



# **VEHICULAR 2024**

The Thirteenth International Conference on Advances in Vehicular Systems,  
Technologies and Applications

ISBN: 978-1-68558-134-3

March 10th –14th, 2024

Athens, Greece

## **VEHICULAR 2024 Editors**

Costin Untaroiu, Virginia Tech, USA

Lasse Berntzen, University of South-Eastern Norway, Norway

# VEHICULAR 2024

## Forward

The Thirteenth International Conference on Advances in Vehicular Systems, Technologies and Applications (VEHICULAR 2024), held between March 10<sup>th</sup> and March 14<sup>th</sup>, 2024, continued a series of international events on the state-of-the-art technologies for information dissemination in vehicle-to-vehicle and vehicle-to-infrastructure and focusing on advances in vehicular systems, technologies and applications.

Mobility brought new dimensions to communication and networking systems, making possible new applications and services in vehicular systems. Wireless networking and communication between vehicles and with infrastructure have specific characteristics from other conventional wireless networking systems and applications (rapidly changing topology, specific road direction of vehicle movements, etc.). These led to specific constraints and optimizations techniques; for example, power efficiency is not as important for vehicle communications as it is for traditional ad hoc networking. Additionally, vehicle applications demand strict communications performance requirements that are not present in conventional wireless networks. Services can range from time-critical safety services, traffic management, to infotainment and local advertising services. They are introducing critical and subliminal information. Subliminally delivered information, unobtrusive techniques for driver's state detection, and mitigation or regulation interfaces enlarge the spectrum of challenges in vehicular systems.

We take here the opportunity to warmly thank all the members of the VEHICULAR 2024 technical program committee, as well as all the reviewers. The creation of such a high-quality conference program would not have been possible without their involvement. We also kindly thank all the authors who dedicated much of their time and effort to contribute to VEHICULAR 2024. We truly believe that, thanks to all these efforts, the final conference program consisted of top-quality contributions. We also thank the members of the VEHICULAR 2024 organizing committee for their help in handling the logistics of this event.

We hope that VEHICULAR 2024 was a successful international forum for the exchange of ideas and results between academia and industry and for the promotion of progress in vehicular systems, technologies and applications.

### **VEHICULAR 2024 Chairs**

#### **VEHICULAR 2024 Steering Committee**

Khalil El-Khatib, University of Ontario Institute of Technology – Oshawa, Canada

Éric Renault, ESIEE Paris, France

Xiaohong Peng, Birmingham City University, UK

Yuping He, University of Ontario Institute of Technology, Canada

#### **VEHICULAR 2024 Publicity Chairs**

José Miguel Jiménez, Universitat Politècnica de Valencia, Spain

Sandra Viciano Tudela, Universitat Politècnica de Valencia, Spain

## **VEHICULAR 2024 Committee**

### **VEHICULAR 2024 Steering Committee**

Khalil El-Khatib, University of Ontario Institute of Technology – Oshawa, Canada  
Éric Renault, ESIEE Paris, France  
Xiaohong Peng, Birmingham City University, UK  
Yuping He, University of Ontario Institute of Technology, Canada

### **VEHICULAR 2024 Publicity Chairs**

José Miguel Jiménez, Universitat Politècnica de Valencia, Spain  
Sandra Viciano Tudela, Universitat Politècnica de Valencia, Spain

### **VEHICULAR 2024 Technical Program Committee**

Vahdat Abdelzad, University of Waterloo, Canada  
Nor Fadzilah Abdullah, National University of Malaysia (UKM), Malaysia  
Mohammed Al-Ansi, University Malaysia Perlis (UniMAP), Malaysia  
Sufyan T. Faraj Al-Janabi, University of Anbar, Ramadi, Iraq  
Mustafa S. Al-Jumaily, University of Tennessee, Knoxville, USA  
Ali Alfoudi, Al-Qadisiyah University, Iraq  
Ala'a Al-Momani, Ulm University, Germany  
Adel Aneiba, Birmingham City University, UK  
Muhammad Asim, Chung-Ang University, Seoul, South Korea  
Hakan Aydin, Karadeniz Technical University, Turkey  
Manlio Bacco, CNR-ISTI, Italy  
Andrea Baiocchi, University of Roma "Sapienza", Italy  
Paolo Barsocchi, ISTI (Institute of Information Science and Technologies) | Italian National Research Council (C.N.R.), Pisa, Italy  
Paulo C. Bartolomeu, University of Aveiro, Portugal  
Marcel Baunach, Graz University of Technology, Austria  
Rahim (Ray) Benekohal, University of Illinois at Urbana-Champaign, USA  
Sylvia Bhattacharya, Kennesaw State University, USA  
Neila Bhourj, Université Gustave Eiffel, France  
Konstantinos Blekas, University of Ioannina, Greece  
Eugen Borcoci, University Politehnica of Bucharest, Romania  
Alexandros-Apostolos A. Boulogeorgos, University of Piraeus, Greece  
Alyssa Byrnes, University of North Carolina at Chapel Hill, USA  
Roberto Caldelli, CNIT, Florence, Italy  
Rodrigo Capobianco Guido, São Paulo State University (UNESP), Brazil  
Antonio Carcaterra, Sapienza University of Rome, Italy  
Pedro Cardoso, Universidade do Algarve, Portugal  
Marcos F. Caetano, University of Brasilia, Brazil  
Florent Carlier, Centre de Reserche en Education de Nantes / Le Mans Université, France  
Juan Carlos Ruiz, Universitat Politècnica de Valencia, Spain

Rodrigo Castelan Carlson, Federal University of Santa Catarina, Brazil  
Francois Chan, Royal Military College, Canada  
Rui Chen, Xidian University, China  
Gihwan Cho, Jeonbuk University, Korea  
Adam Cohen, University of California, Berkeley, USA  
Gianpiero Costantino, Institute of Informatics and Telematics (IIT) | National Research Council (CNR), Italy  
Yousef-Awwad Daraghmi, Palestine Technical University-Kadoorie, Palestine  
David de Andrés, Universitat Politècnica de València, Spain  
Fawad Ud Din, McGill University, Canada  
Liza Dixon, Independent Researcher, Germany  
Konrad Doll, University of Applied Sciences Aschaffenburg, Germany  
Zoran Duric, George Mason University, USA  
Péter Ekler, Budapest University of Technology and Economics, Hungary  
Mostafa Emam, University of the Bundeswehr Munich, Germany  
Suzi Iryanti Fadilah, Universiti Sains Malaysia, University  
Mariano Falcitelli, Photonic Networks & Technologies National Laboratory of CNIT, Italy  
Abraham O. Fapojuwo, University of Calgary, Canada  
Gustavo Fernandez Dominguez, Center for Digital Safety & Security | AIT Austrian Institute of Technology, Austria  
Irene Fiesoli, University of Florence, Italy  
Francesco Flammini, Mälardalen University, Sweden  
Pierfrancesco Foglia, Università di Pisa, Italy  
Clovis Francis, Arts et Métiers ParisTech, Châlons en Champagne, France  
Miguel Franklin de Castro, Federal University of Ceará, Brazil  
Tomonari Furukawa, University of Virginia, USA  
Varun Garg, UMass Lowell, USA  
Pedro Pablo Garrido Abenza, Universidad Miguel Hernandez de Elche, Spain  
Malek Ghanes, Centrale Nantes, France  
Lee Gillam, University of Surrey, UK  
Apostolos Gkamas, University Ecclesiastical Academy of Vella of Ioannina, Greece  
Sezer Goren, Yeditepe University, Turkey  
Alberto Gotta, National Research Council - Institute of Information Science and Technologies "A. Faedo" (CNR-ISTI), Italy  
Heinrich Gotzig, Valeo, Germany  
Javier Gozalvez, Universidad Miguel Hernandez de Elche, Spain  
Abel Guilhermino da Silva Filho, Federal University of Pernambuco - UFPE, Brazil  
Marco Häberle, University of Tuebingen, Germany  
Rami Hamdi, Hamad Bin Khalifa University, Qatar Foundation, Qatar  
Kyungtae (KT) Han, Toyota North America, USA  
Petr Hanáček, Brno University of Technology, Czech Republic  
Hong Hande, Huawei Technologies, Singapore  
Fazirulhisyam Hashim, Universiti Putra Malaysia (UPM), Malaysia  
Yuping He, University of Ontario Institute of Technology, Canada  
Moritz Höser, Bauhaus Luftfahrt e. V., Taufkirchen, Germany  
Javier Ibanez-Guzman, Renault S.A., France  
Hocine Imine, IFSTTAR/LEPSIS, France  
Uzair Javaid, National University of Singapore, Singapore

Dush Nalin Jayakody, Tomsk Polytechnic University, Russia  
Terje Jensen, Telenor, Norway  
Yiming Ji, Georgia Southern University, USA  
Felipe Jiménez Alonso, Technical University of Madrid, Spain  
Magnus Jonsson, Halmstad University, Sweden  
Filbert Juwono, Curtin University, Malaysia  
Thabet Kacem, University of the District of Columbia, USA  
Chuyo Kaku, Jiangsu Chaoli Electric Co. Ltd., China  
Gorkem Kar, Bahcesehir University, Turkey  
Frank Kargl, Institute of Distributed Systems | Ulm University, Germany  
Sokratis K. Katsikas, Norwegian University of Science and Technology, Norway  
Tetsuya Kawanishi, Waseda University, Japan  
John Kenney, Toyota InfoTech Labs, USA  
Norazlina Khamis, Universiti Malaysia Sabah, Malaysia  
Asil Koc, McGill University, Montreal, Canada  
Lisimachos Kondi, University of Ioannina, Greece  
Spyros Kontogiannis, University of Ioannina, Greece  
Anastasios Kouvelas, ETH Zürich, Switzerland  
Zdzislaw Kowalczyk, Gdansk University of Technology, Poland  
Francine Krief, Bordeaux INP, France  
Reiner Kriesten, University of Applied Sciences Karlsruhe, Germany  
Ryo Kurachi, Nagoya University, Japan  
Gyu Myoung Lee, Liverpool John Moores University, UK  
Sebastian Lindner, Hamburg University of Technology, Germany  
Lianggui Liu, Zhejiang Shuren University, China  
M.Carmen Lucas-Estañ, Universidad Miguel Hernández de Elche, Spain  
Dalila B. Megherbi, University of Massachusetts, USA  
Zoubir Mammeri, IRIT - Paul Sabatier University, France  
Sunil Manvi, REVA University, India  
Mirco Marchetti, University of Modena and Reggio Emilia, Italy  
Philippe Martinet, Inria Center at Côte d'Azur University, France  
P. Takis Mathiopoulos, University of Athens, Greece  
Ioannis Mavromatis, University of Bristol, UK  
Rashid Mehmood, King Abdul Aziz University, Saudi Arabia  
José Manuel Menéndez, Universidad Politécnica de Madrid, Spain  
Maria Luisa Merani, University of Modena and Reggio Emilia, Italy  
Lyudmila Mihaylova, The University of Sheffield, UK  
Gerardo Mino Aguilar, Benemérita Universidad Autónoma De Puebla, Mexico  
Naveen Mohan, KTH, Sweden  
Bruno Monsuez, ENSTA ParisTech, France  
Umberto Montanaro, University of Surrey, UK  
Luís Moutinho, Escola Superior de Gestão e Tecnologia de Águeda (ESTGA) - University of Aveiro / Instituto de Telecomunicações, Portugal  
Vasco N. G. J. Soares, Instituto de Telecomunicações / Instituto Politécnico de Castelo Branco, Portugal  
Mena Nagiub, Valeo Schalter und Sensoren GmbH, Germany  
Jose Eugenio Naranjo Hernandez, Universidad Politécnica de Madrid | Instituto Universitario de Investigación del Automóvil (INSIA), Spain  
Ridha Nasri, Orange Labs, France

Keivan Navaie, Lancaster University, UK  
Tomas Olovsson, Chalmers University of Technology, Gothenburg, Sweden  
Rodolfo Orjuela, IRIMAS-Université de Haute-Alsace (UHA), France  
Patrik Österberg, Mid Sweden University, Sweden  
Gerald Ostermayer, University of Applied Sciences Upper Austria, Hagenberg, Austria  
Ilias Panagiotopoulos, Harokopio University of Athens, Greece  
Sugandh Pargal, IIT Kharagpur, India  
Antonio M. Pascoal, Institute for Systems and Robotics - IST | Univ. Lisbon, Portugal  
Al-Sakib Khan Pathan, United International University, Bangladesh  
Robert M. Patton, Oak Ridge National Laboratory, USA  
Xiaohong Peng, Birmingham City University, UK  
Paulo J. G. Pereirinha, Polytechnic of Coimbra | IPC/ISEC | INESC Coimbra, Portugal  
Fernando Pereñíguez García, University Defense Center | Spanish Air Force Academy, Murcia, Spain  
Valerio Persico, University of Napoli Federico II, Italy  
Ivan Petrunin, Cranfield University, UK  
Paulo Pinto, Universidade Nova de Lisboa, Portugal  
Ioannis Politis, Aristotle University of Thessaloniki, Greece  
Srinivas Pulugurtha, The University of North Carolina at Charlotte, USA  
Mahmoud Rahat, Halmstad University, Sweden  
Hesham Rakha, Virginia Tech Transportation Institute, USA  
Mohd Fadlee A Rasid, Universiti Putra Malaysia, Malaysia  
Éric Renault, ESIEE Paris, France  
Martin Ring, Robert Bosch GmbH, Germany  
Geraldo P. Rocha Filho, University of Brasília, Brazil  
Aymeric Rousseau, Argonne National Laboratory, USA  
Javier Rubio-Loyola, CINVESTAV, Mexico  
João Rufino, Instituto de Telecomunicações - Pólo Aveiro, Portugal  
Aduwati Sali, UPM, Malaysia  
José Santa Lozano, Technical University of Cartagena (UPCT), Spain  
José Santa, Technical University of Cartagena, Spain  
Nico Saputro, Parahyangan Catholic University, Bandung, Indonesia  
Marios Savvides, Carnegie Mellon University, USA  
Barbara Schütt, FZI Research Center of Information Technology, Germany  
Alireza Shahrabi, Glasgow Caledonian University, Scotland, UK  
Rajan Shankaran, Macquarie University, Australia  
Susmit Shannigrahi, Tennessee Tech University, USA  
Prinkle Sharma, University of Massachusetts Dartmouth, USA  
Shih-Lung Shaw, University of Tennessee Knoxville, USA  
Dana Simian, Lucian Blaga University of Sibiu, Romania  
Pranav Kumar Singh, Central Institute of Technology Kokrajhar, India  
Michal Sojka, Czech Technical University in Prague, Czech Republic  
Marko Sonkki, Ericsson, Germany  
Chokri Souani, Higher Institute of Applied Sciences and Technology of Sousse, Tunisia  
Essam Sourour, Prince Sattam Bin Abdul-Aziz University (PSAU), Saudi Arabia  
Mujdat Soyuturk, Marmara University, Turkey  
Anand Srivastava, IIT Delhi, India  
Pawan Subedi, The University of Alabama, Tuscaloosa, USA  
Qasim Sultan, Chung-Ang University, Seoul, South Korea

Qingquan Sun, California State University San Bernardino, USA  
Akimasa Suzuki, Iwate Prefectural University, Japan  
Philipp Svoboda, TU Wien, Austria  
Wai Yuen Szeto, The University of Hong Kong, Hong Kong  
Getaneh Berie Tarekegn, National Taipei University of Technology, Taiwan  
Indira Thouvenin, Université de technologie de Compiègne, France  
Angelo Trotta, University of Bologna, Italy  
Bugra Turan, Koc University, Istanbul, Turkey  
Dimitris Tzanis, Technical University of Crete / Hellenic Institute of Transport - Centre for Research and Technology Hellas, Greece  
Klaus David, University of Kassel, Germany  
Costin Untaroiu, Virginia Tech, USA  
Massimo Villari, Università di Messina, Italy  
Alexey Vinel, Halmstad University, Sweden  
Ankur Vora, Intel, SanJose, USA  
Hao Wang, University of Michigan, Ann Arbor, USA  
Hong Wang, Oak Ridge National Laboratory | US Department of Energy, USA  
You-Chiun Wang, National Sun Yat-sen University, Taiwan  
Duminda Wijesekera, George Mason University, USA  
Ramin Yahyapour, Gesellschaft für wissenschaftliche Datenverarbeitung mbH Göttingen (GWDG), Germany  
Bo Yang, University of Tokyo, Japan  
Gioele Zardini, ETH Zurich, Switzerland  
Salim M Zaki, Dijlah University, Baghdad, Iraq  
David Zage, Intel Corporation, USA  
Christos Zaroliagis, University of Patras, Greece  
Sherali Zeadally, University of Kentucky, USA  
Argyrios Zolotas, Cranfield University, UK

## Copyright Information

For your reference, this is the text governing the copyright release for material published by IARIA.

The copyright release is a transfer of publication rights, which allows IARIA and its partners to drive the dissemination of the published material. This allows IARIA to give articles increased visibility via distribution, inclusion in libraries, and arrangements for submission to indexes.

I, the undersigned, declare that the article is original, and that I represent the authors of this article in the copyright release matters. If this work has been done as work-for-hire, I have obtained all necessary clearances to execute a copyright release. I hereby irrevocably transfer exclusive copyright for this material to IARIA. I give IARIA permission to reproduce the work in any media format such as, but not limited to, print, digital, or electronic. I give IARIA permission to distribute the materials without restriction to any institutions or individuals. I give IARIA permission to submit the work for inclusion in article repositories as IARIA sees fit.

I, the undersigned, declare that to the best of my knowledge, the article does not contain libelous or otherwise unlawful contents or invading the right of privacy or infringing on a proprietary right.

Following the copyright release, any circulated version of the article must bear the copyright notice and any header and footer information that IARIA applies to the published article.

IARIA grants royalty-free permission to the authors to disseminate the work, under the above provisions, for any academic, commercial, or industrial use. IARIA grants royalty-free permission to any individuals or institutions to make the article available electronically, online, or in print.

IARIA acknowledges that rights to any algorithm, process, procedure, apparatus, or articles of manufacture remain with the authors and their employers.

I, the undersigned, understand that IARIA will not be liable, in contract, tort (including, without limitation, negligence), pre-contract or other representations (other than fraudulent misrepresentations) or otherwise in connection with the publication of my work.

Exception to the above is made for work-for-hire performed while employed by the government. In that case, copyright to the material remains with the said government. The rightful owners (authors and government entity) grant unlimited and unrestricted permission to IARIA, IARIA's contractors, and IARIA's partners to further distribute the work.

## Table of Contents

A Comparative Analysis of Single-Input Single-Output Stationarity Time and Pathloss in Suburban Environments for Vehicle-to-Infrastructure Channel Using Veneris Ray-Tracing and Real Data <i>Nor El Islam Dahmouni, Mohammed Mallik, Pierre Laly, Esteban Egea Lopez, and Davy P Gaillot</i>	1
Gaze and Coordination in Collision Avoidance between Personal Mobilities <i>Yuki Ninomiya, Shota Matsubayashi, Kazuhisa Miwa, Hitoshi Terai, Naoki Akai, Daisuke Deguchi, and Hiroshi Murase</i>	7
Replicating the Nature of Cooperative Behavior in the First-Person Perspective Task <i>Shota Matsubayashi, Yuki Ninomiya, Kazuhisa Miwa, Hitoshi Terai, Takuma Yamaguchi, Hiroyuki Okuda, and Tatsuya Suzuki</i>	11
Towards a Resource-Aware K-Selection Model for Optimizing V2X Communication in Autonomous Vehicles <i>Olanrewaju Ahmed, David Grace, and Kayode Popoola</i>	15
Autonomous Platooning of General Connected Vehicles Using Bayesian Receding Horizon Control <i>Gilchrist Johnson, Tomonari Furukawa, and B. Brian Park</i>	21
The Smart Highway to Babel: the coexistence of different generations of Intelligent Transport Systems <i>Oscar Amador, Ignacio Soto, Maria Calderon, and Manuel Uruena</i>	27
Offloading Platooning Applications from 5.9 GHz V2X to Radar Communications: Effects on Safety and Efficiency <i>Elena Haller, Galina Sidorenko, Oscar Amador, and Emil Nilsson</i>	33
A Numerical Investigation of Deformable Soil-Tire Interaction <i>Dhruv Jasoliya, Alexandrina Untaroiu, and Costin Untaroiu</i>	39

# A Comparative Analysis of Single-Input Single-Output Stationarity Time and Pathloss in Suburban Environments for Vehicle-to-Infrastructure Channel Using Veneris Ray-Tracing and Real Data

Nor El Islam Dahmouni  
Univ. Lille, CNRS, UMR  
8520-IEMN, F-59000 Lille, France  
email: norelislam.dahmouni@univ-  
lille.fr

Mohammed Mallik  
Univ. Lille, CNRS, UMR  
8520-IEMN, F-59000 Lille,  
France  
email: mohammed.mallik@imt-  
nord-europe.fr

Pierre Laly  
Univ. Lille, CNRS, UMR  
8520-IEMN, F-59000 Lille, France  
email: pierre.laly@univ-lille.fr

Esteban Egea Lopez  
ITC Department,  
Univ. Politécnica de Cartagena,  
30202 Cartagena, Spain  
email: esteban.egea@upct.es

Davy P.Gaillot  
Univ. Lille, CNRS, UMR  
8520-IEMN, F-59000 Lille, France  
email: davy.gaillot@univ-lille.fr

**Abstract**— This paper presents a comparative study of stationarity time ( $T_s$ ) of non-Wide-Sense Stationarity Uncorrelated Scattering (non-WSSUS) channel and path-loss characteristics between a Ray-tracing Veneris simulator and real-world data of Vehicle-to-Infrastructure (V2I) communication of Single-Input Single-Output (SISO) channel in a suburban environment at 5.89 GHz. The WSSUS assumption is often used to model wireless channels in order to simplify the analysis and design of communication systems. However, this assumption is not always valid for V2I channels, which can be highly dynamic and non-stationary. In this paper, a Ray-tracing simulator, namely Veneris, is used to generate synthetic V2I channel data. This data is then compared to real-world V2I channel data collected by a radio channel sounder, namely MaMIMOSA, in a suburban environment. The results show that the simulator accurately predicted the channel stationarity time of the real-world V2I channel, with a median of 560 ms compared to 550 ms for real data. Additionally, a Jensen-Shannon divergence value of 0.05 was found, suggesting a relative similarity between the simulated and real data distributions. The path-loss exponent factor was 3.5 for the simulator and 3.1 for real data.

**Keywords**-WSSUS; GLSF; CCF; V2I; 5G.

## I. INTRODUCTION

5G is considered a major breakthrough for Vehicle-to-Infrastructure (V2I) communication, where the precise understanding of radio propagation channels is fundamental to reliable and robust wireless communication systems. These requirements are crucial for vehicular communication applications, especially for Intelligent Transportation Systems (ITS), which are developed by two main groups: The Third Generation Partnership Project (3GPP), which focuses on the Cellular-Vehicle-to-Everything (C-V2X) standard, and European Telecommunications Standards Institute (ETSI), based on IEEE 802.11p standard, known as ITS-G5 or Direct Short Range Communication (DSRC) in United States [1][2]. In addition, the crucial importance of a thorough and detailed

characterization of the propagation channel becomes evident in the process of modeling and designing communication systems. A comprehensive characterization of the properties of the propagation channel leads to precise modeling, fostering the development of reliable, robust, and interoperable communication systems. The characterization of the radio propagation channel can be described using a variety of channel modeling techniques, including statistical modeling based on time-frequency domain measurement campaigns or deterministic modeling-based simulations [8].

## II. STATE OF THE ART

Ray-tracing, a deterministic modeling technique, has been widely used to characterize 5G radio channels in various environments, including urban, suburban, rural, tunnel, indoor, etc. [7][21]. For vehicular communication, numerous studies are based on Ray-tracing models for the analysis and estimation of vehicle propagation channel characteristics. These studies specifically focus on small-scale fading characteristics, signal statistics, coverage, and data rate prediction [23][24], as well as signal strength degradation [22]. Additionally, a time-varying channel modeling for low terahertz urban V2I communication is presented in [6]. In a separate study, the comparison between Ray-tracing and stochastic models is explored, particularly for urban V2I Terahertz communication channels [20].

A key feature of channel modeling, designing, and analyzing wireless propagation channels is the assumption of Wide-Sense Stationary and Uncorrelated Scattering (WSSUS). Propagation channel models conventionally incorporate the WSSUS assumptions [3][9]. The WSSUS assumptions imply that the channel mean and autocorrelation  $H(t, f)$  remain constant over time  $t$  and frequency  $f$ , or in other words, the second-order channel statistics are independent of time and frequency. This assumption simplifies transceiver design by providing simple mathematical models for the channel, enabling the use of less complex channel estimation or precoding techniques [10].

From a functional perspective, the analysis of non-WSSUS channel statistics could help with optimizing adaptive transmission schemes and beamforming techniques, as well as improving the overall system performance [11][12]. However, due to the high mobility of transmitters and receivers and the appearance of dynamic scatters in vehicular communication, V2I channel characteristics change rapidly over time, leading to violations of WSSUS assumptions, resulting in non-stationary behavior [9] due to the time-varying nature of Multi-Path Components (MPC). This implies that we can describe the time-varying fading process of vehicular channels by assuming that they exhibit local stationarity within a limited time and frequency range. It is therefore necessary to characterize the propagation channel and define the stationarity regions (generally the stationarity time) where the WSSUS hypothesis is valid.

A comprehensive framework for estimating time and frequency stationarity has been developed in [3][4]. The time- and frequency-dependent Generalized Local Scattering Function (GLSF)  $\hat{C}(t, f, \nu, \tau)$  for non-WSSUS channels is derived by extending the scattering function  $C(\tau, \nu)$  for WSSUS channels. The stationarity region, defined by its time and frequency stationarity limits  $T_s$  and  $F_s$ , respectively, can be derived from the GLSF using the four-dimensional Fourier transform of the GLSF, namely the Channel Correlation Function (CCF) [3]. As reported in [13] for similar scenarios, the minimum frequency stationarity is significantly greater than 150 MHz. Since ITS technologies operating at 5.9 GHz typically use bandwidths of less than 20 MHz, the radio channel is considered to be stationary in terms of frequency. Consequently, this study focuses exclusively on analyzing stationarity time  $T_s$ .

In [24], a simulator designed for non-WSSUS channels, to analyze the performance of V2X communication systems, based on Monte Carlo and Cisoid-sum models, is described in detail. Moreover, [25] presents a tapped delay line model specifically adapted to non-WSSUS Vehicle-to-Vehicle (V2V) channel scenarios. In [26], an autoregressive modeling approach for the simulation of non-stationary vehicle channels is presented, focusing on measurements to compare real data, but not directly with a deterministic Ray-tracing model. In addition, a Ray-tracing model has been developed and compared with real-world data in terms of small and large-scale channel parameters in a dense urban environment for Multiple-Input Multiple-Output (MIMO) V2I communication. The study considers the channel to be WSS and does not take into account the non-stationary behavior, as presented in [27].

Despite considerable progress in channel modeling and Ray-tracing for radio propagation channels, as well as for non-WSSUS channels in vehicular communication systems, there remains a notable gap in comprehensive comparisons between real measurement data and Ray-tracing models for non-WSSUS V2I propagation channels, particularly for the stationarity time (WSS), as identified in the current literature.

This paper presents a comparative analysis of Single-Input Single-Output (SISO) channel stationarity time and path-loss in a suburban environment at 5.89 GHz, comparing simulated Channel Transfer Functions (CTF) from the Veneris framework Ray-tracing model [16], and real measurement campaign data collected using a MaMIMOSA channel sounder [5]. The same configuration setup and scenario were employed for both simulations and measurements. The remainder of this paper is organized as follows. Section III introduces the scenario and setup. Section IV fully characterizes and compares the channel path-loss statistics between the simulated CTFs and real measurement data. Additionally, it includes estimations and comparisons of the stationarity time  $T_s$  over distance for both simulated and real data. Finally, Section V concludes the discussion by summarizing key findings implications, and future perspectives.

### III. SCENARIO AND SETUP

In this section, we introduce our environment chosen for measurement and simulation on the campus of the University of Lille (ULille), France. The suburban environment consists of 3-4 story buildings spaced 5-10 m apart, with dense vegetation and trees up to 30 m high. Additionally, there is an industrial hall (8m in height) with a framework of metal portals, an overhanging sloping roof, and metal cladding. Traffic on the road was relatively low, with a maximum speed of 50 km/h, but many cars were parked along the boulevard during the drive-test. Two speed bumps, separated by 150 meters, are present in the used measurement road (Figure 1).

#### A. Real data Measurement

The measurements were performed using the MaMIMOSA radio channel sounder with an 80 MHz bandwidth at 5.89 GHz, developed by a joint team from the ULille in France and Ghent University (UGent) in Belgium. The MaMIMOSA sounder is a real-time massive MIMO radio channel sounder that is specifically designed for V2X applications. It is equipped with a massive 64-antenna array for transmission (Tx) and up to 16 individual antennas for reception (Rx). The MaMIMOSA hardware and software capabilities allow for the sounding parameters to be freely adapted to the investigated scenario, demonstrating its versatility and flexibility [5][14]. The Tx was a massive square array of 64 antennas, but only one antenna was used in this study. The Tx was installed as a Road-Side Unit (RSU) on the sidewalk at a height of 2 meters above the ground. An omnidirectional Rx antenna was placed on the roof of a van at a height of 3 meters, as shown in Figure 2. For the mobility scenario, the van moved away from the Tx at a constant speed of 40 km/h over a total distance of 300 m, such that a Line-Of-Sight (LOS) path was always present, as shown in Figure 1. The 5.89 GHz MaMIMOSA used frequency corresponds to the frequency band offered by ITS derived from the 5.9 GHz ITS-G5 and C-V2X technologies.

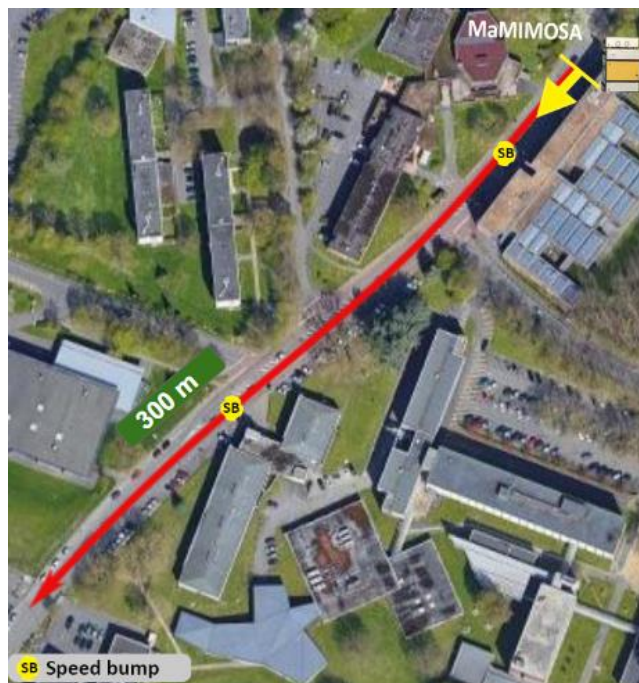


Figure 1. A top view of the measurement campaign for stationarity in a suburban environment.



Figure 2. Tx-Rx antenna systems.

During the drive-test, 13670 time-varying CTFs of ~1 ms were measured over a total Tx-Rx distance of 300 m. These CTFs are organized into 5 frames of 2752 CTFs spaced by an interblock time of 1 ms. Each CTF contains 818 frequency samples spaced by eight subcarriers, which were selected across the 80 MHz bandwidth. The maximum Doppler span is  $\pm 250$  Hz (corresponding to a maximum speed of 46 km/h) with a Doppler resolution of 0.181 Hz. The measurement campaign and frame configuration are detailed in [15].

### B. Ray-tracing Data

The Ray-tracing simulator Veneris uses the same scenario environment (Figure 3) and setup parameters of real data measured from the MaMIMOSA sounder for the simulation part, developed by Telecommunications Network Engineering Group (GIRTEL) of Polytechnic University of Cartagena (UPCT), Spain. Veneris is a comprehensive and realistic simulation environment for research on vehicular networks and cooperative automated driving, as well as a valuable tool for simulating general wireless networks requiring 3D environment-aware propagation simulation. It consists of the following components: a traffic simulator, implemented on top of the Unity game engine and including a realistic vehicle model as well as a set of driving and lane change behaviors that reproduce traffic dynamics; Opal, a Ray-launching GPU-based propagation simulator, which is an open source Ray-tracing propagation simulator for electromagnetic characterization. Opal is an integral part of the Veneris framework and can be used as a stand-alone simulator or can be integrated with the Unity game engine. It is implemented in C++ and utilizes NVIDIA OptiX, and a set of modules that facilitate bidirectional coupling with the widely used network simulator, namely Objective Modular Network Testbed in C++ (OMNET++). The functional and configurational aspects of Veneris are presented in [16][17].

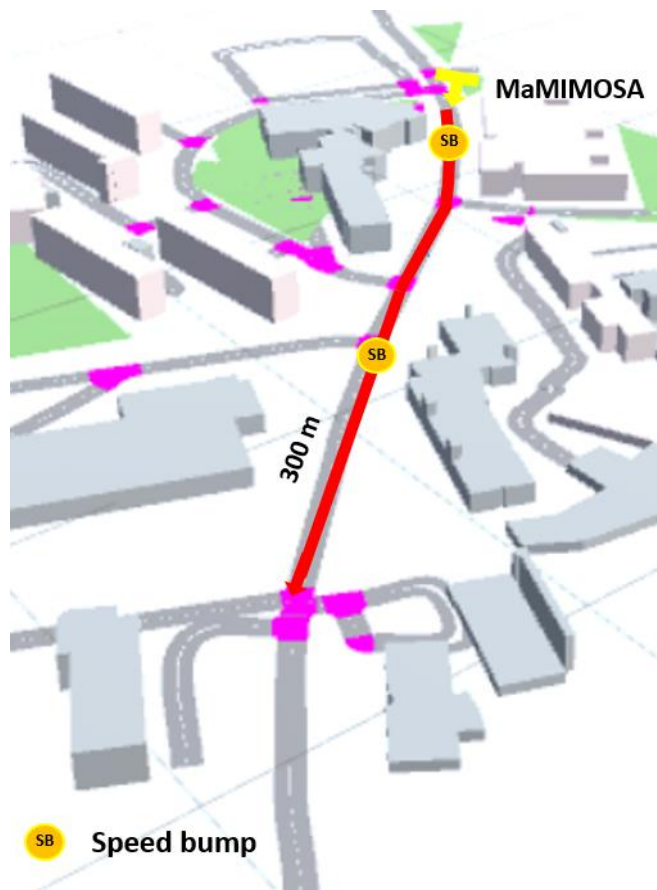


Figure 3. Veneris interface for the same scenario at 5.9 GHz.

TABLE 1. CONFIGURATION PARAMETERS

Parameters	Configuration
Carrier frequency	5.89 GHz
Measurement bandwidth	80 MHz
Frequency points	818
Delay resolution	12.5 ns
Doppler resolution	0.181 Hz
CTF duration	~ 1 ms
Total CTF number	13760
Interblock time	1 ms
Transmit power	0 dBm
Tx – Rx height	2 m / 3 m

The same setup configuration and frame were used in the Veneris configuration, with the antenna power as shown in Table 1, which summarizes the configuration parameters for both real and simulated measurements.

#### IV. RESULTS AND DISCUSSION

The signal power variation of simulation data compared to real data over distance must be checked before analyzing the stationarity time and path-loss characteristics.

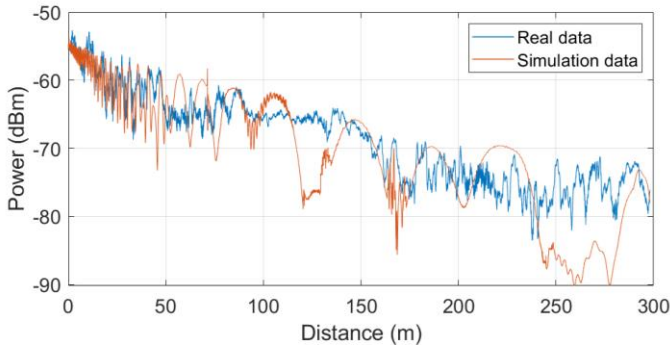


Figure 4. Received power for real and simulation data.

Figure 4 shows the received signal power in dBm for both real-world data and simulation over the Tx-Rx distance. A similar trend is observed in the received power. Within the first 50 meters, there is a power attenuation from -55 dBm to -65 dBm with rapid small-scale fluctuations attributed to the dense multipath component caused by nearby buildings. Beyond 50 meters up to 300 meters, there is a slow pronounced attenuation, ranging from -65 dBm to -80 dBm for real data and -90 dBm for simulation data. Overall, the real and simulation data are in good agreement. The main difference is that the real data is more noisy due to environmental factors. This suggests that the simulation model is accurate.

##### A. Propagation loss

The empirical model for Path-Loss (PL) as a function of the Tx-Rx distance is given by the following expression:

$$PL(d)_{dB} = PL(d_0)_{dB} + 10 \times n \times \log_{10} \left( \frac{d}{d_0} \right) \quad (1)$$

with  $n$  the path-loss attenuation exponent, which is equal to 2 in free space, and  $PL(d_0)$  dB the attenuation measured at a reference distance of  $d_0=80$  m based on [18].

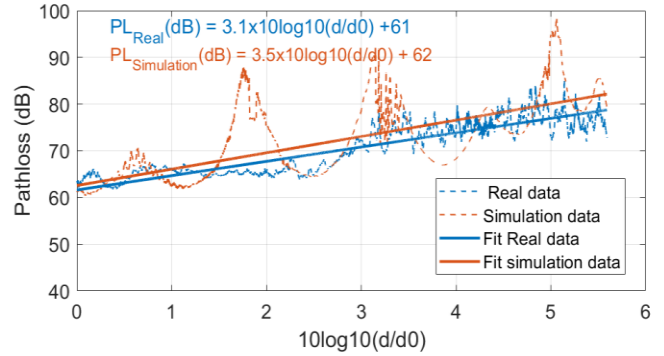


Figure 5. Path-loss fit for real-world and simulation data.

Figure 5 compares the PL plot of real-world data to the simulation plot based on equation (1). The PL exponent factor ( $n$ ) is calculated using linear regression and found to be 3.1 and 3.5 for real-world and simulated PL, respectively. These results agree with previous research on similar scenarios with LOS [18][19].

##### B. Stationarity time evaluation

Based on GLSF, and its 4D Fourier transform the CCF  $A(\Delta v, \Delta \tau; \Delta t, \Delta f)$  [3][4].

$$A(\Delta v, \Delta \tau; \Delta t, \Delta f) = TF^{4D} \{ \hat{C}(t, f; v, \tau) \} \quad (2)$$

The stationarity time  $T_s$  could be calculated as:

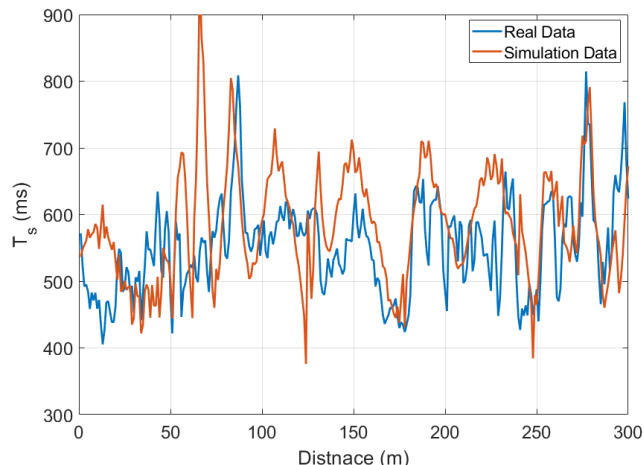
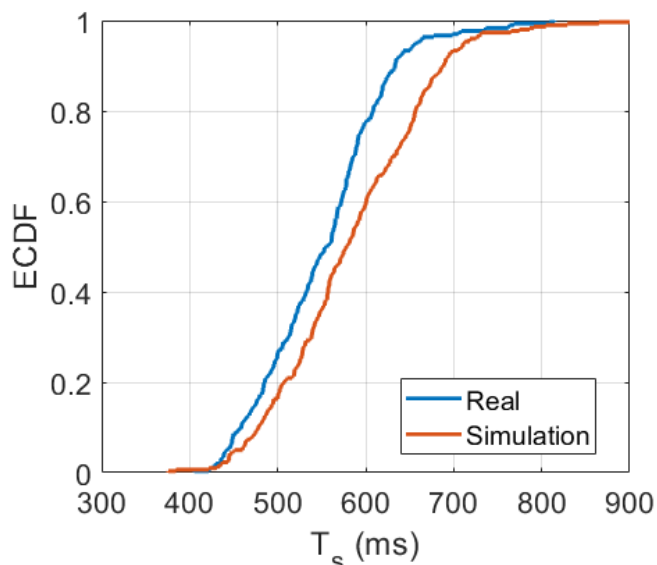
$$T_s = \frac{1}{\overline{\Delta v}} \quad (3)$$

where  $\overline{\Delta v}$  is the Doppler correlation deduced from the CCF Doppler first moment as follows [3][4]

$$\overline{\Delta v} = \frac{1}{\|A\|_1} \int \int \int |\Delta v| A(\Delta v, \Delta \tau; \Delta t, \Delta f) dv d\tau dt df \quad (4)$$

where  $\|A\|_1$  is the first norm of the CCF along the three dimensions.

The sampled CTF, the discrete representation of the GLSF CCF, and the calculation of  $T_s$  are presented and detailed in [15]. In order to estimate stationarity time over distance, we used 10 interleaved GLSF corresponding to 934.34 ms [15].


 Figure 6. Stationarity time  $T_s$  over distance for real and simulated data.

 Figure 7. ECDF of Stationarity time  $T_s$  for real and simulated data.

Figures 6 and 7 show the stationarity time  $T_s$  of real and simulated data over distance and their Empirical Cumulative Distribution Function (ECDF), respectively. The results show that the real and simulated  $T_s$  follow similar trends and distributions, with medians of 550 ms and 560 ms, respectively. Additionally, using the Jensen–Shannon divergence method, which is bounded between 0 and 1 for quantifying the similarity between two probability distributions, where a value of 0 implies identical distributions, and 1 suggests maximal dissimilarity between the distributions, a value of 0.05 is found, meaning that the two probability distributions are relatively similar. This indicates that the Veneris Ray-tracing simulator can accurately reflect the physical properties of the real propagation channel. Table 2 summarizes some statistics of  $T_s$ .

TABLE 2. COMPARISON OF STATIONARITY TIME BETWEEN REAL DATA AND SIMULATION

	Median	Std	Min
<b><math>T_s</math> real</b>	550 ms	74 ms	418 ms
<b><math>T_s</math> simulation</b>	560 ms	86 ms	396 ms

## V. CONCLUSION & FUTURE WORK

This paper presented a comparative study of non-WSSUS SISO channel stationarity time and path-loss characteristics between the Veneris Ray-tracing simulator and real-world data of V2I communication in a suburban environment at 5.89 GHz. The simulator accurately predicted the channel stationarity time of the real-world V2I channel, with a median of 560 ms compared to 550 ms for real data. Furthermore, a Jensen–Shannon divergence value of 0.05 was found, indicating a relative similarity between the simulated and real data distributions. The path-loss exponent factor was 3.5 for the simulator and 3.1 for real data. These results suggest that the simulator can accurately reflect the stochastic physical properties of the channel, making it a reliable tool for evaluating the performance of V2I communication systems in different suburban environments.

In future work, we will extend this paper by comparing the simulator in massive MIMO array configurations to evaluate the statistical spatial behavior of the stationarity time  $T_s$  across the massive array and the angular properties of the MPCs, such as the Angles of Arrival (AoA) and the Angles of Departure (AoD) values and spreads.

## ACKNOWLEDGMENT

This work has been partially funded by Grant PID2020-112675RB-C41 funded by (MCIN/AEI/10.13039/50110001103). E. Egea-Lopez thanks the European Association on Antennas and Propagation (EurAAP) for funding the STSM under which this work was done.

## REFERENCES

- [1] F. Arena, G. Pau, and A. Severino, "A review on IEEE 802.11 p for intelligent transportation systems," *Journal of Sensor and Actuator Networks*, vol. 9, no. 2, pp. 22, 2020.
- [2] A. Alalewi, I. Dayoub, and S. Cherkaoui, "On 5G-V2X use cases and enabling technologies: A comprehensive survey," *IEEE Access*, vol. 9, pp. 107710-107737, 2021.
- [3] G. Matz, "On non-WSSUS wireless fading channels," *IEEE Transactions on Wireless Communications*, vol. 4, no. 5, pp. 2465-2478, 2005.
- [4] G. Matz, "Doubly underspread non-WSSUS channels: Analysis and estimation of channel statistics," in *2003 4th IEEE Workshop on Signal Processing Advances in Wireless Communications-SPAWC 2003 (IEEE Cat. No. 03EX689)*, pp. 190-194, 2003.
- [5] D. P. Gaillot et al., "Measurement of the V2I massive radio channel with the MaMIMOSA sounder in a suburban environment," in *2021 15th European Conference on Antennas and Propagation (EuCAP)*, pp. 1-4, 2021.
- [6] Y. Chen and C. Han, "Time-varying channel modeling for low-terahertz urban vehicle-to-infrastructure communications," in *2019 IEEE Global Communications Conference (GLOBECOM)*, pp. 1-6, 2019.
- [7] M. Ghaddar, J. M. García-Pardo, I. B. Mabrouk, M. Lienard, and P. Degauque, "UTD-Based Ray Tracing MIMO Channel Modeling for the Next Generation Communications within

- Underground Tunnels," *IEEE Transactions on Antennas and Propagation*, 2023.
- [8] G. Tiberi et al., "An efficient ray tracing propagation simulator for analyzing ultrawideband channels," in *2007 IEEE International Conference on Ultra-Wideband*, pp. 794-799, 2007.
- [9] F. Hlawatsch and G. Matz, "Wireless communications over rapidly time-varying channels," Academic Press, 2011.
- [10] A. F. Molisch, "Wireless communications," vol. 34, John Wiley & Sons, 2012.
- [11] O. Renaudin, V.-M. Kolmonen, P. Vainikainen, and C. Oestges, "Non-stationary narrowband MIMO inter-vehicle channel characterization in the 5-GHz band," *IEEE Transactions on Vehicular Technology*, vol. 59, no. 4, pp. 2007-2015, 2010.
- [12] U.A.K. Chude-Okonkwo, R. Ngah, and T. Abd Rahman, "Time-scale domain characterization of non-WSSUS wideband channels," *EURASIP Journal on Advances in Signal Processing*, vol. 2011, no. 1, pp. 1-20, 2011.
- [13] L. Bernadó, T. Zemen, F. Tufvesson, A. F. Molisch, and C.F. Mecklenbräuker, "The (in-) validity of the WSSUS assumption in vehicular radio channels," in *2012 IEEE 23rd International Symposium on Personal, Indoor and Mobile Radio Communications (PIMRC)*, pp. 1757-1762, 2012.
- [14] P. Laly et al., "Massive radio channel sounder architecture for 5G mobility scenarios: MaMIMOSA," in *2020 14th European Conference on Antennas and Propagation (EuCAP)*, pp. 1-5, 2020.
- [15] N. E. I. Dahmouni et al., "On the Stationarity Time of a Vehicle-to-Infrastructure Massive Radio Channel in a Line-of-Sight Suburban Environment," *Sensors*, vol. 22, no. 21, p. 8420, 2022.
- [16] E. Egea-Lopez, F. Losilla, J. Pascual-Garcia, and J. M. Molina-Garcia-Pardo, "Vehicular networks simulation with realistic physics," *IEEE Access*, vol. 7, pp. 44021-44036, 2019.
- [17] E. Egea-Lopez, J.M. Molina-Garcia-Pardo, M. Lienard, and P. Degauque, "Opal: An open source ray-tracing propagation simulator for electromagnetic characterization," *Plos One*, vol. 16, no. 11, p. e0260060, 2021.
- [18] T. S. Rappaport, K. Blankenship, and H. Xu, "Propagation and radio system design issues in mobile radio systems for the glomo project," Virginia Polytechnic Institute and State University, 1997.
- [19] N. H. Talib et al., "An efficient algorithm for large-scale RFID network planning," in *2019 IEEE Jordan International Joint Conference on Electrical Engineering and Information Technology (JEEIT)*, pp. 519-524, 2019.
- [20] Y. Li, Y. Chen, D. Yan, K. Guan, C. Han, "Channel Characterization and Ray-Tracing Assisted Stochastic Modeling for Urban Vehicle-to-Infrastructure Terahertz Communications," *IEEE Transactions on Vehicular Technology*, vol. 72, no. 3, pp. 2748-2763, 2022.
- [21] D. He et al., "The design and applications of high-performance ray-tracing simulation platform for 5G and beyond wireless communications: A tutorial," *IEEE Communications Surveys & Tutorials*, vol. 21, no. 1, pp. 10-27, 2018.
- [22] B. Colo, A. Fouda, and A. S. Ibrahim, "Ray tracing simulations in millimeter-wave vehicular communications," in *2019 IEEE 30th Annual International Symposium on Personal, Indoor and Mobile Radio Communications (PIMRC)*, pp. 1-4, 2019.
- [23] D. Kong et al., "V2I mmWave Connectivity for Highway scenarios," in *2018 IEEE 29th annual international symposium on personal, indoor and mobile radio communications (PIMRC)*, pp. 111-116, 2018.
- [24] J. Zhao, L. Xiong, D. He, and J. Du, "Channel characteristics of rail traffic tunnel scenarios based on ray-tracing simulator," *Wireless Communications and Mobile Computing*, vol. 2018, 2018.
- [25] Y. Li et al., "A TDL based non-WSSUS vehicle-to-vehicle channel model," *International Journal of Antennas and Propagation*, vol. 2013, 2013.
- [26] M. Yusuf et al., "Autoregressive Modeling Approach for Non-Stationary Vehicular Channel Simulation," *IEEE Transactions on Vehicular Technology*, vol. 71, no. 2, pp. 1124-1131, 2021.
- [27] K. H. Ng, E. K. Tameh, A. Doufexi, M. Hunukumbure, and A. R. Nix, "Efficient multielement ray tracing with site-specific comparisons using measured MIMO channel data," *IEEE Trans. Veh. Technol.*, vol. 56, no. 3, pp. 1019-1032, 2007.

# Gaze and Coordination in Collision Avoidance between Personal Mobilities

Yuki Ninomiya

*Institute of Innovation for Future Society  
Nagoya University*

Aichi, Japan

e-mail: ninomiya.yuki.t1

@f.mail.nagoya-u.ac.jp

Shota Matsubayashi

*Institute of Innovation for Future Society  
Nagoya University*

Aichi, Japan

e-mail: matsubayashi.shota.v0

@f.mail.nagoya-u.ac.jp

Kazuhisa Miwa

*Graduate School of Informatics  
Nagoya University*

Aichi, Japan

e-mail: miwa@is.nagoya-u.ac.jp

Hitoshi Terai

*Faculty of Humanity-Oriented Science and Engineering  
Kindai University*

Fukuoka, Japan

e-mail: terai@fuk.kindai.ac.jp

Naoki Akai

*Graduate School of Engineering  
Nagoya University*

Aichi, Japan

e-mail: akai@nagoya-u.jp

Daisuke Deguchi

*Graduate School of Informatics  
Nagoya University*

Aichi, Japan

e-mail: ddeguchi@nagoya-u.jp

Hiroshi Murase

*Graduate School of Informatics  
Nagoya University*

Aichi, Japan

e-mail: murase@nagoya-u.jp

**Abstract**—In collision avoidance between pedestrians, they smoothly avoid collisions. In Personal Mobility (PM) collision avoidance, eye movement information, which is not often used in pedestrian collision avoidance, may be a powerful source of information. This is because information from body movements is limited in the case of PMs. This study shows the relationship between gaze and the opponent's coordination behavior in collision avoidance between PMs. Only the Follower who passed later through the collision point gazed at the opponent more when they adjusted their own behavior more. This study extends the findings on collision avoidance behavior between pedestrians and provides insight into collision avoidance behavior between PMs.

**Keywords** - collision avoidance; gaze; coordination.

## I. INTRODUCTION

We avoid collisions with others as we walk through crowded places, such as supermarkets, hospitals, and airports. Collision avoidance between pedestrians is achieved smoothly by using a common strategy among pedestrians to determine their roles of going first or going second [1]. In this paper, the role of the person who passes through the collision point first is defined as the Leader, and the role of the person who passes through the collision point later is defined as the Follower.

On the other hand, recently, due to the development of Personal Mobility (PM), there has been an increase of shared spaces where different types of mobility other than pedestrians are present [2]. Some reports suggest that the safety in such shared spaces is better than in conventional segregated spaces [3]. Specifically, it has been reported that driver attention to pedestrians improves [3], vehicle speeds decrease, traffic congestion decreases, and accident rates decrease [4].

In a shared space, the interaction partners are not only pedestrians but also various mobilities including PMs. Therefore, the need for knowledge on collision avoidance behavior via PMs is expected to increase in the future. The purpose of this study is to investigate the factors that influence collision avoidance behavior via PMs.

Studies of collision avoidance among pedestrians have shown that pedestrians acquire roles and adjust their behavior accordingly [5][6]. Coordination behavior in collision avoidance uses information that varies with the crossing situation, such as the crossing angle and its rate of change, and the estimated time to collision [1][5]–[7]. For example, pedestrians adjust their walking speed and walking path according to the crossing angle and available space [1]. In addition, it has been reported that when avoiding a collision in a face-to-face situation, pedestrians make avoidance decisions based on the direction of the oncoming person's feet [7]. On the other hand, there has also been progress in examining factors that do not contribute to collision avoidance between pedestrians. For example, it has been shown that gaze at the other person does not affect coordination behavior in collision avoidance between pedestrians [8]. In other words, in collision avoidance between pedestrians, coordination behavior is based on information, such as location, speed, and body movements, such as body orientation and foot direction.

In the case of collision avoidance between PMs, the information available for coordination behavior is more limited compared to the case of a pedestrian partner. Specifically, while coordination behavior with a pedestrian partner uses information on body motions, such as body and foot orientation [7][8], in the case of a PM partner, body motion information

is limited because there is no up-and-down motion of the legs in both the seated and standing positions. Therefore, the available body motion information is limited to the direction of the head and eye movements. In other words, in the case of collision avoidance between PM passengers, unlike in the case of pedestrians, gaze may be a valuable source of information for coordination behavior.

In fact, it has been shown that gaze plays an important role in traffic negotiation situations with a partner whose behavior cannot be estimated from body motion. For example, in traffic negotiations between cars and pedestrians, it is known that a pedestrian's direct gaze at the oncoming lane elicits more concessive behavior from the car [9][10]. However, the relationship between gaze and coordination behavior in collision avoidance between PMs has not been clarified.

In this study, we examine the relationship between gaze and coordination behavior in collision avoidance between PMs. In examining the relationship between gaze and coordination behavior, it is necessary to examine the influence of gaze depending on the role. There is a difference in the required coordination behavior between the Leader and the Follower. The Follower adjusts speed and path more than the Leader in collision avoidance situations [5][6]. Similarly, the relationship between gaze and coordination behavior may differ depending on these roles.

Therefore, this study examines the relationship between gaze and coordination behavior in collision avoidance between PMs, considering this role. Specifically, we examine the following three points. First, we examine the difference in gaze between the Leader and the Follower. Then, we confirm whether there is a difference in coordination behavior depending on the roles of the Leader and the Follower. Finally, by examining the correlation between gaze and coordination behavior of the Leader and Follower, we examine whether there is a role-dependent difference in the relationship between gaze and coordination behavior in collision avoidance between PMs.

## II. METHOD

### A. Participants

Twenty participants ( $N_{female} = 17$ ,  $N_{male} = 3$ ,  $M_{age} = 41.95$ ,  $SD_{age} = 14.95$ ) were recruited through a recruitment agency. 4 participants participated in the experiment per day.

### B. Apparatus

Eye movement and position data during collision avoidance were measured. Eye movements were measured with Tobii Glasses 2 manufactured by Tobii Technology Co. The pose and velocity information was obtained using the 2D-LiDAR-based localization system (presented in [11]). The vehicle used was a WHILL Model C manufactured by WHILL Inc. (Figure 1).

### C. Tasks

The task was to board a PM and cross paths with other participants only by operating acceleration and deceleration.



A) Whill model C

B) Position of 2D-LiDAR

Figure 1. PM (A) and 2D-LiDAR position (B).

The paths were designed to intersect at the center of the paths, which were 10 m straight from each other (Figure 2). A straight line, such as A→G in Figure 2 means path in one trial. Three angles of intersection (60, 90, and 120 degrees) were provided. The two participants switched sides so that the direction from which the other person came was not fixed to either the left or right. One set of 24 trials, two rounds of 3 (crossing angle) × 2 (reciprocation) × 2 (direction of the other person), was used. For example, in the case of a pair of participants x and y, the x participant moves a set of paths (A→G→A) × 2→(B→H→B) × 2→(C→I→C) × 2, while the y participant moves a set of paths (L→F→L) × 2→(K→E→K) × 2→(J→D→J) × 2. Subsequently, x and y exchanged sets of paths.

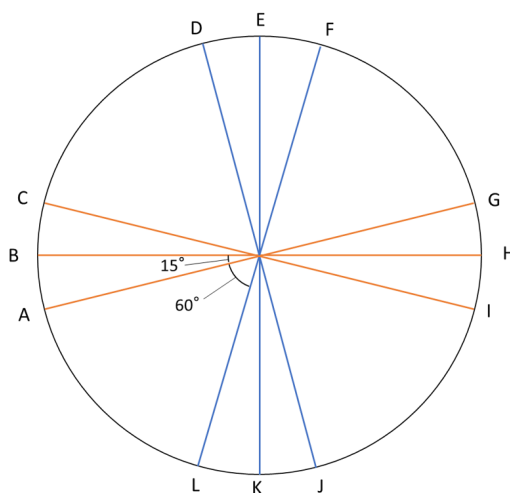


Figure 2. The path design in tasks.

### D. Procedure

First, informed consent was conducted. After the task explanation, participants practiced 12 trials to familiarize them-

selves with the operation of the PM. They then participated in the main task. In this task, all combinations of two out of four participants participated in a set. That is, the total number of sets was six, and each participant participated in three sets of the experiment. The time he/she did not participate was considered a rest period.

### III. RESULTS

#### A. Difference in the gaze toward the opponent between Follower and Leader

We analyzed the video recorded by the eye tracker. Gaze toward the opponent was defined as the overlap of the coordinates of the gaze position and the position of the opponent in the video. The amount of gaze in each trial was calculated by dividing the number of logs in which each participant gazed by the total number of logs recorded every 100 hz (Table I). To examine differences in the amount of gaze by role, a paired t-test comparing the amount of gaze was conducted, and significantly more gaze was observed for the Follower ( $t(535) = -28.55, p < .001$ ).

TABLE I  
MEAN (SD) OF AMOUNT OF GAZE AND OPERATION

	Leader	Follower
Gaze	.014(.023)	.083(.053)
Operation	3.97(1.58)	4.30(1.54)

To examine the nature of gaze for each role, we plotted the time from the beginning of the trial on the horizontal axis and the number of trials in which gaze was performed at that point on the vertical axis (Figure 3). The results showed that the Follower continued to gaze until the middle of the trial, while the Leader rarely gazed after gazing at the beginning of the trial. In other words, the Follower gazed more, and continued to gaze until the middle of the trial, when coordination behavior was required.

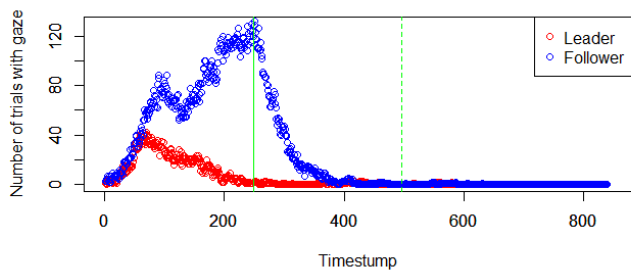


Figure 3. Timing of the gaze toward the opponent. The green dotted line indicates the average end time of a trial, and the green solid line indicates half of that time.

#### B. Difference in the coordination behavior between Follower and Leader

Differences in coordination behavior by role were examined. In this study, the coordination behavior in collision avoidance

was limited to acceleration/deceleration. In other words, the more acceleration/deceleration during the trial, the more it contributed to the coordination behavior. However, acceleration/deceleration after passing through the intersection is not a coordination behavior for collision avoidance.

Therefore, the amount of operation to reach the intersection of the paths of the Follower and Leader was calculated. Specifically, we calculated the amount by which the speed of the Leader and Follower changed (Table I). This value represents the amount of speed change per unit of time. That is, the value is larger when there is a sudden acceleration or deceleration. The point of intersection is the point of intersection between the start and goal of the two vehicles, and the value is used until the vehicle enters a 1m circle centered at the point of intersection.

The operation volumes of the Follower and Leader were then compared using a paired t-test. The analysis showed that the Follower had more operations than the Leader ( $t(535) = -3.81, p < .001$ ).

#### C. Relationship between gaze toward the opponent and coordination behavior.

To examine the relationship between the gaze and coordination behavior for each collision avoidance role, Pearson's product-moment correlations were calculated for each value (Table II). The results showed that, regardless of the role, gaze was significantly correlated with the amount of operation of the opponent. On the other hand, the Leader's gaze was not significantly correlated with the amount of their own operations, while the Follower's gaze was significantly correlated with the amount of their own operations.

TABLE II  
CORRELATION BETWEEN GAZE TOWARD OPPONENT AND OPERATION BY ROLE (\* :  $p < .05$ , \*\*\* :  $p < .001$ )

	Leader's Operation	Follower's Operation
Leader's Gaze	.08	.09*
Follower's Gaze	.10*	.14***

### IV. DISCUSSION

The purpose of this study was to examine the relationship between gaze toward the opponent and coordination behavior in collision avoidance between PMs. The results of the experiment are summarized with a focus on the difference between the roles of the Leader and the Follower.

The Follower had more gaze toward the opponent and more coordination behavior (amount of manipulation) than the Leader. This is consistent with the findings of previous studies in pedestrians that coordination behavior is mainly performed by the Follower [5][6]. Our findings provide empirical evidence that the Follower performs more gaze toward the partner, as well as coordination behavior.

The important point is that the relationship between gaze and coordination behavior was different between the Leader and Follower. First, there was no role-dependent difference in the fact that gaze toward the opponent was positively

correlated with the opponent's coordination behavior. This suggests that regardless of the role, gaze toward the opponent has a role in promoting the opponent's coordination behavior. This point was not observed in the case of collision avoidance between pedestrians. This means that gaze toward the opponent is a powerful source for coordination behavior in situations where information is limited, such as in PMs.

On the other hand, the Follower's gaze was related to the amount of their own operations, but the Leader's gaze was not related to the amount of their own operations. This result can be interpreted that only the Follower gazed more when they coordinated behavior with their opponent. This interpretation is supported by the fact that the Follower's gaze was mainly focused on the opponent before reaching the point of intersection where coordination behavior was performed, and that the Follower, who performed more coordination behavior than the Leader, gazed more than the Leader. These results suggest that the gaze toward the opponent is performed for different purposes depending on the role of collision avoidance. Specifically, the Leader's gaze is intended to encourage the opponent to coordinate behavior, while the Follower's gaze may be intended to coordinate their own behavior in addition to encouraging the opponent to coordinate behavior.

#### V. CONCLUSION AND FUTURE WORK

The purpose of this study was to examine the relationship between gaze toward the opponent and coordination behavior in collision avoidance between PMs. This study extends the knowledge of pedestrian-to-pedestrian collision avoidance behavior and provides insight into PM-to-PM collision avoidance behavior by the following contributions. First, we extended the knowledge that Follower coordinates behavior in pedestrian-pedestrian collision avoidance to the case of PMs. Second, we provided evidence that gaze is involved in coordination behavior in collision avoidance between PMs, unlike in collision avoidance between pedestrians. Finally, we showed that the relationship between gaze and coordination behavior differs depending on the role in collision avoidance, and that only the Follower gazes towards the opponent to coordinate their own behavior. Future work should extend the discussion to the functions of gaze to smoothness and role determination in collision avoidance.

#### ACKNOWLEDGMENT

Support for this work was given by JSPS KAKENHI Grant Number 22H03912 and 22H00211, and by Toyota Motor Corporation (TMC). However, note that this article solely reflects the opinions and conclusions of its authors and not TMC or any other Toyota entity.

#### REFERENCES

- [1] P. Basili, M. Sağlam, T. Kruse, M. Huber, A. Kirsch, and S. Glasauer, "Strategies of locomotor collision avoidance," *Gait & Posture*, vol. 37, pp. 385–390, 3 2013. [Online]. Available: <https://doi.org/10.1016/j.gaitpost.2012.08.003>
- [2] A. Karndacharuk, D. J. Wilson, and R. Dunn, "A review of the evolution of shared (street) space concepts in urban environments," *Transport Reviews*, vol. 34, pp. 190–220, 3 2014. [Online]. Available: <https://doi.org/10.1080/01441647.2014.893038>
- [3] I. Kaparias, M. G. Bell, A. Miri, C. Chan, and B. Mount, "Analysing the perceptions of pedestrians and drivers to shared space," *Transportation Research Part F: Traffic Psychology and Behaviour*, vol. 15, pp. 297–310, 5 2012. [Online]. Available: <https://doi.org/10.1016/j.trf.2012.02.001>
- [4] B. Hamilton-Baillie, "Shared space: Reconciling people, places and traffic," *Built Environment*, vol. 34, pp. 161–181, 5 2008.
- [5] A.-H. Olivier, A. Marin, A. Créteil, A. Berthoz, and J. Pettré, "Collision avoidance between two walkers: Role-dependent strategies," *Gait & Posture*, vol. 38, pp. 751–756, 9 2013. [Online]. Available: <https://doi.org/10.1016/j.gaitpost.2013.03.017>
- [6] A. G. Knorr, L. Willacker, J. Hermsdörfer, S. Glasauer, and M. Krüger, "Influence of person- and situation-specific characteristics on collision avoidance behavior in human locomotion," *Journal of Experimental Psychology: Human Perception and Performance*, vol. 42, pp. 1332–1343, 9 2016. [Online]. Available: <https://doi.org/10.1037/xhp0000223>
- [7] N. Watanabe, H. Mikado, and T. Omori, "Construction of collision avoidance behavior model induced by visual motion," *2011 IEEE International Conference on Fuzzy Systems (FUZZ-IEEE 2011)*, pp. 2732–2736, 6 2011. [Online]. Available: <https://doi.org/10.1109/FUZZY.2011.6007626>
- [8] S. D. Lynch, J. Pettre, J. Bruneau, R. Kulpa, A. Cretual, and A.-H. Olivier, "Effect of virtual human gaze behaviour during an orthogonal collision avoidance walking task," *2018 IEEE Conference on Virtual Reality and 3D User Interfaces (VR)*, pp. 136–142, 3 2018. [Online]. Available: <https://doi.org/10.1109/VR.2018.8446180>
- [9] N. Guéguen, S. Meineri, and C. Eyssartier, "A pedestrian's stare and drivers' stopping behavior: A field experiment at the pedestrian crossing," *Safety Science*, vol. 75, pp. 87–89, 6 2015. [Online]. Available: <https://doi.org/10.1016/j.ssci.2015.01.018>
- [10] N. Guéguen and C. Jacob, "Direct look versus evasive glance and compliance with a request," *The Journal of Social Psychology*, vol. 142, pp. 393–396, 6 2002. [Online]. Available: <https://doi.org/10.1080/00224540209603907>
- [11] N. Akai, "Reliable Monte Carlo localization for mobile robots," *Journal of Field Robotics*, vol. 40, pp. 595–613, 5 2023. [Online]. Available: <https://doi.org/10.1002/rob.22149>

# Replicating the Nature of Cooperative Behavior in the First-Person Perspective Task

Shota Matsubayashi

*Institutes of Innovation for Future Society (InFuS)*

*Nagoya University*

Aichi, Japan

e-mail: matsubayashi.shota.v0@f.mail.nagoya-u.ac.jp

Yuki Ninomiya

*Institutes of Innovation for Future Society (InFuS)*

*Nagoya University*

Aichi, Japan

e-mail: ninomiya.yuki.t1@f.mail.nagoya-u.ac.jp

Kazuhisa Miwa

*Graduate School of Informatics*

*Nagoya University*

Aichi, Japan

e-mail: miwa@is.nagoya-u.ac.jp

Hitoshi Terai

*Faculty of Humanity-Oriented Science and Engineering*

*Kindai University*

Fukuoka, Japan

e-mail: terai@fuk.kindai.ac.jp

Takuma Yamaguchi

*Graduate School of Engineering*

*Nagoya University*

Aichi, Japan

e-mail: t\_yamaguchi@nuem.nagoya-u.ac.jp

Hiroyuki Okuda

*Graduate School of Engineering*

*Nagoya University*

Aichi, Japan

e-mail: h\_okuda@nuem.nagoya-u.ac.jp

Tatsuya Suzuki

*Graduate School of Engineering*

*Nagoya University*

Aichi, Japan

e-mail: t\_suzuki@nuem.nagoya-u.ac.jp

**Abstract**—The nature of cooperative behavior has been shown to reach self-goal earlier and achieve self-benefit by reducing interruption to others using the bird’s-eye perspective task. This study examines whether the nature of cooperative behavior is replicated in the first-person perspective task using a driving simulator. The results showed that behavioral performance was nearly identical in the bird-eye perspective experiment and the first-person perspective tasks. This finding indicates that the nature of cooperative behavior was confirmed in the realistic first-person perspective and that the bird-eye perspective task has high validity in verifying moving behavior.

**Keywords**—cooperative behavior; shared space.

## I. INTRODUCTION

### A. Cooperative Behavior in Traffic

The cooperative behavior of humans plays an important role in traffic. Previous studies have considered acceleration or deceleration for others as the typical cooperative behavior [1]–[3]. Such cooperative behavior promotes efficiency and safety [4] and generates positive emotions in the surrounding individuals [5][6]. Conversely, uncooperative behavior can cause serious accidents and delays [7][8] and arouse stress and anger [9]. In recent years, cooperative behavior that takes into account the others surrounding us has been developed from the perspective of social robotics [10]–[12].

### B. Nature of Cooperative Behavior

The main scope of previous studies is separated space, where each traffic participant is provided with its own space, such as a sidewalk for pedestrians or a motorway for vehicles. However, such separated space is replaced by shared space.

In the shared space, all traffic participants can move bidimensionally [13] and it is not clear who has priority to cross [14]. We have shown what kind of cooperative behavior individuals take in the shared space [15].

Our previous study [15] examined the nature of cooperative behavior using the Bird’s-Eye Perspective (BEP) experiment (Figure 1). Participants were required to move to their goals by operating a joystick in the simulated space shared with the other autonomous agents. Participants were given one of the following three instructions, and their behavioral performance was compared across the three conditions: “Reach your goal while considering others” (cooperative condition), “You have enough time and can go to your goal slowly” (nonurgent condition), and “You do not have enough time and should reach your goal as fast as you can” (urgent condition).

The results showed that the urgent behavior decreased

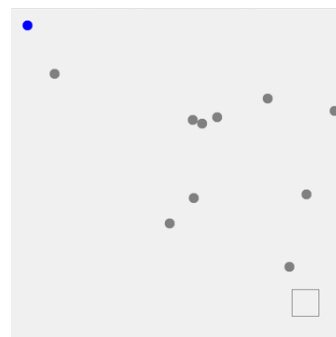


Figure 1. Overview of the bird-eye perspective task [15].

completion time compared to no instruction baseline, but increased the amount of interruption to others. Meanwhile, the cooperative and nonurgent behavior increased completion time. Furthermore, only the cooperative behavior decreased the amount of interruption compared to the baseline. An additional comparison among the three conditions showed that completion time and interruption were lower in the cooperative condition than in the nonurgent condition. We concluded that the nature of cooperative behavior is to reach the self-goal earlier and to achieve self-benefit by reducing interruption to others.

### C. Difference in Perspective

In the authors' previous task, participants had a BEP [15]. However, in actual situations, individuals move in a First-Person Perspective (FPP). Therefore, it is necessary to examine whether the nature of cooperative behavior can be reproduced in FPP. This study examines cooperative behavior compared to urgent and nonurgent behavior in the experiment in the FPP using a driving simulator.

Although there are not many studies that directly compare the BEP and FPP, several studies have suggested the effect of perspective on moving behavior. For example, in a maze task, it is more difficult to accurately understand the positional relationship from the FPP than from BEP [16]. In addition, providing a highly objective perspective influences moving behavior [17]. This experiment shows that adding BEP reduces lateral deviation when driving straight ahead and increases speed when turning left or right. Individuals evaluate the risk of contact with vehicles higher in FPP than in third-person perspective [18].

In the non-traffic field, the effect of FPP has also been shown. Virtual experience in the FPP using virtual reality elicits stronger physiological responses, emotional experiences, and subjective reactions than in the third-person perspective [19]–[21].

Based on these previous studies, the following effects can be predicted when the perspective is changed to FPP in the moving task as a shared space. First, cooperative behavior may not reduce the interruption to others in the FPP although it does in the BEP. This is because it is more difficult to understand the positional relationship in the FPP than in the BEP. Conversely, the nature of cooperative behavior may be observed in the FPP as well as in the BEP. This is because the FPP evokes a stronger emotional experience of cooperation or consideration. Examination of the effect of perspective on cooperative behavior is also important to use BEP and FPP tasks for verification of cooperative behavior.

The rest of the paper is structured as follows. Section 2 describes the experimental method and Section 3 describes the results of the experiment. In Section 4, we discuss the difference in the effect of perspectives and the applicability of the tasks.



Figure 2. Overview of the first-person perspective task.

## II. METHOD

### A. Participants

A total of 24 participants joined the experiment ( $M_{age} = 48.08$ ,  $SD_{age} = 12.18$ ). Informed consent was obtained from participants prior to the experiment. This experiment was approved by the Institutional Review Board at the Institutes of Innovation for Future Society (InFuS), Nagoya University (approval number: 2021-13).

### B. Stimulus

The task in the previous study [15] was changed from BEP to FPP using a driving simulator (Figure 2). A total of seven displays were used to project the images from the FPP using Unity [22]. A vehicle was placed in the center of the displays, and the joystick used in the BEP task was set to control the vehicle. The up/down directions of the joystick corresponded to forward/backward movement, and the left/right directions corresponded to left/right turns, while the joystick input corresponded directly to the direction of travel in the BEP task. A trial was defined as lasting until participants reached their own goals.

### C. Procedure

The procedure was almost identical to the BEP task. After some practice trials with the joystick, a total of five sets were performed. In Sets 1 and 2, participants were asked to reach their goals without any instructions. In Sets 3, 4, and 5, participants performed the same task after receiving one of three instructions, i.e., cooperative, urgent, or nonurgent instructions, or no instruction. Trials with no instruction were regarded as baseline. The order of instructions was counterbalanced across participants. A set consisted of 12 trials, including four trials each with 16, 24, and 32 other autonomous agents.

The index of moving performance was also the same as in the BEP experiment. The completion time corresponds to the time it took participants to reach their goal, and the amount of interruption corresponds to the total time it took participants to interfere with other agents. If an agent was in the direction of another agent and the distance between them was less than 3 meters, it was considered to be an interruption.

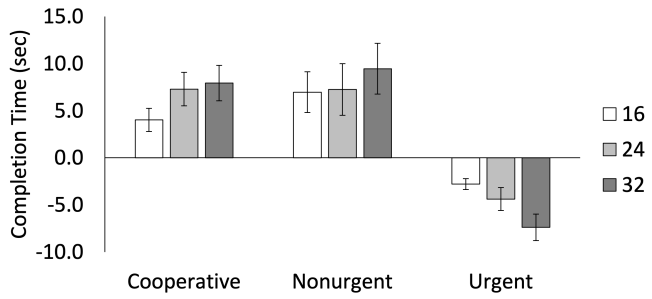


Figure 3. Means of Completion Time. Values indicate the differences from baseline with no instruction. Error bars indicate standard errors. The legend indicates the number of other agents.

### III. RESULTS

One participant was excluded due to incomplete data, and the remaining 23 participants were analyzed.

#### A. Completion Time

The values in Figure 3 indicate the differences from baseline. One-sample  $t$ -tests were performed with the baseline for all conditions. The results show significant differences from the baseline in all nine conditions. The completion time in the cooperative and nonurgent conditions was significantly longer, while the completion time in the urgent condition was shorter than baseline. Comparisons of the results of  $t$ -tests between the BEP and the FPP are shown in Table I.

As in the BEP experiment, direct comparisons were made between the cooperative and nonurgent conditions. The results of the 2 (instructions)  $\times$  3 (number of others) ANOVA showed that there were no main effects of instructions ( $F(1, 22) = 0.411, p = .527, \eta_p^2 = .018$ ) and number of others ( $F(2, 44) = 2.796, p = .071, \eta_p^2 = .112$ ), nor interaction between instructions and number of others ( $F(2, 44) = 1.110, p = .341, \eta_p^2 = .047$ ).

Therefore, the trend of cooperative behavior could be observed for completion time in the FPP task, although there was no salient difference from the nonurgent condition.

#### B. Interruption

The same  $t$ -tests were performed for interruption (Figure 4). The results showed significant differences from baselines in all but 24 others conditions in the cooperative and nonurgent conditions. This means that the amount of interruption was less in the cooperative and nonurgent conditions and greater in the urgent condition. A direct comparison showed that there were no main effects of instructions ( $F(1, 22) = 0.002, p = .962, \eta_p^2 = .000$ ) and number of others ( $F(2, 44) = 2.270, p = .115, \eta_p^2 = .093$ ), nor interaction between instructions and number of others ( $F(2, 44) = 0.533, p = .590, \eta_p^2 = .023$ ).

Therefore, the trend of cooperative behavior was also observed for interruption in the FPP task, although there was no salient difference from the nonurgent condition. The results that interruption was not reduced in some cases are consistent with the results in the BEP experiment (Table I).

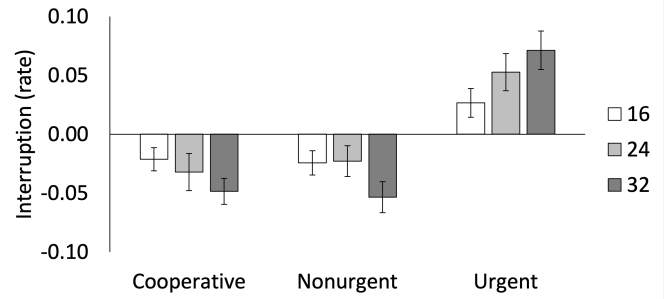


Figure 4. Means of Interruption Rate. Values indicate the differences from baseline with no instruction. Error bars indicate standard errors. The legend indicates the number of other agents.

TABLE I  
RESULTS OF ONE-SAMPLE  $t$ -TESTS WITH BASELINE.

	Bird's-eye pers.			First-person pers.		
	5	10	20	16	24	32
Completion Time						
Cooperative	+	+	+	+	+	+
Nonurgent	+	+	+	+	+	+
Urgent	-	-	-	-	-	-
Interruption						
Cooperative	-	-	-	-	-	-
Nonurgent	-	-	-	-	-	-
Urgent	+	+	+	+	+	+

Notes: “+” indicates a significant positive value and “-” indicates a significant negative value compared to the baseline based on the results of one-sample  $t$ -tests with baseline.

### IV. DISCUSSION

This study examined whether the nature of cooperative behavior observed in the BEP task was replicated in the FPP task. The results of the baseline comparison showed that behavioral performance was almost identical in the BEP and FPP tasks. That is, both cooperative and nonurgent behavior increased completion time and decreased interruption compared to baseline. Surprisingly, interruption was affected by the number of other agents in both experiments. Thus, this research shows that the nature of cooperative behavior is independent of perspective. This also indicates the high effectiveness and reliability of the BEP task as an experimental paradigm for verifying various moving behaviors.

However, the direct comparison revealed some differences between the BEP and FPP tasks. Significant differences between the cooperative and nonurgent conditions were found for completion time and interruption in the BEP task, but these differences were not found in the FPP task.

#### A. Effect of Perspective

In general, the nature of cooperative behavior was somewhat less salient in the FPP task than in the BEP task, although these trends were similar. One possible reason for this is that it is difficult to understand the positional relationship between oneself and others in the FPP [16]. From the FPP, individuals could only get the positional information in front of them. Thus, they may not notice the presence of others approaching

from the left or right and may inadvertently obstruct others. In addition, the FPP makes it difficult to identify the path to the goals, which leads to an increase in completion time in the cooperative condition. As a result, the differences with the nonurgent condition may be eliminated. In other words, the reason for the increase in completion time in the cooperative condition may be that individuals often accelerate or decelerate and make large turns to obtain as much positional information as possible.

### B. Fidelity and Validity of Bird's-eye View Experiment

The results of this study show that the nature of cooperative behavior was confirmed in the realistic FPP, and the BEP task has high validity for verifying moving behavior. In the BEP task, participants can obtain objective information more easily than in actual traffic situations. In addition, the fidelity of the BEP task is considered to be lower than the FPP task. In general, low-fidelity environments have the advantage of facilitating factor control, but the behavior observed in such an environment may not be realistic or reliable.

However, the moving behavior in the BEP task is generally consistent with that in the FPP task, and its validity is also sufficiently high. Therefore, we conclude that the BEP task is useful to verify cooperative behavior even in complex traffic situations. Furthermore, these findings suggest that our tasks may be useful for verification of other various behavior.

### ACKNOWLEDGMENT

Support for this work was given by JSPS KAKENHI Grant Number 22H03912 and 22H00211, and by Toyota Motor Corporation (TMC). However, note that this article solely reflects the opinions and conclusions of its authors and not TMC or any other Toyota entity.

### REFERENCES

- [1] P. Hidas, "Modelling vehicle interactions in microscopic simulation of merging and weaving," *Transportation Research Part C: Emerging Technologies*, vol. 13, no. 1, pp. 37–62, 2005.
- [2] T. Stoll, F. Müller, and M. Baumann, "When cooperation is needed: the effect of spatial and time distance and criticality on willingness to cooperate," *Cognition, Technology and Work*, vol. 21, no. 1, pp. 21–31, 2019.
- [3] T. Stoll, M. Lanzer, and M. Baumann, "Situational influencing factors on understanding cooperative actions in automated driving," *Transportation Research Part F: Traffic Psychology and Behaviour*, vol. 70, pp. 223–234, 2020.
- [4] M. Fiosins, B. Friedrich, J. Görmer, D. Mattfeld, J. P. Müller, and H. Tchouankem, *A Multiagent Approach to Modeling Autonomic Road Transport Support Systems*. Cham: Springer International Publishing, 2016, pp. 67–85.
- [5] D. H. Mcknight, M. Carter, J. B. Thatcher, and P. F. Clay, "Trust in a specific technology: An investigation of its components and measures," *ACM Transactions on Management Information Systems*, vol. 2, no. 2, pp. 1–25, 2011.
- [6] M. Zimmermann, L. Fahrmeier, and K. J. Bengler, "A Roland for an Oliver? Subjective perception of cooperation during conditionally automated driving," *2015 International Conference on Collaboration Technologies and Systems, CTS 2015*, pp. 57–63, 2015.
- [7] J. Tang, F. Liu, W. Zhang, R. Ke, and Y. Zou, "Lane-changes prediction based on adaptive fuzzy neural network," *Expert Systems with Applications*, vol. 91, pp. 452–463, 2018.
- [8] S. Matsubayashi, H. Terai, and K. Miwa, "Development of a Driving Model That Understands Other Drivers' Characteristics," in *HCII 2020*, vol. 2, no. 1918, 2020, pp. 29–39.
- [9] A. Riener, K. Zia, A. Ferscha, C. Ruiz Beltran, and J. J. Minguez Rubio, "Traffic flow harmonization in expressway merging," *Personal and Ubiquitous Computing*, vol. 17, no. 3, pp. 519–532, 2013.
- [10] M. Heesen, M. Baumann, J. Kelsch, D. Nause, and M. Friedrich, "Investigation of cooperative driving behaviour during lane change in a multi-driver simulation environment," in *Human Factors: a view from an integrative perspective*, D. De Waard, K. Brookhuis, F. Dehais, C. Weikert, S. Röttger, D. Manzey, S. Biede, F. Reuzeau, and P. Terrier, Eds., 2012. [Online]. Available: <https://elib.dlr.de/79384/>
- [11] G. Kong, J. Cai, J. Gong, Z. Tian, L. Huang, and Y. Yang, "Cooperative Following of Multiple Autonomous Robots Based on Consensus Estimation," *Electronics*, vol. 11, no. 20, p. 3319, oct 2022. [Online]. Available: <https://www.mdpi.com/2079-9292/11/20/3319>
- [12] B. Sabetghadam, R. Cunha, and A. Pascoal, "Cooperative motion planning with time, energy and active navigation constraints," in *2018 IEEE/OES Autonomous Underwater Vehicle Workshop (AUV)*, 2018, pp. 1–6.
- [13] F. Weifeng, Y. Lizhong, and F. Weicheng, "Simulation of bi-direction pedestrian movement using a cellular automata model," *Physica A: Statistical Mechanics and its Applications*, vol. 321, no. 3–4, pp. 633–640, 2003.
- [14] J. Uttley, Y. M. Lee, R. Madigan, and N. Merat, "Road user interactions in a shared space setting: Priority and communication in a UK car park," *Transportation Research Part F: Traffic Psychology and Behaviour*, vol. 72, pp. 32–46, 2020.
- [15] S. Matsubayashi, K. Miwa, H. Terai, A. Shimojo, and Y. Ninomiya, "Self-Benefit and Others' Benefit in Cooperative Behavior in Shared Space," *Human Factors: The Journal of the Human Factors and Ergonomics Society*, vol. 66, no. 4, pp. 961–974, 2024.
- [16] M. Nakanishi, Y. Higa, and K. Iwanaga, "Effects of difference in the viewpoint on the user's behaviors in the 3d virtual space : First person view and third person view," *Bulletin of Japanese Society for the Science of Design*, vol. 58, no. 1, pp. 17–24, 2011.
- [17] K. Teranishi, T. Ohtsubo, S. Nakamura, Y. Matsuba, and M. Nakanishi, "Effects of Different Visual-support Viewpoints upon Behavior and Cognition in Spatial Mobility," *Transactions of Society of Automotive Engineers of Japan*, vol. 50, no. 3, pp. pp 883–890, 2019.
- [18] C. Castanier, F. Paran, and P. Delhomme, "Risk of crashing with a tram: Perceptions of pedestrians, cyclists, and motorists," *Transportation Research Part F: Traffic Psychology and Behaviour*, vol. 15, no. 4, pp. 387–394, 2012.
- [19] D. Berntsen and D. C. Rubin, "Emotion and vantage point in autobiographical," *Cognition & Emotion*, vol. 20, no. 8, pp. 1193–1215, 2006.
- [20] C. Gonzalez-Lienres et al., "Being the Victim of Intimate Partner Violence in Virtual Reality: First- Versus Third-Person Perspective," *Frontiers in Psychology*, vol. 11, pp. 1–13, 2020.
- [21] M. Slater et al., "A virtual reprise of the Stanley Milgram obedience experiments," *PLoS ONE*, vol. 1, no. 1, 2006.
- [22] J. K. Haas, "A history of the unity game engine," *Diss. Worcester Polytechnic Institute*, vol. 483, no. 2014, p. 484, 2014.

# Towards a Resource-Aware K-Selection Model for Optimizing V2X Communication in Autonomous Vehicles

Olanrewaju Ahmed, David Grace, Kayode Popoola

School of Physics Engineering and Technology

University of York

York, UK

e-mail: moa531@york.ac.uk

e-mail: david.grace@york.ac.uk

e-mail: kayodepopoola@alumni.york.ac.uk

**Abstract** - The rise of autonomous vehicles is accompanied by the emergence of bandwidth-intensive applications like real-time 3D map downloads, necessitating improved bandwidth utilization. While clustering has proven effective in prior research to partially address this challenge, existing works often assume a perfect cluster formation without accounting for outliers, and the selection of the number of clusters ( $k$ ) tends to be resource-agnostic. This paper presents the preliminary findings from the initial cluster analysis phase, laying the foundation for a resource-aware  $k$ -selection model. This model aims to optimize bandwidth resources and alleviate throughput bottlenecks between Vehicle-to-Infrastructure (V2I) and Vehicle-to-Vehicle (V2V) links. The cluster analysis part of our work examines the variation in sizes of various vehicular cluster components concerning changes in cluster range ( $d$ ) and the number of clusters ( $k$ ). Notably, our approach considers unclustered vehicles, acknowledging their impact on bandwidth utilization. Our results reveal a consistent pattern and correlation between the size of different vehicular components and the variables considered ( $k$  and  $d$ ). Drawing insights from this understanding of vehicular cluster behaviour, we propose an approach to optimize V2I and V2V bandwidth usage while minimizing throughput bottlenecks between V2V and V2I links. This resource-aware  $k$ -selection model holds the potential to significantly enhance the efficiency and performance of Vehicle-to-Everything (V2X) communication in the era of autonomous vehicles, contributing to the realization of a seamless and high-throughput vehicular communication network.

**Keywords**-Cluster; bandwidth; V2X; V2V; sidelink.

## I. INTRODUCTION

Clustering approaches has gained significant interest in V2X research in recent years, and this is due to the potential it holds with regards to mitigating stability issues emanating from the dynamic characteristic of vehicular network topology as demonstrated in the works in [1]-[4]. However, with the increasing growth in autonomous driving, accompanied with rise in data-intensive driving applications and use cases has raised questions concerning the quality of vehicular links and their capacity to cope with these emerging applications. Cluster-based approaches has been suggested to improve link performances either by shortening of link length, resource allocation or by hot-spot based relaying. Though cluster-based relaying has been touted to minimize bandwidth resource contention in Cellular-V2X (C-V2X) [4][5], and cluster-based resource allocation have been suggested to maximize resource

utilization [6][7], the potential of these approaches can be limited by a little considered factor. Outlying or unclustered vehicles. Also, it is unrealistic to continuously minimize cluster threshold to minimize link length, as this could either indiscriminately increase number of clusters or number of unclustered vehicles.

We seek an approach that could exploit the optimal selection of number of clusters to consolidate on the resource gains potential of cluster-based relaying and resource allocation.

Most approaches of selecting number of clusters ( $k$ ) are resource agnostic and have only considered the compactness of clusters [8]-[12]. For example, the gap method described in [12] compares cluster compactness value with a null reference point. The popular elbow method described in [10] uses a visual observation to select an edge point at which within-cluster-sum of squared error difference starts to diminish. Calinski-Harabasz [8], David Bouldin [9] and Silhouette [11] approaches all considered both intra-cluster compactness and inter-cluster separation. All these approaches though have been used in clustering process of vehicular nodes in V2X networks and Vehicular ad hoc Networks (VANETs), they are all resource agnostics and have little consideration for unclustered vehicles.

Our approach focusses on building on the idea of cluster-based relay and resource allocation to further optimize utilization of V2X bandwidth resources by selecting optimal number of clusters ( $k$ ) with consideration for available resources, free vehicles, and cluster boundary threshold. The goal is to maximize the use of both V2I and V2V bandwidth resources. We approach the conundrum by first analysing the relationship between the variables considered, then find a solution that minimizes the V2I links and maximum cluster size, which in turn maximizes the resources available to both V2I and V2V users. The analysis is done in the context of mode-3 centralised resource allocation, where separate dedicated resources are allocated for V2I and V2V communication. The results obtained from the analysis demonstrates a specific pattern of variation of number of V2I users along changes in number of clusters and distance threshold which suggest an understanding that for a dedicated allocation approach there exist a point where the minimum number of V2I users will offer the maximum V2I bandwidth. A similar observation is observed for V2V users with respect to

maximum cluster size variation. Having, completed the analysis, we proceeded to develop an optimization problem to maximize bandwidth utilization. that the optimal number of cluster (k) solution and cluster boundary threshold that yields the maximum bandwidth/user.

The rest of this paper describes in detail the cluster analysis and the proposed optimization. In Section 2, a description of the overall system model is presented, which includes the cluster and resource allocation model. Section 3 presents the cluster analysis, describing variations across number of clusters and distance threshold. Section 4 presents the proposed k-selection optimization model while Section 5 concludes the paper.

## II. SYSTEM MODEL

The consideration of cluster-based relay necessitates a description of the topology and the communication model underpinning the topology. The topology is developed in the context of a 2-hop downlink transmission path proposed for download of urgently needed real-time traffic data. Vehicles are grouped into clusters where the Cluster Heads (CHs) serve as a relay and a download hotspot for the rest of Cluster Members (CMs). The 2-hop downlink transmission path consist of the cluster backhaul or the Base Station to Cluster Head downlink (BS-to-CH) and the Cluster Head to Cluster Member (CH-to-CM) sidelink. The CH-to-CM V2V side links are modelled in an urban environment as described in [13]. The pathloss and shadowing model we employed for the backhaul is based on the channel model defined in [14].

Concerning interference, we used different interference schemes for the V2I/N links and the V2V sidelink. For the

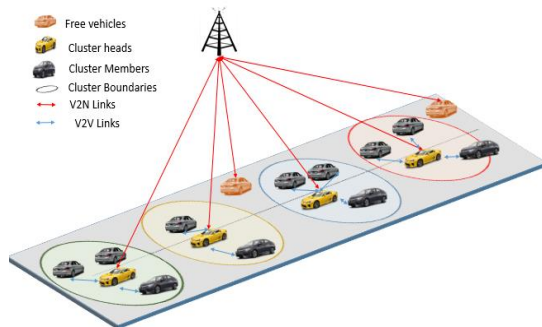


Figure 1. System Model of Cluster Based C-V2X.

V2I/N links, we adopted frequency reuse of 1 and hexagonal cell coverage with the BS at the centre of the hexagon. We assume a variation of Fractional Frequency Reuse (FFR) is used by the base station to allocate resources to the V2I/N nodes/links. We have decided to limit our discussion about the type or implementation of the FFR scheme, since the type of scheme adopted has no impact on the downlink interference considered in our scenario.

For the V2V sidelink, the frequency allocation and interference are cluster-based. A typical vehicular node uses a different channel from those used by its co-cluster members and same bandwidth channel to CMs of other

clusters that poses least interference. A simple depiction of the interference and resource allocation approach used is depicted in Figure 2. The coloured bar at the top represents the entire resource allocated for V2V sidelink communication, while each colour represents the equal bandwidth resource blocks allocated to each V2V CH-to-CM sidelink. The dotted lines represent interference while the continuous lines represent received signal link. Note that the resource bar has size different colours, each colour represents the resource blocks attached to each user and the size of each block is defined by the maximum cluster size,  $C_{sz(max)}$ .

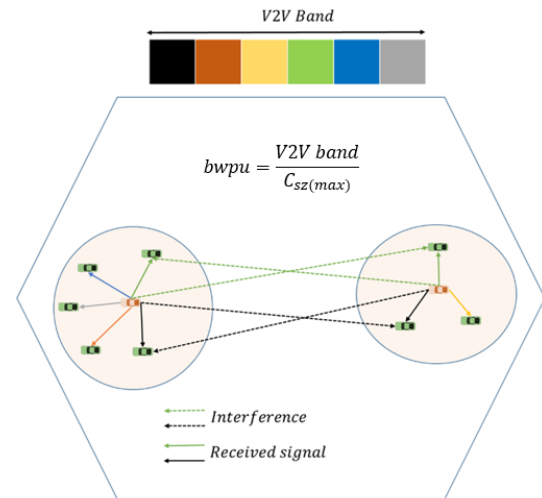


Figure 2. A Depiction of Interference Coordination and Resource Allocation for V2V Sidelink Communication.

## III. CLUSTER ANALYSIS

In effort to maximize bandwidth per user-link and minimize the potential bottleneck between V2I and V2V links along relay transmission path, we seek to investigate the variation of the sizes of different vehicular node components with changes in cluster boundary thresholds and number of clusters.

The resource assignment used in this model assumes a dedicated resource slice for C-V2X, with a further dedicated and distinct bandwidth resource to V2I and V2V links. Our approach to optimizing the use of the V2I bandwidth resource per user link and reducing the cluster backhaul bottleneck is by minimizing the number of V2I user links contending for the resource. Likewise, for maximizing the V2V side-link resource per user link, we approach this by minimizing the maximum cluster size at each clustering instance, building on our V2V resource allocation scheme described in Section II. To do this, a study of the relationship between the number of different vehicle designation (CH, CM and FV) and cluster parameters, such as the number of clusters and cluster distance thresholds needs to be explored.

Our study shows how the number of V2I, and maximum cluster size varies with different cluster radius threshold and different number of clusters. In Figure 3, we present a plot of the average number of V2I users across

different k-values against a varying distance threshold between 300m to 1000m.

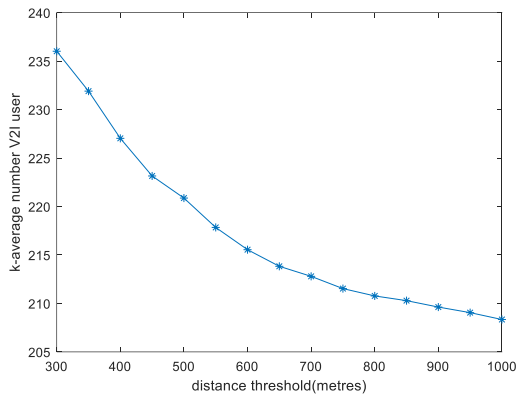


Figure 3. Average Number of V2I User Links across Number of Clusters vs Distance Threshold.

Figure 3 indicates that the number of V2I users drops with increasing distance threshold range being considered, with a total variation of 27 users across threshold range. The minimum number of V2I users is observed at the maximum threshold, implying that this point potentially meets the requirement of minimizing the number of users contending for V2I bandwidth resources.

The plot in Figure 4 shows the variation of average number of V2I users across distance against number of clusters. The number of clusters considered ranges across the total number of vehicles, from 1 to 400. It is observed that at just one cluster, the average number of V2I vehicles across distance threshold is approximately 375, which is essentially the total number of vehicles less the number of CMs in the cluster. This means we have an average of 25 CMs in the first clusters across distance threshold and the total number of free vehicles is around 374, which represents the total number of V2I vehicles less the CH of the single cluster.

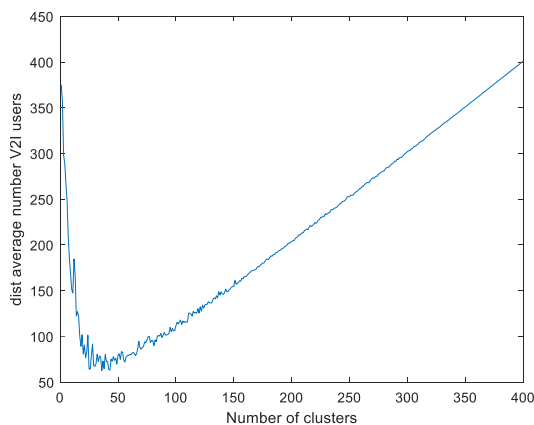


Figure 4. Plot of Average Number of V2I User links Across Distance Threshold Vs Number of Clusters.

However, as the number of clusters increase, the number of V2I vehicles and links drops until a point is reached where a further increase in the number of clusters increases the number of V2I vehicles or links. This points

(number of clusters, number of V2I user links) is reached at approximately (36, 66). From this point onwards there is an almost linear increase in the number of V2I user links with number of clusters, until a point where every individual vehicle is a CH of its own cluster at (400,400).

A 3D-plot showing a comprehensive variation of V2I along distance threshold and number of clusters is presented in Figure 5.

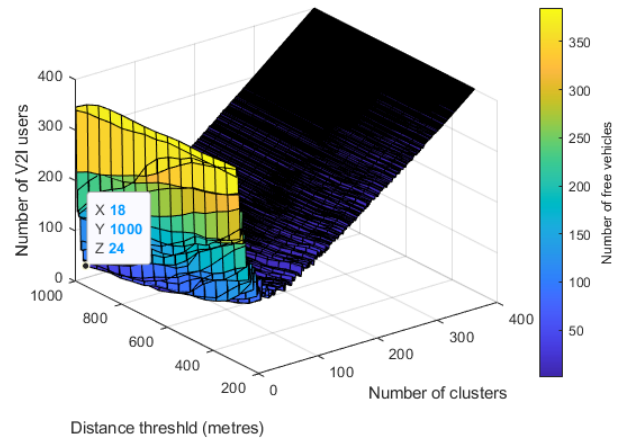


Figure 5. Surface Plot Showing Variation of V2I and FV User Links Across Distance Threshold and Number of Clusters.

It also shows the variation of number of free vehicles links within the number V2I user links. The FV links continues to decrease across increasing number of clusters and increasing distance threshold.

The minimum number of V2I users is obtained at 18 clusters and 1000m of cluster distance threshold. At this point the number of free vehicles, 6 is the total number of V2I user links, 24 less the number of clusters, 18.

For the CH-to-CM V2V side-links, it is understandable that the number of side-links is the total number of vehicles less the CHs and FVs. But one important parameter in the V2V side-link context is the maximum cluster size, which defines the number of side-links or the number of CMs in the most populated cluster. The importance is particularly related to how resource allocation is done in our V2V resource reuse scheme described in Section II. The resources allocated to each CH-to-CM side-link is directly determined by and inversely proportional to maximum cluster size. Figure 6 shows how average maximum cluster size across distance threshold behave in response to changes in the number of clusters. As number of clusters increases, the average maximum cluster size over all distance threshold considered increases, until a specific number of clusters is reached (in this case about 8 clusters). At this point, a further increase in the number of clusters reduces the maximum cluster size achievable until a point where the number of clusters equals the number of nodes in context, at which point cluster size is 1 and at minimum.

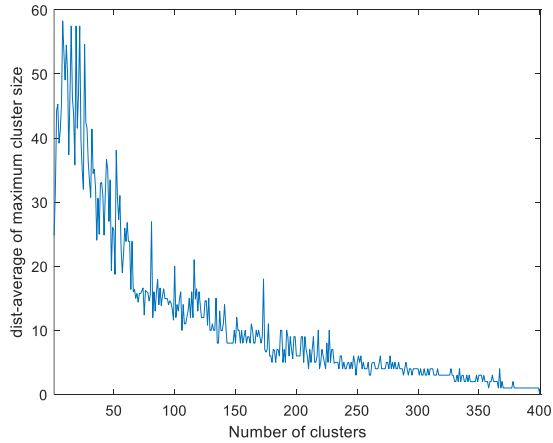


Figure 6. Plot of Average Maximum Cluster Size across Distance Threshold Vs Number of Clusters.

Figure 7, on the other hand, presents the variation of average maximum cluster size across number of clusters against distance threshold.

The plot clearly indicates that the maximum cluster size increases with increasing distance threshold, however compared to the variation across number of clusters, it is observed that the changes in maximum cluster size here is relatively small, with a total variation of less than 3 vehicles as compared to a maximum cluster size variation of approximately 57 vehicles observed in Figure 6.

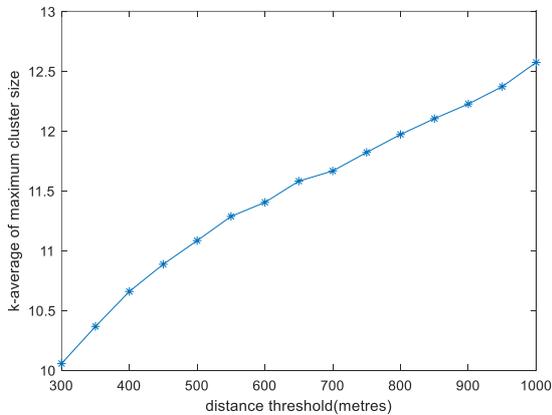


Figure 7. Plot of Average Maximum Cluster Size across Number of Clusters Vs Distance Threshold.

The investigation extends beyond the mere comprehension of the dynamics exhibited by distinct components within vehicular nodes in response to variations in distance thresholds and number of clusters. The outcomes gleaned from this analysis offer valuable indications for the strategic optimization of bandwidth resource utilization and the amelioration of potential bottlenecks in cluster backhaul.

#### IV. PROPOSED OPTIMAL-K PROBLEM

Our aim is to maximize the bandwidth available to both V2I and V2V links and potentially minimize throughput bottleneck along relay transmission path. Unlike traditional

k-selection schemes, we seek to understand the relationship between the k-value, number of unclustered vehicles and how they affect the bandwidth resources at the disposal of V2I and V2V links.

For each number of clusters,  $k_x$  ranging across the entire number of vehicles as described by the set,  $K$  in equation (1), the corresponding centroid positions are evaluated using k-means and k-means++.

$$K = \{k_x: 1 \leq x \leq n\} \quad (1)$$

For each value of  $k_x$ , considering a superset,  $Z$  comprising of a set of Signal-to-Noise Ratio (SNR) values,  $\zeta_t$ . Each set,  $\zeta_t$  comprises of evaluated SNR values between each vehicle  $V_t \in V$  and all centroids,  $i$  as defined in equations (2), (3) and (4) and each cluster has a corresponding cluster head,  $Ch_i$  as in equation (5)

$$Z \supseteq \{\zeta_t: 1 \leq t \leq n\} \quad (2)$$

$$V = \{V_t: 1 \leq t \leq n\} \quad (3)$$

$$\zeta_t = \{\zeta_i: 1 \leq i \leq k_x\} \quad (4)$$

$$C = \{c_i: 1 \leq i \leq k_x\} \quad (5)$$

where  $n$  is number of vehicles,  $V$  is a set of all vehicles,  $k_x$  represents the number of centroids,  $t$  represents the index of specific vehicle and  $i$  is the index of a specific cluster, CH, or centroid.

Also, we consider a set of distance thresholds defining the radius within which clusters are bounded to be  $d_{th}$ , we define a set of SNR threshold,  $SNR_{th}$  as a function of  $d_{th}$  as described in Equation (6). Where the function is based on sidelink pathloss, Received Signal Strength (RSS) and noise.

$$f(d_{th}) \rightarrow \zeta_{th} \quad (6)$$

Having estimated  $\zeta_{th}$ , we associate each vehicle to centroids with which the vehicle has maximum SNR,  $\zeta_t$  and whose  $\zeta_t$  is below the threshold. For every value of  $k_x$  number of centroids, we have cluster identities ranging from 1 to  $k_t$  and mapped to each vehicle and saved as a set of vehicle cluster identity,  $C_L$  as presented in equation (7) with the size of each cluster,  $C_s$  defined in equation (8). The maximum cluster size,  $C_{max}$  is identified and the number of free vehicles,  $F_v$  is evaluated as presented in equations (9) and (10).

$$C_L = \underset{1 \leq t \leq n}{\forall \zeta_t} \left\{ \underset{1 \leq i \leq k_x}{\operatorname{argmax}} (\zeta_t \geq \zeta_{th}, c_i) \right\} \quad (7)$$

$$C_L = \{C_t: 1 \leq t \leq n\}$$

$$C_s = \{C_{s_i}, 1 \leq i \leq k_x: n(c_i \in C_L)\} \quad (8)$$

We then exploit the variation in number of CHs, number of FVs and maximum cluster size,  $C_{max}$  with the distance threshold and number of clusters to maximize the bandwidth available per V2I and V2V link. Both  $C_{max}$  and  $F_v$  are estimated as presented in equations (9) and (10), respectively.

$$C_{max} = \max\{C_s\} \quad (9)$$

$$F_v = n - \sum_{i=1}^{k_x} C_{si} \quad (10)$$

Recalling resource allocation approach, where V2V and V2I links are allocated distinct dedicated frequency band and V2I bands are dedicated and separate from bands used by other BS users, we have decided to approach k-selection in a way that maximizes usage of both V2V and V2I bandwidth resources per link. This approach seeks to keep the bandwidth allocated to V2I and V2V as close as possible with the bandwidth allocated to V2I links greater than the bandwidth allocated to V2V side links. The optimization problem is defined in equations (11) to (17), with the multi-objective functions are presented in equations (11) and (12), while the constraints are presented in equations (14) to (17).

$$\frac{B_{v2i}}{k_x + F_v} + \frac{B_{v2v}}{C_{max}} \text{ Maximize} \quad (11)$$

$$\frac{B_{v2i}}{k_x + F_v} - \frac{B_{v2v}}{C_{max}} \text{ Minimize} \quad (12)$$

The first objective function presented in the optimization expression in (11) seeks to maximize the combined bandwidth per V2I and V2V link, consequently seeking to reach a compromise between the number of V2I links and cluster size. While maximizing the bandwidth per user link, the second objective function presented in the optimization expression in (12) seeks to minimize the difference between V2I and V2V bandwidth per user link. The aim is to prevent excessive skewing of bandwidth towards V2I, which could in turn portend redundant throughput at the backhaul.

We then combine the objective functions to a single super objective function which when maximized, its optimal solution is used to find the maximum combine V2I and V2V bandwidth per user-link. The super objective function is expressed in (13).

$$\frac{B_{v2i}}{k_x + F_v} + \frac{B_{v2v}}{C_{max}} - \left( \frac{B_{v2i}}{k_x + F_v} - \frac{B_{v2v}}{C_{max}} \right) \text{ Maximize} \quad (13)$$

The objective functions are constrained by the conditions expressed in the inequalities between (14) and (17). The first inequality presented in (14) limits the V2V and V2I optimal bandwidth pair to a pair that where V2I bandwidth is greater than V2V bandwidth. The reason for this is to guarantee some performance reliability for CH's V2I links that shoulders relaying responsibility. A performance issue for CH V2I links has a multiplier effect on CMs. The constraint in (15) limits the k-selection solution to a range number of clusters within which the condition that V2V bandwidth per user link can only be as big as V2I link bandwidth per user can be satisfied. This is useful to keep the number of clusters within the range that sustains the proximity advantage defined by traditional k-selection methods. Here, we used a quantitative silhouette-

based elbow method similar to the approach used in [15]. The inequality in (16) and (17) constrains the objective functions to values where  $k_x$  and  $C_{max}$  is greater than 1 and to values where  $B_{v2i}, B_{v2v}, k_{elb}$  and  $F_v$  is non-zero. This is to exclude extremities from solution options.

$$\frac{B_{v2i}}{k_x + F_v} \geq \frac{B_{v2v}}{C_{max}} \quad (14)$$

$$k_{elb} + 2 \geq k_x \geq k_{elb} \quad (15)$$

$$k_x, C_{max} > 1 \quad (16)$$

$$B_{v2i}, B_{v2v}, k_{elb}, F_v > 0 \quad (17)$$

Here,  $B_{v2i}$  is the total bandwidth resource allocated for V2I communication,  $B_{v2v}$  is the total bandwidth resource allocated for V2V communication and  $k_{elb}$  is the optimal k-value as estimated using the quantitative elbow method.

## V. CONCLUSION

This research addresses the critical challenges arising in the V2X communication landscape, particularly within the context of autonomous vehicles. The preliminary findings presented herein underscore the significance of a resource-aware approach to the selection of the number of clusters (k) in vehicular networks. Existing clustering methodologies, while effective, often overlook the presence and impact of unclustered or free vehicles, thus necessitating a more comprehensive analysis.

Through a meticulous investigation of the dynamics within vehicular clusters, considering variations in cluster range (dth) and the number of clusters (k), this study reveals consistent patterns and correlations between the number of vehicular components and the variables. Noteworthy insights have emerged, indicating that within a dedicated resource allocation approach, there exist points across the different variables where V2I and V2V bandwidth can be maximized.

The proposed resource-aware k-selection model, rooted in these findings, holds substantial promise for enhancing the efficiency and performance of V2X communication. By optimizing the utilization of bandwidth resources and mitigating potential bottlenecks, this model contributes to the realization of a seamless and high-throughput vehicular communication network. Future work will delve deeper into the optimization problem presented, refining the model, and validating its efficacy through simulations and real-world implementations. This research seeks to propel advancements in V2X communication, aligning with the transformative potential of autonomous vehicles in reshaping the landscape of transportation efficiency and safety.

## REFERENCES

- [1] G. Liu, N. Qi, J. Chen, C. Dong, and Z. Huang, "Enhancing clustering stability in VANET: A spectral clustering-based approach," *China Communications*, vol. 17, no. 4, pp. 140–151, 2020, doi: 10.23919/JCC.2020.04.013.

- [2] M. A. Saleem *et al.*, "Expansion of Cluster Head Stability Using Fuzzy in Cognitive Radio CR-VANET," *IEEE Access*, vol. 7, pp. 173185–173195, 2019, doi: 10.1109/ACCESS.2019.2956478.
- [3] M. Alowish, Y. Shiraishi, Y. Takano, M. Mohri, and M. Morii, "Stabilized Clustering Enabled V2V Communication in an NDN-SDVN Environment for Content Retrieval," *IEEE Access*, vol. 8, pp. 135138–135151, 2020, doi: 10.1109/ACCESS.2020.3010881.
- [4] K. Abboud and W. Zhuang, "Stochastic modeling of single-hop cluster stability in vehicular ad hoc networks," *IEEE Trans Veh Technol*, vol. 65, no. 1, pp. 226–240, Jan. 2016, doi: 10.1109/TVT.2015.2396298.
- [5] Z. Khan and P. Fan, "A multi-hop moving zone (MMZ) clustering scheme based on cellular-V2X," *China Communications*, vol. 15, no. 7, pp. 55–66, Jul. 2018, doi: 10.1109/CC.2018.8424603.
- [6] K. Sehla, T. Mai, T. T. M. T. Nguyen, G. Pujolle, and P. B. Velloso, "A New Clustering-based Radio Resource Allocation Scheme for C-V2X," *IFIP Wireless Days*, vol. 2021-June 2021, doi: 10.1109/WD52248.2021.9508289.
- [7] J. Zhao *et al.*, "Cluster-based resource selection scheme for 5G V2X," *IEEE Vehicular Technology Conference*, vol. 2019-April, pp. 5–9, 2019, doi: 10.1109/VTCSpring.2019.8746637.
- [8] X. Wang and Y. Xu, "An improved index for clustering validation based on Silhouette index and Calinski-Harabasz index," *IOP Conf Ser Mater Sci Eng*, vol. 569, no. 5, p. 052024, Jul. 2019, doi: 10.1088/1757-899X/569/5/052024.
- [9] J. Xiao, J. Lu, and X. Li, "Davies Bouldin Index based hierarchical initialization K-means," *Intelligent Data Analysis*, vol. 21, no. 6, pp. 1327–1338, Jan. 2017, doi: 10.3233/IDA-163129.
- [10] C. Yuan and H. Yang, "Research on K-Value Selection Method of K-Means Clustering Algorithm," *J 2019, Vol. 2, Pages 226-235*, vol. 2, no. 2, pp. 226–235, Jun. 2019, doi: 10.3390/J2020016.
- [11] N. Kaoungku, K. Suksut, R. Chanklan, K. Kerdprasop, and N. Kerdprasop, "The silhouette width criterion for clustering and association mining to select image features," *Int J Mach Learn Comput*, vol. 8, no. 1, pp. 69–73, Feb. 2018, doi: 10.18178/IJMLC.2018.8.1.665.
- [12] T. Robert, W. Guenther, and H. Trevor, "Estimating the number of clusters in a data set via gap statistics," *Journal of the Royal Statistical Society. Series B*, vol. 63, no. 2, pp. 411–423, 2001, Accessed: Feb. 20, 2024. [Online]. Available: <https://hastie.su.domains/Papers/gap.pdf>
- [13] ETSI Technical Committee Intelligent Transport Systems (ITS), "Intelligent Transport Systems (ITS) Access Layer; Part 1: Channel Models for the 5,9 GHz frequency band," Sophia Antipolis Cedex, 2020. [Online]. Available: [https://www.etsi.org/deliver/etsi\\_tr/103200\\_103299/10325701/01.01.01\\_60/tr\\_10325701v010101p.pdf](https://www.etsi.org/deliver/etsi_tr/103200_103299/10325701/01.01.01_60/tr_10325701v010101p.pdf)
- [14] TSGR, "TR 138 901 - V14.3.0 - 5G; Study on channel model for frequencies from 0.5 to 100 GHz (3GPP TR 38.901 version 14.3.0 Release 14)," 2018. [Online]. Available: <https://portal.etsi.org/TB/ETSIDeliverableStatus.aspx>
- [15] C. Shi, B. Wei, S. Wei, W. Wang, H. Liu, and J. Liu, "A quantitative discriminant method of elbow point for the optimal number of clusters in clustering algorithm," *EURASIP J Wirel Commun Netw*, vol. 2021, no. 1, pp. 1–16, Dec. 2021, doi: 10.1186/S13638-021-01910-W/FIGURES/6.

# Autonomous Platooning of General Connected Vehicles Using Bayesian Receding Horizon Control

Gilchrist Johnson  
*VICTOR Lab*  
 University of Virginia  
 Charlottesville, VA, USA  
 email: gilchristjohnson@virginia.edu

Tomonari Furukawa  
*VICTOR Lab*  
 University of Virginia  
 Charlottesville, VA, USA  
 email: tomonari@virginia.edu

B. Brian Park  
*Link Lab*  
 University of Virginia  
 Charlottesville, VA, USA  
 email: bp6v@virginia.edu

**Abstract**—This paper focuses on futuristic connected vehicles and presents a strategy for autonomous platooning of general connected vehicles including low-speed utility vehicles, which drive over various terrains, not limited to roads. In such general environments, the goal of a following vehicle is to keep following its preceding vehicle with minimum distance and without collision. Since the vehicles are connected, the following vehicle in the proposed strategy receives the controls of its immediate preceding vehicle through communications and predicts a future pose of the preceding vehicle in a receding horizon. Further, the prediction incorporates the inertial motion and is probabilistically executed in the framework of Recursive Bayesian Estimation by fusing the two distributions predicted by a particle filter through Gaussian approximation. The performance of the proposed strategy was investigated using simulated golf carts with a drive-by-wire system. The proposed strategy has been found to improve the accuracy of the conventional following by 30.4%.

**Index Terms**—autonomous following; connected vehicles; recursive bayesian estimation; receding horizon control.

## I. INTRODUCTION

The last two decades have seen the dramatic advancement of vehicle autonomy including autonomous platooning, which allows a sequence of vehicles to drive autonomously. While the leader vehicle may also be automated, the first interest of autonomous platooning results in autonomously navigating a follower vehicle such that it keeps a targeted distance from its preceding vehicle during the entire navigation. Autonomous following has become the primary concern of autonomous platooning.

Past work on autonomous vehicles can be primarily studied in two applications. With society's interest, recent efforts have been most exerted on autonomous driving where vehicles are expected to be driven with a minimum or target distance to minimize traffic congestion while avoiding collision [1]. Since roads are structured well having planar surfaces with various marks and signs, such as lanes, the majority of the work was conducted on the detection and localization of such objects and autonomous following in the reduced free space [2]. Because vehicles on public roads are not connected to each other, follower vehicles determine their final control actions based on what they can observe using their sensors.

The second application is often known in the name of multi-robot cooperation. Formation control is a synchronous approach where all the robots including the leader are controlled to maintain the pre-designed formation [3][4]. This is not the

approach of interest in this paper since the paper is concerned with the autonomous control of a following vehicle only. The other popular approach is the leader-follower approach where each of the follower robots sequentially and independently determines its path after the path of the leader is given [5]–[7], which is along with the interest of this paper and has been widely studied. Some early work planned a path to pass through waypoints whereas trajectories specifying states in full-led follower robots subject to dynamic behavior more accurately [8]. Extended work includes that of [9] which developed a collision avoidance strategy for environments with obstacles that do not allow the maintenance of the pre-designed formation. Communication between the leader robot and a follower robot was proposed by [10] to transmit the follower's path computed by the leader after the leader redesigned its path for obstacle avoidance. The technique works well if the leader robot is autonomous. However, the full autonomy of the leader robot in the real world is still unrealistic, so autonomous following should be developed for manually operated leader vehicles.

This paper presents a strategy for autonomous following of general connected vehicles including low-speed utility vehicles. The proposed technique does not rely on traffic marks and signs to drive over various terrains and enhances its autonomous following capability by using vehicle connectivity; the following vehicle receives the controls of its immediate preceding vehicle through communications and predicts a future pose of the preceding vehicle in a receding horizon. Further, the prediction incorporates the inertial motion and is probabilistically executed in the framework of Recursive Bayesian Estimation (RBE) by fusing the two distributions predicted by a Particle Filter (PF) through Gaussian approximation.

The paper is organized as follows. The next section describes the mathematical foundation of the leader vehicle estimation problem and two conventional techniques to achieve autonomous following. Section III presents the technique which is proposed to enhance autonomous following leveraging vehicle connection. Experimental studies are conducted in Section IV, and conclusions and future work are summarized in the final section.

## II. RECURSIVE BAYESIAN ESTIMATION

### A. Leader and Follower Vehicle Models

Consider a leader vehicle  $l$  with its unknown global state given by  $\mathbf{x}^l \in \mathcal{X}^l$ , the motion of which is generically modeled by

$$\mathbf{x}_k^l = \mathbf{f}^l(\mathbf{x}_{k-1}^l, \mathbf{w}_k^l), \quad (1)$$

where  $\mathbf{w}_k^l$  is a motion noise. This leader vehicle is observed by an autonomous follower vehicle  $f$ , the global state of which is evolved with the motion model

$$\mathbf{x}_k^f = \mathbf{f}^f(\mathbf{x}_{k-1}^f, \mathbf{u}_k^f, \mathbf{w}_k^f), \quad (2)$$

where  $\mathbf{x}_k^f \in \mathcal{X}^f$  and  $\mathbf{u}_k^f \in \mathcal{U}^f$  represent the state and control input of the follower vehicle, respectively, and  $\mathbf{w}_k^f \in \mathcal{W}^f$  is the motion noise of the follower vehicle.

The follower vehicle will be equipped with various sensors including those for self-localization and those for observation of targets of interest and environments. To focus on autonomous following, the pose of the follower vehicle is assumed to be known exactly, so only the model of the sensor for leader vehicle localization is thus formulated:

$${}^f\mathbf{z}_k^l = {}^f\mathbf{h}^l(\mathbf{x}_k^l, \mathbf{x}_k^f, {}^f\mathbf{v}_k^l) \quad (3)$$

where  ${}^f\mathbf{z}_k^l$  is the observation of the leader vehicle by the sensor on the follower vehicle, and  ${}^f\mathbf{v}_k^l$  represents the observation noise [13].

### B. Recursive Bayesian Estimation

In the context of autonomous following, the RBE generically estimates belief on the leader vehicle in the global coordinate frame. This is done by representing the belief in terms of a Probability Density Function (PDF) and recursively updating it through prediction and correction. Let us consider a generic scenario where a sequence of observations of the leader vehicle by the follower vehicle is given by  ${}^f\tilde{\mathbf{z}}_{1:k}^l \equiv \{{}^f\tilde{\mathbf{z}}_{\kappa}^l | \forall \kappa \in \{1, \dots, k\}\}$ . Note here that  $(\cdot)$  represents an instance of variable  $(\cdot)$ . Given the initial belief  $p(\mathbf{x}_0^l)$  and the sequence of observations  ${}^f\tilde{\mathbf{z}}_{1:k}^l$ , the lead vehicle belief at time step  $k$ ,  $p(\mathbf{x}_k^l | {}^f\tilde{\mathbf{z}}_{1:k}^l, \tilde{\mathbf{x}}_{1:k}^f)$ , is updated as follows:

**Prediction:** Computes the follower vehicle belief at  $k$   $p(\mathbf{x}_k^l | {}^f\tilde{\mathbf{z}}_{1:k-1}^l, \tilde{\mathbf{x}}_{1:k-1}^f)$  from the belief updated at  $k-1$   $p(\mathbf{x}_{k-1}^l | {}^f\tilde{\mathbf{z}}_{1:k-1}^l, \tilde{\mathbf{x}}_{1:k-1}^f)$ . The prediction is carried out by Chapman-Kolmogorov equation:

$$p(\mathbf{x}_k^l | {}^f\tilde{\mathbf{z}}_{1:k-1}^l, \tilde{\mathbf{x}}_{1:k-1}^f) = \int_{\mathcal{X}^l} p(\mathbf{x}_k^l | \mathbf{x}_{k-1}^l) p(\mathbf{x}_{k-1}^l | {}^f\tilde{\mathbf{z}}_{1:k-1}^l, \tilde{\mathbf{x}}_{1:k-1}^f) d\mathbf{x}_{k-1}^l, \quad (4)$$

where  $p(\mathbf{x}_k^l | \mathbf{x}_{k-1}^l)$  is a Markov motion model defined by (1).

**Correction:** Computes the robot and target belief  $p(\mathbf{x}_k^l | {}^s\tilde{\mathbf{z}}_{1:k}^l, \tilde{\mathbf{x}}_{1:k}^f)$  given the predicted belief  $p(\mathbf{x}_k^l | {}^f\tilde{\mathbf{z}}_{1:k-1}^l, \tilde{\mathbf{x}}_{1:k-1}^f)$  and the new observation  ${}^f\tilde{\mathbf{z}}_k^l$  at the new state  $\tilde{\mathbf{x}}_k^f$ . The equation is derived by applying formulas

for marginal distribution and conditional independence and given by

$$p(\mathbf{x}_k^l | {}^f\tilde{\mathbf{z}}_{1:k}^l, \tilde{\mathbf{x}}_{1:k}^f) = \frac{l(\mathbf{x}_k^l | {}^f\tilde{\mathbf{z}}_k^l, \tilde{\mathbf{x}}_k^f) p(\mathbf{x}_k^l | {}^f\tilde{\mathbf{z}}_{1:k-1}^l, \tilde{\mathbf{x}}_{1:k-1}^f)}{\int_{\mathcal{X}^l} l(\mathbf{x}_k^l | {}^f\tilde{\mathbf{z}}_k^l, \tilde{\mathbf{x}}_k^f) p(\mathbf{x}_k^l | {}^f\tilde{\mathbf{z}}_{1:k-1}^l, \tilde{\mathbf{x}}_{1:k-1}^f) d\mathbf{x}_k^l}, \quad (5)$$

where  $l(\mathbf{x}_k^l | {}^f\tilde{\mathbf{z}}_k^l, \tilde{\mathbf{x}}_k^f)$  represents the likelihood of  $\mathbf{x}_k^l$  given observation  ${}^f\tilde{\mathbf{z}}_k^l$ .

There are two approaches that have been commonly used for the autonomous control of the follower vehicle. The inexpensive approach is observation based and determines the next control of the follower vehicle  $\mathbf{u}_{k+1}^f$  using the latest observation  ${}^f\tilde{\mathbf{z}}_k^l$  and the current state  $\tilde{\mathbf{x}}_k^f$ ; the control  $\mathbf{u}_{k+1}^f$  is found such that the belief resembles the observation likelihood:

$$J\left(l(\mathbf{x}_k^l | {}^f\tilde{\mathbf{z}}_k^l, \tilde{\mathbf{x}}_k^f)\right) = \left\| \mathbf{g}\left(l(\mathbf{x}_k^l | {}^f\tilde{\mathbf{z}}_k^l, \tilde{\mathbf{x}}_k^f)\right) - \left(\mathbf{x}_{k+1}^f + \mathbf{d}_k\right) \right\|_2 \rightarrow \min_{\mathbf{u}_{k+1}^f} \quad (6)$$

where

$$\mathbf{x}_{k+1}^f = \mathbf{f}^f(\tilde{\mathbf{x}}_k^f, \mathbf{u}_{k+1}^f, \tilde{\mathbf{w}}_{k+1}^f), \quad (7)$$

$\mathbf{g}(\cdot)$  returns the centroid of the likelihood, and  $\mathbf{d}_k$  is the desired gap of the follower vehicle to the leader vehicle.  $\|\cdot\|$  is an  $L^2$  norm.

The more intelligent approach identifies a sequence of  $n_c$  controls,  $\mathbf{u}_{k+1:k+n_c}^f$ , by predicting the belief recursively up to the  $(k+n_c)$ -th time step in the framework of receding horizon control (RHC):

$$J\left(p(\mathbf{x}_{k+n_c}^l | {}^f\tilde{\mathbf{z}}_{1:k}^l, \tilde{\mathbf{x}}_{1:k}^f)\right) = \left\| \mathbf{g}\left(p(\mathbf{x}_{k+n_c}^l | {}^f\tilde{\mathbf{z}}_{1:k}^l, \tilde{\mathbf{x}}_{1:k}^f)\right) - \left(\tilde{\mathbf{x}}_{k+n_c}^f + \mathbf{d}_k\right) \right\|_2 \rightarrow \min_{\mathbf{u}_{k+1:k+n_c}^f} \quad (8)$$

where

$$p(\mathbf{x}_{k+\kappa}^l | {}^f\tilde{\mathbf{z}}_{1:k}^l, \tilde{\mathbf{x}}_{1:k}^f) = \int_{\mathcal{X}^l} p(\mathbf{x}_{k+\kappa}^l | \mathbf{x}_{k+\kappa-1}^l) p(\mathbf{x}_{k+\kappa-1}^l | {}^f\tilde{\mathbf{z}}_{1:k}^l, \tilde{\mathbf{x}}_{1:k}^f) d\mathbf{x}_{k+\kappa-1}^l, \quad (9a)$$

$$\mathbf{x}_{k+\kappa}^f = \mathbf{f}^f(\tilde{\mathbf{x}}_{k+\kappa-1}^f, \mathbf{u}_{k+\kappa}^f, \tilde{\mathbf{w}}_{k+\kappa}^f) \quad (9b) \\ \forall \kappa \in \{1, \dots, n_c\}$$

It is to be noted that (8) may be represented with an integral payoff instead of the terminal payoff.

Both approaches work well if the leader vehicle has a predictable motion and moves within the range the follower vehicle can track. However, the motion of the leader vehicle is, precisely, given not by (1) but by

$$\mathbf{x}_k^l = \mathbf{f}^l(\mathbf{x}_{k-1}^l, \mathbf{u}_k^l, \mathbf{w}_k^l), \quad (10)$$

where the control of the leader vehicle,  $\mathbf{u}_k^l$ , significantly affects its motion in addition to the motion noise  $\mathbf{w}_k^l$ . If the intention

of the leader vehicle,  $\mathbf{u}_{k+1:k+n_c}^l$ , is beyond the expectation, the follower vehicle may not be able to track the leader vehicle successfully. The number of steps to look ahead  $n_c$ , as a consequence, cannot be large, which results in unstable controls.

### III. AUTONOMOUS PLATOONING

#### A. Overview

Figure 1 illustrates the proposed technique for autonomous platooning. The technique is built on conventional methods but incorporates novel leader intention prediction, which was originally proposed by the authors for robotic escorting [11][12]. The following vehicle estimates the current pose of the leader vehicle  $\mathbf{x}_k^l$  and predicts its future pose  $\mathbf{x}_{k+n_p}^{l,\alpha}$  from the current pose using the RBE as the conventional following does. Here, the superscript  $\alpha$  indicates the conventional following whereas  $n_p$  indicates the number of steps to look ahead by the proposed technique. However, the future pose of the leader vehicle in the proposed technique is additionally predicted as  $\mathbf{x}_{k+n_p}^{l,\beta}$  using the current leader vehicle data transmitted through connection to the follower vehicle including the steering angle and the vehicle speed, which cannot be observed well. Here, the superscript  $\beta$  indicates the prediction using the leader vehicle's control. The proposed technique then fuses the two predictions and determines future controls  $\mathbf{u}_{k+1:k+n_p}^f$  using the RHC. Prediction using the vehicle control data is an additional effective source for follower control because the current control is often the intention of the leader vehicle in a longer time horizon. The number of steps to look ahead by the proposed technique,  $n_p$ , is thus larger than that of the conventional technique  $n_c$ , and the prediction by the proposed technique is also expected to be more accurate. The follower vehicle, thus, can potentially achieve more smooth and successful platooning even in noisier environments.

#### B. Prediction Using Particle Filter

The steering angle of the leader vehicle cannot be observed from the follower vehicle whereas the speed of the leader vehicle cannot be accurately measured from the follower vehicle due to the dynamic relative motion. Since it receives the precise steering angle and vehicle speed through connection,  $\tilde{\mathbf{u}}_k^l$ , the follower vehicle can identify what the leader vehicle intends to do. Let the intended control that may be used up to the time step  $k + n_p$  be  $\mathbf{u}_{k \rightarrow n_p}^l \sim \mathcal{N}(\tilde{\mathbf{u}}_k^l, \Sigma_k^{l,u})$ . Using the PF, the pose of the leader vehicle can be then predicted by leveraging the intention as

$$\mathbf{x}_{k+\kappa,i}^\beta = \mathbf{f}^\beta \left( \mathbf{x}_{k+\kappa-1}^{\beta,i}, \mathbf{u}_{k \rightarrow n_p}^{\beta,i}, \mathbf{w}_k^{\beta,i} \right), \quad \forall \kappa \in [1, \dots, n_p], \forall i \in [1, \dots, N], \quad (11)$$

where  $\mathbf{w}_k^{\beta,i} \sim \mathcal{N}(\bar{\mathbf{w}}_k^\alpha, \Sigma_k^{\beta,w})$ , and  $N$  is the number of particles.

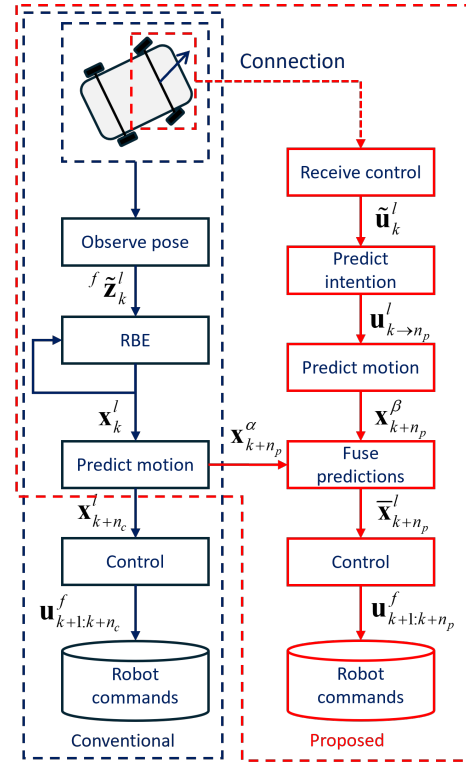


Figure 1. Conventional platooning vs. proposed platooning.

The pose can also be predicted using the motion model without the control as

$$\mathbf{x}_{k+\kappa+1}^{\alpha,i} = \mathbf{f}^\alpha \left( \mathbf{x}_{k+\kappa}^{\alpha,i}, \mathbf{w}_k^{\alpha,i} \right), \quad \forall \kappa \in [1, \dots, n_p], \forall i \in [1, \dots, N], \quad (12)$$

where  $\mathbf{w}_k^{\alpha,i} \sim \mathcal{N}(\bar{\mathbf{w}}_k^\alpha, \Sigma_k^{\alpha,w})$ . Note that the PF is used in the proposed technique because the motion model is non-Gaussian; the particles of both predictions will be spread in a non-Gaussian manner in the state space due to the nonlinearity of the motion models. Clearly, prediction with control is more accurate if the current control lasts long in the future whereas prediction with the current pose and without control is more accurate if the current control is given transitionally. The level of confidence of the predictions is determined by  $\Sigma_k^{\alpha,w}$ ,  $\Sigma_k^{\beta,w}$  and  $\Sigma_k^{l,u}$ . While  $\Sigma_k^{\alpha,w}$  in the model without control modeling is much larger than  $\Sigma_k^{\beta,w}$ , the control uncertainty  $\Sigma_k^{l,u}$ , which is added to  $\mathbf{f}^\beta$ , becomes the factor to determine which prediction is more certain.

#### C. Receding Horizon Control Based on the Hybrid Prediction

Once they have been spread over the state space, the two sets of particles must be fused to ultimately determine the control action. The proposed approach uniquely approximates each distribution as a Gaussian distribution. This approximation is valid since random noise dominates the distribution over time.

By definition, the mean and the covariance of each distribution is calculated as

$$\bar{\mathbf{x}}_{k+n_p}^{(\cdot)} = \frac{1}{N} \sum_{i=1}^N \mathbf{x}_{k+n_p}^{(\cdot),i} \quad (13a)$$

$$\Sigma_{k+n_p}^{(\cdot)} = \frac{1}{N} \sum_{i=1}^N \left( \mathbf{x}_{k+n_p}^{(\cdot),i} - \bar{\mathbf{x}}_{k+n_p}^{(\cdot)} \right) \left( \mathbf{x}_{k+n_p}^{(\cdot),i} - \bar{\mathbf{x}}_{k+n_p}^{(\cdot)} \right)^\top \quad (13b)$$

where  $(\cdot)$  is prediction without control  $\alpha$  or prediction with control  $\beta$ , and  $\top$  represents the transpose of the matrix. The mean of the probability distribution combining the two distributions can be then derived through the multiplication:

$$\bar{\mathbf{x}}_{k+n_p}^l = \frac{\Sigma_{k+n_p}^\beta}{\Sigma_{k+n_p}^\alpha + \Sigma_{k+n_p}^\beta} \bar{\mathbf{x}}_{k+n_p}^\alpha + \frac{\Sigma_{k+n_p}^\alpha}{\Sigma_{k+n_p}^\alpha + \Sigma_{k+n_p}^\beta} \bar{\mathbf{x}}_{k+n_p}^\beta. \quad (14)$$

Now that the target pose of the leader vehicle in the  $n_p$  step lookaheads is identified, the RHC determines a sequence of control actions of the follower vehicle by minimizing the objective function:

$$J \left( \bar{\mathbf{x}}_{k+n_p}^l \right) = \left\| \bar{\mathbf{x}}_{k+n_p}^l - \left( \mathbf{x}_{k+n_p}^f + \mathbf{d}_k \right) \right\|_2 \rightarrow \min_{\mathbf{u}_{k+1:k+n_p}^f} \quad (15)$$

where

$$\mathbf{x}_{k+\kappa}^f = \mathbf{f}^f \left( \mathbf{x}_{k+\kappa-1}^f, \mathbf{u}_{k+\kappa}^f, \tilde{\mathbf{w}}_{k+\kappa}^f \right), \quad \forall \kappa \in \{1, \dots, n_p\}. \quad (16)$$

#### IV. EXPERIMENTAL RESULTS

##### A. Experimental Settings

The proposed technique was evaluated using two golf carts in a simulated environment, which are available to the authors for real-world demonstration in the future. Each cart has a full set of components for autonomous platooning including a communication module for vehicle connection, a stereo camera for relative pose measurement, a GPS and IMU for global positioning, and a drive-by-wire system for computer-controlled actuation. The simulated carts used the same components. Figure 2(a) shows the real cart whereas their simulated version is shown in Figure 2(b). In order to validate the efficacy of the proposed platooning technique over conventional techniques, the two conventional techniques described in Section II were also used for autonomous platooning. One was observation based with no prediction and connection, and the other was with prediction but without connection. Since the aim of the experimental analysis is the proof-of-concept, the motion models of the leader cart and the follower cart were for the two-dimensional space and given by

$$x_k^{(\cdot)} = v_k^{(\cdot)} \cos \theta_k^{(\cdot)} \quad (17a)$$

$$y_k^{(\cdot)} = v_k^{(\cdot)} \sin \theta_k^{(\cdot)} \quad (17b)$$

$$\theta_k^{(\cdot)} = \frac{v_k^{(\cdot)}}{L} \tan \gamma_k^{(\cdot)}, \quad (17c)$$



(a) Golf cart.



(b) Simulated golf cart.

Figure 2. Physical vs. simulated systems.

where  $\mathbf{x}_k^{(\cdot)} = [x_k^{(\cdot)}, y_k^{(\cdot)}, \theta_k^{(\cdot)}]^\top$  is the set of state variables, and  $\mathbf{u}_k^{(\cdot)} = [v_k^{(\cdot)}, \gamma_k^{(\cdot)}]^\top$  is the set of control variables.  $(\cdot)$  is  $l$  or  $f$ . For the leader cart model with no control information, the motion model with the controls of the average observed speed  $\bar{v}_k^l$  and 0 steering angle was used since it is valid to assume that the cart moves straight with the current orientation. The relative difference  $\mathbf{d}_k = [d_{x,k}, d_{y,k}, d_{\theta,k}]^\top$  places the follower cart behind the leader cart in the same orientation:

$$d_{x,k} = d \cos \theta_k^l \quad (18a)$$

$$d_{y,k} = d \sin \theta_k^l \quad (18b)$$

$$d_{\theta,k} = 0, \quad (18c)$$

where  $d$  is the targeted distance. In the numerical simulation, the leader cart was programmed to drive a winding path since the proposed technique is effective when the cart is turning. Table I lists the parameters used in the experiment.

TABLE I  
PARAMETERS FOR EXPERIMENT

Parameter	Value
$L$	1.2 [m]
$\bar{v}_k^l$	8.5 [m/s]
$d$	4 [m]
$\Sigma_k^{l,u}$	[0.1, 0, 0, 0.087] [m,m,m]
$\tilde{\mathbf{w}}_k^\alpha$	[0.5, 0.5] [m,m]
$\Sigma_k^{\alpha,w}$	[0.05, 0, 0, 0.017] [m,m,m,m]
$\tilde{\mathbf{w}}_k^\beta$	[0.5, 0.5] [m,m]
$\Sigma_k^{\beta,w}$	[0.5, 0, 0, 0.087] [m,m,m,m]
$N$	1000

##### B. Results

Figure 3 shows the results of the proposed platooning technique compared to those of the two conventional techniques. Figure 3(a) first shows the paths of the follower cart by the proposed and the conventional techniques in addition to those of the leader cart and the ideal follower cart. The path of the ideal follower cart  $\mathbf{x}_k^{\text{ideal}}$ , given that of the leader cart  $\mathbf{x}_k^l$  is given by

$$\mathbf{x}_k^{\text{ideal}} = \mathbf{x}_k^l - \mathbf{d}_k. \quad (19)$$

The closer the path to that of the ideal follower cart, the better the path. It is seen that the path of the proposed technique is significantly better than that of the conventional techniques. The observation based technique with neither prediction nor connection is shown to have the worst path partly because the control of the leader cart is not observable and partly because this limited observation is the only source of information to determine the control of the follower cart; if the observation is noisy, the control fluctuates according to the noisy observation and thus becomes inaccurate. The prediction based technique with no connection performs better but is still inefficient when compared to the proposed technique. This is due to the lack of information on the control of the leader cart, which makes the prediction of the future pose of the leader cart more accurate. Figure 3(b) shows the error in the orientation of the follower cart with respect to the ideal orientation. The superiority of the proposed technique to the conventional techniques can also be seen in this result since the configuration of the orientation with the proposed technique captures that of the leader cart most.

Figure 3(c) lastly shows the positional error. The positional error is defined by

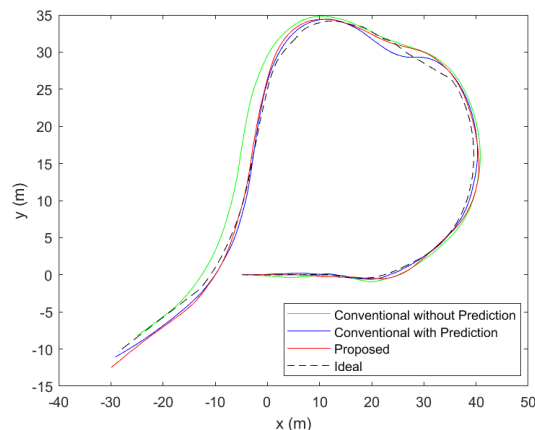
$$E_k^{(\cdot)} = \left\| \mathbf{x}_k^{\text{ideal}} - \bar{\mathbf{x}}_k^f \right\|_2 \quad (20)$$

It is seen that the proposed technique yields the minimum positional errors constantly, which is the result of the prediction using information through vehicle connectivity. The mean positional error of the proposed technique is 3.7% whereas that of the conventional observation and prediction techniques are 8.0% and 5.3%, respectively. The error of the proposed technique is particularly small around 10 seconds when the cart is turning maximally. This is because the technique used information on the turning. The result conclusively shows that the proposed technique has improved the accuracy of the conventional techniques by 30.4%.

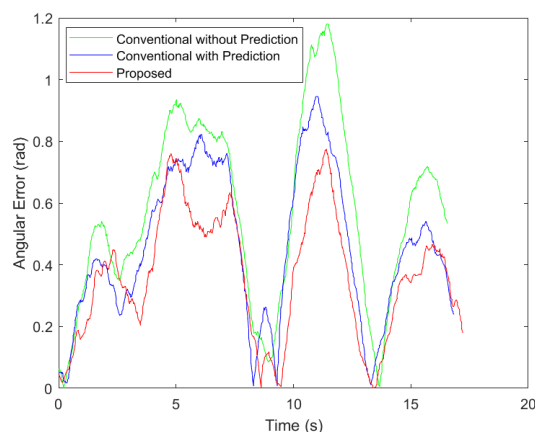
## V. CONCLUSION AND FUTURE WORK

This paper has presented a strategy for autonomous following of general connected vehicles. In the proposed strategy, the following vehicle receives the controls of its immediate preceding vehicle through communications and predicts a future pose of the preceding vehicle using the PF and the Gaussian fusion. The autonomous control of the follower vehicle is finally determined through the RHC. The performance of the proposed strategy was investigated using simulated golf carts with a drive-by-wire system. The results show that the proposed strategy improved the accuracy by 30.4%, and it was particularly effective when the leader cart was turning sharply.

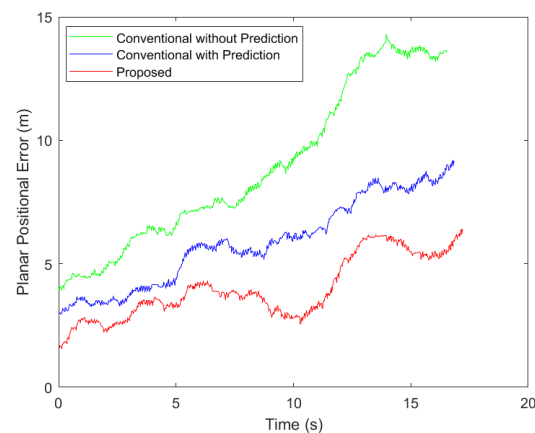
The paper shows only the preliminary results and much future work is possible. Ongoing work includes experimental validation using the real golf carts, modeling of uncertainties and the effect, and the reduction of communication delay. Communication delay weakens the effect of the proposed technique, so minimizing it is an essential task to complete.



(a) Vehicle path.



(b) Angular root mean squared error.



(c) Planar position error.

Figure 3. Simulation results.

## ACKNOWLEDGMENT

This work is sponsored by the US Office of Naval Research (N00014-23-1-2572). The authors would like to express their sincere gratitude to Dr. Tom McKenna at the Office of Naval Research for his invaluable support and advice. Special thanks

also go to Mr. Dean Conte at Mitre Corporation who developed the base technique of this paper during his graduate study.

#### REFERENCES

- [1] D. Milakis, B. van Arem, and B. van Wee, "Policy and society related implications of automated driving: a review of literature and directions for future research," *J. Intel. Transp. Sys.*, vol. 21, no. 4, pp. 324-348, 2017.
- [2] A. AM. Assidiq, O. O. Khalifa, M. R. Islam, and S. Khan, "Real time lane detection for autonomous vehicles," *Int. Conf. Comp. Comm. Eng.*, Kuala Lumpur, pp. 82-88, 2008.
- [3] A. Loria, J. Dasedemir, and N. A. Jarquin, "Leader-follower formation and tracking control of mobile robots along straight paths," *IEEE Trans. Cont. Sys. Tech.*, vol. 24, no. 2, pp. 727-732, 2016.
- [4] M. M. Alam, M. Y. Arafat, S. Mah, and J. Shen, "Topology control algorithms in multi-unmanned aerial vehicle networks: an extensive survey," *J. Network. Comp. Appl.*, vol. 207, 103476, 2022.
- [5] T. Fukao, H. Nakagawa, and N. Adachi, "Adaptive tracking control of a nonholonomic mobile robot," *IEEE Trans. Rob. Auto.*, vol. 16, no. 5, pp. 609-615, 2000.
- [6] B. Madhevan, and M. Sreekumar, "Tracking algorithm using leader follower approach for multi robots," *Proc. Eng.*, vol. 64, pp. 1426-1435, 2013.
- [7] M. Bujarbaruah, Y. R. Sturz, C. Holda, K. H. Johansson, and F. Borrelli, "Learning environment constraints in collaborative robotics: a decentralized leader-follower approach," 2012 IEEE/RSJ Int. Conf. Intel. Rob. Sys., Prague, 2021.
- [8] A. Gasparetto, P. Boscariol, A. Lanzutti, and R. Vidoni, "Path planning and trajectory planning algorithms: a general overview," *Motion and Operation Planning of Robotic Systems*, pp. 3-27, 2015.
- [9] T. Bhavana, M. Nithya, and M. Rajesh, "Leader-follower co-ordination of multiple robots with obstacle avoidance," 2017 Int. Conf. Smart. Tech. Smart Nation, August 2017.
- [10] X. Wu, S. Wang, and M. Xing, "Observer-based leader-following formation control for multi-robot with obstacle avoidance," *IEEE Access*, vol. 7, pp. 14791-14798, 2018.
- [11] D. Conte and T. Furukawa, "Autonomous robotic escort incorporating motion prediction and human intention," 2021 IEEE Int. Conf. Rob. Auto., Xi'an, 2021.
- [12] D. Conte and T. Furukawa, "Autonomous Bayesian escorting of a human integrating intention and obstacle avoidance," *J. Field Rob.*, vol. 39, pp. 679-693, 2022.
- [13] T. Furukawa, F. Bougault, B. Lavis, and H. F. Durrant-Whyte, "Recursive Bayesian search-and-tracking using coordinated UAVs for lost targets," 2006 Int. Conf. Rob. Auto., pp. 2521-2526, 2006

# The Smart Highway to Babel: the Coexistence of Different Generations of Intelligent Transport Systems

Oscar Amador

*School of Information Technology  
Halmstad University  
Halmstad, Sweden  
email: oscar.molina@hh.se*

María Calderón

*Departamento de Ingeniería de Sistemas Telemáticos  
ETSI Telecomunicación  
Universidad Politécnica de Madrid  
Madrid, Spain  
email: maria.calderon@upm.es*

Ignacio Soto

*Departamento de Ingeniería de Sistemas Telemáticos  
ETSI Telecomunicación  
Universidad Politécnica de Madrid  
Madrid, Spain  
email: ignacio.soto@upm.es*

Manuel Uruña

*Escuela Superior de Ingenieros y Tecnología  
Universidad Internacional de la Rioja  
Logroño, Spain  
email: manuel.uruena@unir.net*

**Abstract**—The gap between technology readiness level in Cooperative Intelligent Transport Systems (C-ITS) and its adoption and deployment has caused a phenomenon where at least two types of network access technologies have to coexist. Furthermore, for the case of the European Telecommunications Standards Institute (ETSI) Intelligent Transport Systems protocols, work is being completed in Release 2 of the specification while Release 1 deployments are still underway. This, coupled with industry and consumer trends in the vehicle industry, is bound to cause a scenario where fully C-ITS-enabled vehicles have to coexist with non-C-ITS road users and, at the very least, with different versions of C-ITS. In this paper, we analyze the performance in terms of efficiency and safety of two releases of the ETSI GeoNetworking protocol and we discuss possible paths to tackle the upcoming compatibility and coexistence problems.

**Index Terms**—Coexistence, Contention Based Forwarding, ETSI, GeoNetworking.

## I. INTRODUCTION

The use of C-ITS to maximize road safety and traffic efficiency has been one of the cornerstones upon which future mobility is built. The final stage of Cooperative, Connected and Automated Mobility (CCAM) depends on the presence of C-ITS on all roads and at all times, exchanging information and coordinating their maneuvers [1].

The road to CCAM is divided in three different fronts: *connection* (the ability to exchange information through networks), *cooperation* (the protocols that define how intelligent vehicles react to information and each other's actions), and *automation* (the level of human intervention on the driving task). These fronts have particular stages (e.g., levels of automation [2]), but they share common stages, such as the

*Days in Vision Zero* [1]. These Days (1–4) are incremental steps toward the realization of full CCAM:

- on Day 1, *awareness* starts, and vehicles share their status using messages like Cooperative Awareness Message (CAM) and Decentralized Environmental Notification Message (DENM) (i.e., in the framework established by the ETSI);
- on Day 2, *cooperation* starts, and vehicles exchange information from their sensors using, e.g., Collective Perception Messages (CPMs);
- on Day 3, road users communicate their intentions; and
- on Day 4, road users execute coordinated maneuvers.

These days take into account the evolution of technology. For example, in the *connection* front, Day 1 considers the use of Vehicular ad hoc Networks (VANETs) supported on cellular communications (i.e., LTE) or in WiFi (e.g., ETSI ITS-G5, based on IEEE 802.11p). From Day 2 onward, C-ITSs expect the use of evolved technologies (e.g., 5G, 802.11bd, and technologies beyond these two). The choice between cellular or WiFi is the first hurdle towards the harmonic coexistence of different types of intelligent vehicles, and ETSI develops media-dependent protocols for both approaches [3], [4]. Thus, manufacturers and transportation authorities are given the chance to select one or many technologies.

However, industry and consumer patterns are likely to cause a scenario where vehicles that are produced in 2023, with the technological features present this year, will share the road with fully CCAM-enabled vehicles in 2050 [5]. Even now, figures from the industry show that the average age for a vehicle in Europe ranges from 12 to 14.7 years for cars and

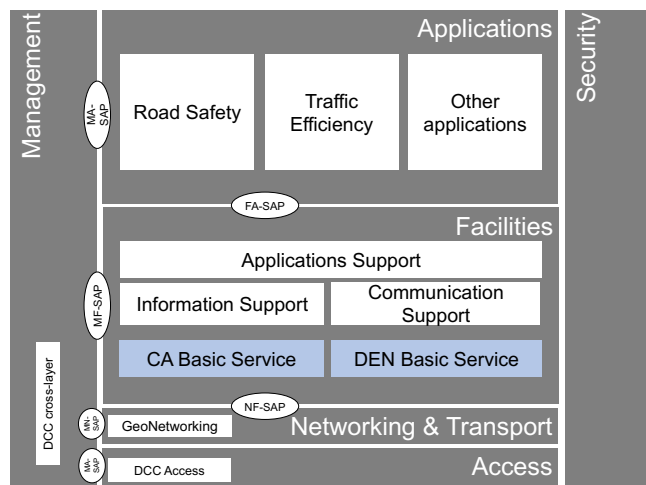


Fig. 1. ETSI ITS Architecture.

trucks, respectively, and some countries have even larger mean values [6]. This means that is highly likely to have a fleet with 1) different technological capabilities, and 2) different versions of the same technology.

In this paper, we present the effect of the coexistence of two versions of one safety-critical protocol: Release 1 of ETSI Contention-Based Forwarding (CBF) [7], and the changes proposed to Release 2, which were originally presented in [8] and [9]. We evaluate efficiency metrics such as the number of transmissions and its variation with larger penetration rates of the newer protocol in scenarios where a message has to be distributed within a Destination Area. Finally, we discuss the likely scenarios for coexistence and possible compatibility between two versions of one protocol.

The rest of the paper is organized as follows: in Section II, we present the two releases of the ETSI CBF protocol; in Section III, we perform an experimental assessment of the penetration rate of the updated protocol on effectivity and efficiency; Section IV presents a discussion on scenarios and alternatives to palliate the problem of having a mixed fleet; and finally, conclusions and future work are presented in Section V.

## II. BACKGROUND

### A. ETSI ITS Architecture

Figure 1 shows the layers and entities of the ETSI ITS architecture. At the very top, the Application layer hosts systems that pursue the goals of all C-ITSs — road safety and traffic efficiency — as well as other functions (e.g., related to infotainment). These applications are supported by the Facilities layer, e.g., by safety-critical Day 1 services like the Cooperative Awareness (CA) and Decentralized Environmental Notification (DEN) basic services. These services exchange messages with other nodes (vehicles and the infrastructure) that allow applications fulfill their roles: for example, a DENM

warns road users about roadworks ahead of the road, and an application can suggest or take a new route.

Messages are generated by services at the Facilities layer and then get sent down the stack to the Networking & Transport layer. Depending on the use case and requirements from applications, a message can be broadcast to neighbors one hop away (i.e., Single-Hop Broadcasting (SHB)), or towards a specific area of interest (Destination Area). The latter is achieved through GeoNetworking [7]. In either case, packets are encapsulated and sent down to the Access layer for transmission.

The Access layer executes Medium Access Control as well as Congestion Control functions. This layer accommodates both WiFi-based and cellular-based access technologies. For the case of WiFi-based access (i.e., ETSI ITS-G5), channel occupation (i.e., Channel Busy Ratio (CBR)) is measured at this layer and, using Decentralized Congestion Control (DCC) [10], each station calculates the share of the medium it can use, which ranges from 0.06% to 3% of the medium, or a message rate between 1 and 40 Hz. This means that, even in extremely low congestion conditions, consecutive messages must wait in the DCC queues for at least 25 ms between each dequeuing. From these queues, frames are then sent to the Enhanced Distributed Channel Access (EDCA) queues where they wait for their time to contend for access to the medium.

The road a message takes from generation to transmission and the possible bottleneck or sinkhole effects that different phenomena, e.g., at the Access layer, can have on protocol performance is accounted for by ETSI protocols. E.g., a CAM can only be generated if the message rate is less or equal to the one allowed by DCC. However, the appearance of new services and the expected effect of having a high number of nodes in proximity of each other has prompted the research community to study these effects continuously [11].

### B. GeoNetworking in ETSI ITS

Routing protocols in conventional computer networks rely on Layer 3 addresses to send data between hosts in remote locations. This is typically achieved through IP addressing. In the context of VANETs, where use cases sometimes require the dissemination of information to a given area, geographical awareness is required for a routing protocol. Hence, GeoNetworking functionalities are included, e.g., in the Networking & Transport layer of the ETSI ITS protocol stack [7]. GeoNetworking allows for messages to reach a Destination Area without the need of maintaining a record of the network addresses of nodes in that area, which would be difficult due to the dynamic nature of vehicular networks.

ETSI defines mechanisms to broadcast information to a geographical Destination Area when:

- the source is outside the Destination Area and the message has to arrive in it (e.g., using Greedy Forwarding or CBF); or
- the message originates from or arrives into the Destination Area and is disseminated using CBF or Simple Forwarding.

Non-Area mechanisms are out of the scope of this paper, but we can summarize Greedy Forwarding as a mechanism where each hop selects its farthest known neighbor and determines it as the next hop toward the Destination Area. These type of mechanisms have been widely studied, and the ETSI-defined version of Greedy Forwarding is evaluated in-depth in [12] and [13].

Regarding Area forwarding mechanisms, Simple Forwarding can be described as a brute-force mechanism where every node that receives a message forwards it immediately (i.e., simple flooding). CBF, on the other hand, makes receivers start a *contention* timer that is proportional to their distance from the last hop before they decide to forward the message. If they listen to a forwarding while they are waiting for their timer to expire, they cancel the timer and drop their copy of the packet.

1) *Inefficiencies in Release 1 of ETSI CBF*: Efforts from the research community have evaluated the performance of ETSI CBF. While the theoretical frame which supports CBF makes it more optimal than, e.g., simple forwarding, the way it interacts with other layers in the ETSI ITS architecture causes phenomena that affect its efficiency.

The interaction between ETSI CBF and the DCC mechanism at the Access layer causes an undesired effect: even if the CBF timer expires, and the decision to forward the packet is made, if there is congestion in the channel or if another packet has just been transmitted, the forwarding is stopped at the DCC queues (for ETSI ITS-G5) or the scheduler (for C-V2X). This means that the actual transmission may not occur when CBF has decided, and this phenomenon can occur in any station, so even if a copy of the message is received during contention, it is not guaranteed that it comes from an optimal forwarder. Furthermore, Release 1 of ETSI GeoNetworking relies Duplicate Packet Detection (DPD) to CBF, so, if a backlogged message from a DCC-affected forwarder is received at a neighbor which had already forwarded or even cancelled its copy will enter the loop once again.

2) *ETSI CBF Release 2*: The issues with DPD and the effect of DCC on Release 1 for ETSI CBF had been studied widely in the literature [12], [14], [15]. Yet, it was the work in [8] and [9] that was presented to ETSI as a change request that was iterated and matured before it reached the necessary consensus to be Release 2 of ETSI CBF.

The differences in Release 2 of Area CBF are:

- The inclusion of DPD inside the CBF algorithm.
- Interfacing with the cross-layer DCC mechanism to offer awareness of the time before DCC allows the next transmission, and account for it when calculating the contention timer (optional for cellular-based communications).
- A procedure to determine if a copy received during contention actually comes from a better forwarder.
- An updated timer formula to account for receptions beyond the maximum expected distance.

However, since Release 2 services might have different requirements and characteristics, it is not clear if Release 1 nodes will be able to receive messages originating from Release 2 nodes, even for safety-critical applications. If this is the case, and nodes executing Release 2 of ETSI CBF coexist with nodes executing Release 1, there might be effects on awareness and efficiency metrics. In the following section, we evaluate these effects in Area CBF in a highway scenario.

### III. EXPERIMENTAL EVALUATION OF COEXISTENT RELEASES

#### A. Simulation Scenario

We evaluate the effect of different ratios of nodes executing Release 1 and 2 of ETSI CBF in a highway scenario where a vehicle is stationary on the shoulder of a road. It starts sending DENMs [16] at 1 Hz with a Destination Area covering 4 km of a road with 4 lanes per direction. The vehicular density is 30 veh/km on each lane. We take measurements for 30 s after a warm-up period of 120 s. We evaluate:

- 1) **Packet-delivery Ratio (PDR)**: the number of successful individual receptions of a message in the Destination Area divided by the total number of vehicles in the area at the time of DENM generation.
- 2) **Number of transmissions**: how many transmissions (i.e., from the source and forwarders) have occurred.

Our toolkit consists of the OMNET++-based simulator Artery [17], which implements the ETSI ITS protocol stack using Vanetta and Veins [18] for the physical model of ETSI ITS-G5. Mobility is controlled by SUMO [19]. A set of vehicles execute ETSI CBF Release 1 [7], and an increasing number of vehicles (see the penetration rate parameter) execute the improvements included in Release 2 as described in [9]. In our set-up, and due to the nature of the message (i.e., Road Hazard Warning (RHW)), we consider Release 2 and Release 1 messages to be mutually understandable. The rest of the parameters are specified in Table I.

TABLE I  
SIMULATION PARAMETERS

Parameter	Values
Access Layer protocol	ITS-G5 (IEEE 802.11p)
Channel bandwidth	10 MHz at 5.9 GHz
Data rate	6 Mbit/s
DCC	ETSI Adaptive DCC
Transmit power	20 mW
Path loss model	Two-Ray interference model [20]
Maximum transmission range	1500 m
CAM packet size	285 bytes
CAM generation frequency	1–10 Hz (ETSI CAM [21])
CAM Traffic Class	TC2
DENM packet size	301 bytes
DENM Traffic Class	TC0 (Source) and TC3 (Forwarders)
DENM lifetime	10 s
DPL size	32 packet identifiers per Source
Default Hop Limit	10
Rel. 2 penetration rate	0, 25, 50, 75, 100%

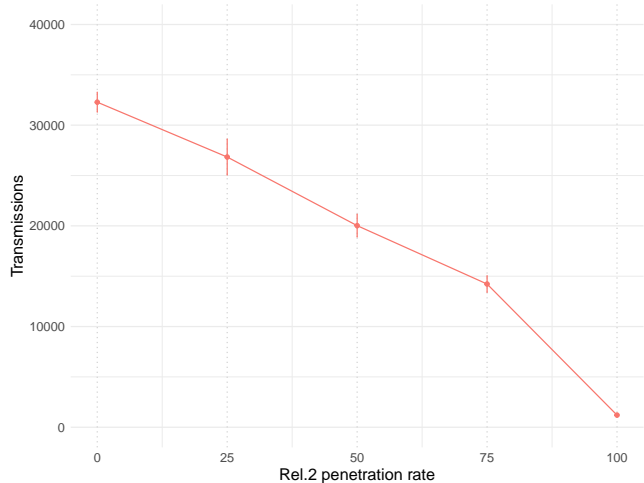


Fig. 2. Number of transmissions in different Release 2 penetration rates.

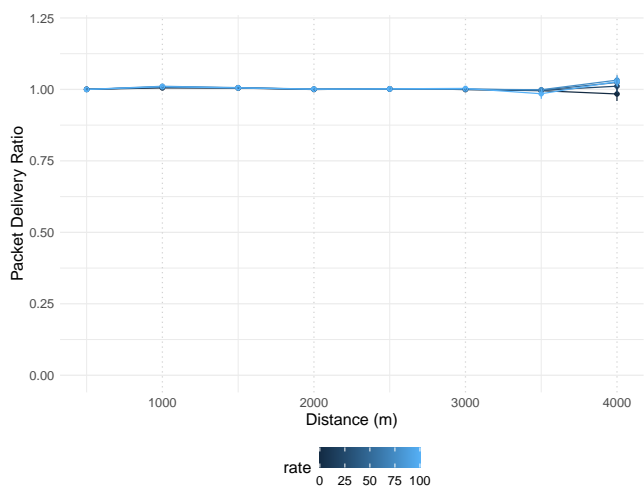


Fig. 3. Packet Delivery Ratio for different Release 2 penetration rates.

## B. Results

Figure 2 shows the effect of even a minority portion of nodes executing a non-optimized protocol. There is beyond an order of magnitude in executed transmissions between the 0% and the 25% penetration rate for Release 2. From there, there is a linear increase until the almost 30:1 ratio between Release 1 and Release 2 in line with the results in [8] and [9].

However, this issue is not reflected in awareness. Figure 3 shows the PDR over the distance in the 4 km-long Destination Area. Lines overlap for most of the distance, up to the last segment where they fan out in favor of higher penetration rates. However, this phenomenon is due to an unbalance in the turnover rate (i.e., the ratio between vehicles entering and exiting the Destination Area after the DENM was generated). These extra vehicles are accounted for since the message is still within validity, and it is relevant to newcomers into the Destination Area.

The main takeaway of this experiment is that, as long as Re-

lease 1 and Release 2 GeoNetworking messages are mutually intelligible, there is an effect on efficiency but not in safety (for the case of multi-hop DENMs from a single source). However, inefficient forwarding will occupy the medium with unnecessary repetitions of messages. Thus, in scenarios where there is more than one source trying to disseminate safety-critical messages, unnecessary transmissions are bound to cause collisions or, at least, to block access to the medium for more necessary messages waiting to be forwarded. Further work needs to be performed on how non-mutually intelligible messages affect performance, since Release 1 is likely to reach higher PDR using brute force, while Release 2 will either yield access to the medium or might find a path to transmit immediately. What is sure is that, in that scenario, safety will be compromised.

## IV. DISCUSSION

We present a study of how the coexistence of two different releases of a protocol, one being an incremental improvement of the other, affects efficiency. For our case, packets were compatible, and Release 1 nodes could understand Release 2 messages and vice versa. However, the road to full CCAM is long, and this might not be the case even in the near future. In this section, we present a discussion on the upcoming scenarios when multiple types and generations of technologies have to coexist.

### A. The upcoming Tower of Babel

Vehicles equipped with ETSI ITS nodes are already on the road communicating with large deployments. Just in the first three quarters of 2023, more than 250,000 C-ITS-equipped Volkswagen ID. cars were delivered [22]. These cars can communicate with each other, with other ETSI ITS-compatible vehicles, and with current deployments such as the one covering the entire Austrian motorway network [23].

However, these vehicles and deployments all use Release 1 services. While some Release 2 features are software-dependant, e.g., new services such as the Vulnerable Road User awareness (VA) basic service, and can be installed during car services or using over-the-air updates, some others will likely require a deeper update (e.g., compatibility with Multi-channel Operation (MCO)).

While backwards-compatibility is a common issue in computer networks, the characteristics of the vehicular market and industry make it especially more difficult. This is one of the first cases where a massive number of *legacy* nodes will likely share spaces with nodes up to 20 years more modern [6]. This will create a scenario where pockets of segregated nodes are bound to destabilize the system, at the very least make it more inefficient, while compromising efficacy and safety.

1) *Past experiences with backwards compatibility:* One example of backwards compatibility is the jump between Transport Layer Security (TLS) 1.2 and 1.3. The 1.3 version was released in RFC 8446 in August 2018 [24]. Its benefits over past versions have been widely studied [25], but there are known examples of problems with its adoption [26].

The main problem with TLS 1.3 is *protocol ossification*. This phenomenon occurs when deployed equipment (e.g., middleboxes) does not recognize new protocols or even extensions to known protocols that were released after they were installed. This causes them to interrupt packets that are valid, but unrecognizable for the middlebox.

The solution for TLS 1.3, and for other examples of ossification, was to encapsulate new messages so that the *wire image* of the packets is acceptable for older middleboxes. This could be a path to follow with safety-critical messages exchanged by nodes executing different releases of ETSI ITS.

At the Access layer, 802.11p (upon which ETSI ITS-G5 is based) and its evolution 802.11bd are somewhat compatible. One of the main differences between 802.11bd and 802.11p is the channel bandwidth — 20 MHz up from 11p’s 10 MHz. However, 11bd can also work in 10 MHz, and does so if it detects nodes using only 10 MHz, thus, falling back into 11p when needed. However, this approach might not be efficient in Future Mobility scenarios, when 11p’s channel capacity might not be able to accommodate the myriad of applications that will try to use the medium.

The foreseeable scenario if nodes cannot process packets from newer releases (i.e., if Release 1 nodes cannot handle Release 2 GeoNetworking traffic) can cause a disruption in Non-Area GeoNetworking [7] if Greedy Forwarding is used. Since it is likely that beacons (e.g., CAMs) will always be compatible, a Release 2 node can select a Release 1 neighbor as the next hop for a message. The next hop will not process the message, and thus it will not reach the Destination Area, since there are no fallback nodes in ETSI Greedy Forwarding. This phenomenon can be avoided, for example, using CBF, where multiple nodes become the next hop and contend to forward the message, increasing the chances of nodes from both releases hearing the forwarded message. Further work will address the impact of this phenomenon on Non-Area forwarding.

2) *Nodes with different technologies*: In the network side, even at Day 1, there is an identified risk of *non-interoperability* [27]. Since ETSI ITS is media-independent, it does not mandate that one access technology shall be used. Thus, there are vehicles and road-side equipment that use, e.g., LTE or 802.11p. ETSI recognizes the scenario and proposes co-existence methods [28] where, for example, vehicles using different technologies share the time domain. This means that cellular-based nodes occupy the C-ITS band for a fraction of the time and WiFi-based nodes use it for the complement. This, however, is not full inter-operability, since nodes using different access technologies will not “listen” to each other, and this approach compromises every metric: efficiency (diminishing the amount of resources), efficacy (messages are not delivered to all connected road users), and thus, safety.

Further work has to be performed within the research and industry communities to 1) determine whether WiFi and cellular can possibly inter-operate, and 2) whether inter-operability is possible, search for a path to evolve in a way that newer versions of access technologies account for older nodes. One

possible approach is to adopt approaches such as Software-Defined Radio (SDR), which would allow equipment to be updated over the air as long as hardware supports newer features, such as different modulation and coding schemes.

This phenomenon will be aggravated when technologies from different Days coexist. For example, a *legacy* node that cannot interpret or even receive intention-sharing or maneuver-coordination message exchanges will likely affect the way CCAM-enabled vehicles converge to a solution. Once again, this will affect traffic efficiency and might hinder road safety. Further work is being performed to assess the effect of a mixed fleet in the optimal performance in CCAM.

### B. The case for ETSI CBF Release 2

For the specific phenomenon in this work, the differences between ETSI CBF Release 1 and 2 are purely software-based. There is no need for extra fields in the headers, or new values in the existing fields. The main differences come in what the algorithm does with information it already used, namely, the position vector from the last hop and the source. It also uses an existing interface to the Management entity to consult the cross-layer DCC mechanism and account for transmission rate control information when calculating a contention timer (although this feature is optional).

We foresee two simple solutions: 1) existing equipment that is able to receive an update adopts Release 2, or 2) Release 2 GeoNetworking messages are encapsulated as Release 1, as was the case for TLS 1.3. Both approaches will ensure safety in given scenarios, but approach 1 guarantees more efficiency, and thus, more availability of resources for other applications.

## V. CONCLUSIONS AND FUTURE WORK

We have presented a study of the coexistence of two releases of a GeoNetworking protocol in the context of ETSI ITS — Release 1 and 2 of ETSI CBF. We have proved that, as long as releases are compatible and nodes can understand each other, safety metrics stay high even if resource efficiency is compromised. Then, we presented a discussion of possible settings that are likely to happen when Future Mobility is completely mature (i.e., Day 4 of Vision Zero), where a Tower of Babel scenario might occur, and road users are segregated into pockets of nodes *speaking* different *languages* (and some not *speaking* at all). Even when the first C in CCAM stands for *cooperative*, this cooperation is not likely to occur when agents are not able to hear and understand each other. Future work includes a more in-depth analysis of the effect of *multi-modal road users* (e.g., disconnected users, legacy fleet) in the optimal performance of the CCAM-enabled fleet (i.e., connected and automated vehicles).

### ACKNOWLEDGMENT

This work was partially supported by SAFER in the project “Human Factors, Risks and Optimal Performance in Cooperative, Connected and Automated Mobility”, the Knowledge Foundation in the project “SafeSmart – Safety of Connected

Intelligent Vehicles in Smart Cities” (2019-2024), and the EL-LIIT Strategic Research Network in the project “6G wireless” – sub-project “vehicular communications”.

## REFERENCES

- [1] European Commission (EC), “Towards a European road safety area: policy orientations on road safety 2011-2020,” July 2010.
- [2] SAE, “Taxonomy and Definitions for Terms Related to Driving Automation Systems for On-Road Motor Vehicles,” SAE International, Standard, Apr. 2021.
- [3] European Telecommunications Standards Institute (ETSI), “Intelligent Transport Systems (ITS); Vehicular Communications; GeoNetworking; Part 4. Geographical addressing and forwarding for point-to-point and point-to-multipoint communications; Sub-part 2: Media-dependent Functionalities for ITS-G5,” ETSI TS 102 636-4-2 - V1.4.1, February 2021.
- [4] —, “Intelligent Transport Systems (ITS); Vehicular Communications; GeoNetworking; Part 4. Geographical addressing and forwarding for point-to-point and point-to-multipoint communications; Sub-part 2: Media-dependent Functionalities for LTE-V2X,” ETSI TS 102 636-4-3 - V1.2.1, August 2020.
- [5] D. Milakis, M. Snelder, B. Arem, B. Wee, and G. Homem de Almeida Correia, “Development and transport implications of automated vehicles in the Netherlands: Scenarios for 2030 and 2050,” *European Journal of Transport and Infrastructure Research*, vol. 17, pp. 63–85, 01 2017.
- [6] European Automobile Manufacturers’ Association, “Average age of the EU vehicle fleet, by country,” accessed: 2024-01-31. [Online]. Available: <https://www.acea.auto/figure/average-age-of-eu-vehicle-fleet-by-country/>
- [7] European Telecommunications Standards Institute (ETSI), “Intelligent Transport Systems (ITS); Vehicular Communications; GeoNetworking; Part 4. Geographical addressing and forwarding for point-to-point and point-to-multipoint communications; Sub-part 1: Media-Independent Functionality,” ETSI EN 302 636-4-1 - V1.4.1, January 2020.
- [8] O. Amador, M. Urueña, M. Calderon, and I. Soto, “Evaluation and improvement of ETSI ITS Contention-Based Forwarding (CBF) of warning messages in highway scenarios,” *Vehicular Communications*, vol. 34, p. 100454, 2022, accessed: 2024-01-31. [Online]. Available: <https://www.sciencedirect.com/science/article/pii/S2214209622000018>
- [9] O. Amador, I. Soto, M. Calderon, and M. Urueña, “Studying and improving the performance of ETSI ITS contention-based forwarding (CBF) in urban and highway scenarios: S-FoT+,” *Computer Networks*, vol. 233, p. 109899, 2023, accessed: 2024-01-31. [Online]. Available: <https://www.sciencedirect.com/science/article/pii/S1389128623003444>
- [10] European Telecommunications Standards Institute (ETSI), “Intelligent Transport Systems (ITS); Decentralized congestion control mechanisms for Intelligent Transport Systems operating in the 5 GHz range; Access layer part,” ETSI EN 102 687 - V1.2.1, April 2018.
- [11] Ó. Amador Molina, “Decentralized congestion control in etsi intelligent transport systems and its effect on safety applications,” 2020.
- [12] R. Riebl, *Quality of Service in Vehicular Ad Hoc Networks: Methodical Evaluation and Enhancements for ITS-G5*. PhD Thesis. De Montfort University, 2021. [Online]. Available: <https://dora.dmu.ac.uk/handle/2086/21186>
- [13] V. Sandonis, I. Soto, M. Calderon, and M. Urueña, “Vehicle to internet communications using the etsi its geonetworking protocol,” *Transactions on Emerging Telecommunications Technologies*, vol. 27, no. 3, pp. 373–391, 2016. [Online]. Available: <https://onlinelibrary.wiley.com/doi/abs/10.1002/ett.2895>
- [14] S. Kühlmorgen, H. Lu, A. Festag, J. Kenney, S. Gernsheim, and G. Fetweis, “Evaluation of Congestion-Enabled Forwarding With Mixed Data Traffic in Vehicular Communications,” *IEEE Transactions on Intelligent Transportation Systems*, vol. 21, no. 1, pp. 233–247, 2020.
- [15] T. Paulin and S. Ruehrup, “On the Impact of Fading and Interference on Contention-Based Geographic Routing in VANETs,” in *2015 IEEE 82nd Vehicular Technology Conference (VTC Fall)*, 2015, pp. 1–5.
- [16] European Telecommunications Standards Institute (ETSI), “Intelligent Transport Systems (ITS); Vehicular Communications; Basic Set of Applications; Part 3: Specifications of Decentralized Environmental Notification Basic Service,” ETSI EN 302 637-3 - V1.3.1, April 2019.
- [17] R. Riebl, H. Günther, C. Facchi, and L. Wolf, “Artery: Extending Veins for VANET Applications,” in *2015 International Conference on Models and Technologies for Intelligent Transportation Systems (MT-ITS)*, 2015, pp. 450–456.
- [18] C. Sommer, R. German, and F. Dressler, “Bidirectionally Coupled Network and Road Traffic Simulation for Improved IVC Analysis,” *IEEE Transactions on Mobile Computing*, vol. 10, no. 1, pp. 3–15, 2011.
- [19] D. Krajzewicz, J. Erdmann, M. Behrisch, and L. Bieker, “Recent Development and Applications of SUMO - Simulation of Urban MObility,” *International Journal On Advances in Systems and Measurements*, vol. 5, no. 3&4, pp. 128–138, December 2012.
- [20] C. Sommer, S. Joerer, and F. Dressler, “On the applicability of Two-Ray path loss models for vehicular network simulation,” in *2012 IEEE Vehicular Networking Conference (VNC)*, 2012, pp. 64–69.
- [21] European Telecommunications Standards Institute (ETSI), “Intelligent Transport Systems (ITS); Vehicular Communications; Basic Set of Applications; Part 2: Specifications of Cooperative Awareness Basic Service,” ETSI EN 302 637-2 - V1.4.1, April 2019.
- [22] Volkswagen Group, “Volkswagen Group delivers 45 percent more all-electric vehicles in first 9 months,” accessed: 2024-01-31. [Online]. Available: <https://www.volkswagen-newsroom.com/en/press-releases/volkswagen-group-delivers-45-percent-more-all-electric-vehicles-in-first-9-months-17771/>
- [23] C-ITS Deployment Group, “ASFINAG, Managing everyday traffic situations more easily with C-ITS / Car2X,” accessed: 2024-01-31. [Online]. Available: <https://c-its-deployment-group.eu/news-events/news/2022-07-27-asfinag-c-its-imagevideo>
- [24] E. Rescorla, “The Transport Layer Security (TLS) Protocol Version 1.3,” RFC 8446, Aug. 2018. [Online]. Available: <https://www.rfc-editor.org/info/rfc8446>
- [25] O. Levillain, “Implementation flaws in tls stacks: Lessons learned and study of tls 1.3 benefits,” in *Risks and Security of Internet and Systems*, J. Garcia-Alfaro, J. Leneutre, N. Cuppens, and R. Yaich, Eds. Cham: Springer International Publishing, 2021, pp. 87–104.
- [26] S. Lee, Y. Shin, and J. Hur, “Return of version downgrade attack in the era of tls 1.3,” in *Proceedings of the 16th International Conference on Emerging Networking EXperiments and Technologies*, ser. CoNEXT ’20. New York, NY, USA: Association for Computing Machinery, 2020, p. 157–168. [Online]. Available: <https://doi.org/10.1145/3386367.3431310>
- [27] C-ROADS, “C-ROADS platform position paper on 5.9 GHz band,” accessed: 2024-01-31. [Online]. Available: [https://www.c-roads.eu/fileadmin/user\\_upload/media/Dokumente/C-Roads\\_Position\\_paper\\_on\\_59GHz\\_final.pdf](https://www.c-roads.eu/fileadmin/user_upload/media/Dokumente/C-Roads_Position_paper_on_59GHz_final.pdf)
- [28] European Telecommunications Standards Institute (ETSI), “Intelligent Transport Systems (ITS); Pre-standardization study on co-channel co-existence between IEEE- and 3GPP- based ITS technologies in the 5 855 MHz - 5 925 MHz frequency band,” ETSI TR 103 766, September 2021.

# Offloading Platooning Applications from 5.9 GHz V2X to Radar Communications: Effects on Safety and Efficiency

Elena Haller, Galina Sidorenko, Oscar Amador, Emil Nilsson

School of Information Technology

Halmstad University

Halmstad, Sweden 30118

Emails: {elena.haller,galina.sidorenko,oscar.molina,emil.nilsson}@hh.se

**Abstract**—Vehicle to anything (V2X) communications are nowadays performed at 5.9 GHz spectrum, either using WiFi-based or Cellular technology. The channel capacity is limited, and congestion control regulates the number of messages that can enter the medium. With user rate growing, overloading becomes a factor that might affect road safety and traffic efficiency. The present paper evaluates the potential of using Radar-Based Communication (RadCom) for offloading the V2X spectrum. We consider a Heavy-Duty Vehicle (HDV) platooning scenario as a case of maneuver coordination where local messages are transmitted by means of RadCom at different penetration rates. Simulations show significant improvements in channel occupancy and network reliability. As a result, RadCom allows for shorter, safer, and more energy efficient inter-vehicle distances.

**Index Terms**—Fuel Efficiency, Optimal distances, Platooning, Radar-based Communications.

## I. INTRODUCTION

Mobility with maximized road safety and traffic efficiency is a goal reflected in the United Nation's Social Development Goals [1], and in global initiatives such as Vision Zero [2], adopted by the European Commission. The road towards future mobility in Vision Zero is divided in stages called *Days*, which go from Day 1 (where we currently are) until Day 4, when Cooperative, Connected and Automated Mobility (CCAM) is expected to be present on all roads and at all times.

Efforts to arrive at the final stage of CCAM include two main fronts: automated mobility and Cooperative Intelligent Transport Systems (C-ITS). The latter uses vehicular communications, such as Vehicular ad hoc Networks (VANETs), that use access technologies such as 802.11p. For Day 1 services, aimed at increasing the awareness of road users, there are technologies such as the Cooperative Awareness (CA) [3] and Decentralized Environmental Notification (DEN) [4] basic services, which are used in the framework defined by the European Telecommunications Standards Institute (ETSI). These services rely on the exchange of messages that inform road users about each other's presence (through Cooperative Awareness Messages (CAMs)) or about risks on the road (using Decentralized Environmental Notification Messages (DENMs)). These messages are exchanged using access technologies such as ETSI ITS-G5 [5], which is based on 802.11p.

Subsequent Days are also expected to rely on messages. Day 2, when *cooperation* starts, uses Collective Perception Messages (CPMs) to exchange information about detected objects [6]. On Day 3, road users share their intentions (e.g., desired trajectories), and finally, on Day 4, vehicles coordinate their maneuvers. These features are expected to be performed by the Maneuver Coordination (MC) service, powered by Maneuver Coordination Messages (MCMs).

Early forms of maneuver coordination are Cooperative Adaptive Cruise Control (CACC) and platooning. These applications are also based on messages. For example, platooning uses CAMs and Platooning Awareness Messages (PAMs) to inform neighbors of the ability to form a platoon and negotiate its start (sent in broadcast mode), and Platooning Control Messages (PCMs) to maintain the platoon (sent in unicast between platoon members) [7].

This means that, from Day 1, the medium will be occupied by a myriad of messages to power services. Even for Day 1, the existence of traffic with different characteristics and priorities can cause problems in efficiency and effectiveness for safety applications [6], [8]. These issues stem from the capacity of the channel to accommodate a certain number of messages before reaching congestion [9], [10]. Thus, if more messages enter the system, e.g., MCMs, PCMs, the ability of the channel to accommodate them will be hindered.

This paper proposes the use of Radar-Based Communication (RadCom) as an alternative channel to offload future mobility use cases, such as platooning. We present a study of the potential saving in terms of medium usage (Channel Busy Ratio (CBR)), and whether such offloading allows reaching the goal of platooning and C-ITSs in general: minimizing risks of accidents (e.g., collisions between road users) and increasing efficiency.

The contributions of this work are:

- 1) A simulation-based study of the effect of offloading Vehicle-to-Vehicle (V2V) communications from the C-ITS medium to bumper-to-bumper RadCom.
- 2) An analysis of the effect of this offloading on minimizing safe inter-vehicle distances in a platoon.

- 3) An analysis of the effect of these distances on traffic and in-vehicle efficiency.

The rest of the paper is organized as follows: in Section II, we explore the related work on platooning and its performance using VANETs; Section III presents our proposal for RadCom-enabled channel offloading; Section IV presents an experimental evaluation of the system; Section VI presents an analysis of our results and its effects on road safety and traffic efficiency; and, finally, Section VII presents the conclusions and our future lines of work.

## II. PLATOONING

Platooning has been widely studied in the context of safety and efficiency. An early example of electronics-assisted platooning is the "Electronic Tow Bar" resulting from the European project PROMOTE-CHAUFFEUR [11]. Further efforts from the industry and research communities are reflected in brand-specific projects SARTRE [12] and COMPANION [13], as well as multi-brand projects like ENSEMBLE [14]. These projects, however, rely mostly on sensing and adaptations in the infrastructure (e.g., lane markings), and use cloud services instead of vehicular communications. In this section, we describe network-enabled platooning, as expected by ETSI and as studied by the research community.

### A. Network-enabled platooning

Platooning is an C-ITS application contemplated in the ETSI ITS framework [7]. As it is for Day 1 applications, it relies on the exchange of messages: CAMs inform about a vehicle's capability to platoon, PAMs are used to negotiate platoon creation, and PCMs are sent between the leader and members (in unicast) to maintain the platoon.

The platoon leader exchanges information with the rest of the members and with other road users. This enables functionalities for platoon safety and efficiency, such as negotiating inter-vehicle distances to enable safe braking in emergency situations [15], or exchanging information on attributes and capabilities (e.g., acceleration/deceleration capability).

While the platoon is enabled, the rest of Vehicle-to-anything (V2X) communications are still used, so there is a possibility that PCMs use a channel different from the main V2X channel (e.g., CCH for ETSI ITS-G5), which is used by other safety-critical applications. However, even if a different channel is used, they are likely to suffer from access layer phenomena, as we explore in Section II-B.

### B. Access phenomena affecting platooning

There are several Access layer phenomena that affect V2X-enabled platooning. Some of these phenomena are inherent to the nature of WiFi-based protocols such as ETSI ITS-G5, such as hidden and exposed nodes; and others are related to channel congestion and how different frameworks deal with it. Figure 1 summarizes the hidden and exposed node phenomena. A and D are hidden nodes for C and B, respectively, and messages they send to each other (A and C) could collide with messages coming from the hidden nodes. Similarly, if A and B want

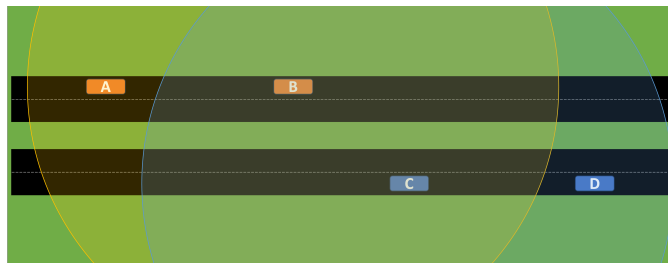


Fig. 1. Hidden and exposed node phenomena in V2X scenarios.

to communicate with each other, communication between C and D can prevent them from accessing the medium. This is the exposed node phenomenon. While there are mechanisms, e.g., back-off procedures in WiFi networks, to counter hidden and exposed nodes, there are access protocols in C-ITS that only use them when unicast communication takes place (e.g., ETSI ITS-G5 does not use exponential back-off for single-hop broadcast traffic, but does so for unicast) [16].

An analysis of CAM-based platooning is performed in [17]. Here, authors present an evaluation of the CA basic service as an enabler for platooning and identify a problem with message synchronization. While CAM synchronization is solved with kinematic generation, PCMs are generated at high, periodic rates [7], and are thus susceptible to collisions due to synchronization.

Furthermore, even if PCMs are sent in unicast mode (as opposed to CAMs and DENMs, which are broadcast), neighbors can overhear these exchanges (i.e., sense the medium as occupied). In moderate to high density scenarios, these exchanges add to the existing channel occupancy and create congestion. The work in [18] analyzes the performance of ETSI DCC in multi-lane platooning scenarios, and proposes the use of congestion control techniques different to adapting message rates (e.g., controlling transmission power).

There is a need for "intra-platoon" communications to occur without interfering with other applications sharing the medium. The use of millimeter wave (mmWave) communications for platooning applications is explored in [19]. The authors use mmWave to rely sensor information using multi-hop dissemination. The difference with our proposal is that, while they consider a generic mmWave antenna, we analyze the possibility of piggy-backing communications specifically on radars with specific attributes and capabilities.

## III. RADCOM-ENABLED PLATOONING

Figure 2 summarizes our proposal to offload intra-platoon communications to RadCom. The top part of the figure (2a) shows the foreseeable status of network-enabled platooning. After negotiating the start of a platoon using CAMs and PAMs, the platoon leaders (dark nodes) start communicating with the members (light nodes) exchanging PCMs in unicast mode. The arches express a conservative range for the wireless signals from each node (yellow for the platoon on the left and blue for the one on the right). These ranges are typically measured above 300 m, but are sometimes greater [20].

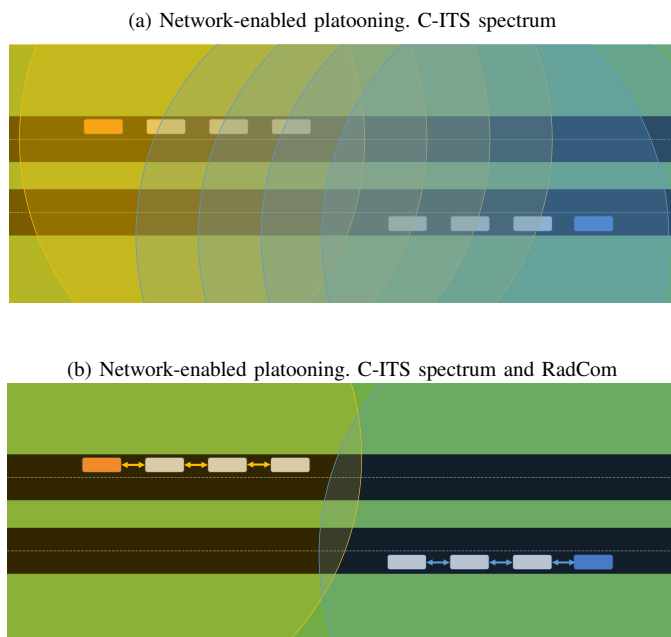


Fig. 2. Representation of offloading intra-platoon communications to RadCom. The yellow and blue shades represent the coverage area for the members of each platoon, yellow for the westbound and blue for the eastbound.

This means that, in scenarios like this, intra-platoon communications will not only interfere with other platoon members, but also with other platoons and even other vehicular communications. Figure 2a shows that the tails of both platoons are within the range of most of the nodes, and are likely to suffer from the exposed node phenomenon, as described in Section II-B.

Figure 2b shows how intra-platoon communications can be offloaded to V2V RadCom. On this example, the leaders can send commands, e.g., through PCMs, and receive feedback or other communications from platoon members through multi-hop RadCom (represented by arrows). Then, radio resources would be available for other applications, e.g., inter-platoon communications. At the very least, this offloading will avoid causing congestion in the C-ITS spectrum.

#### A. RadCom ability to support V2V communications

The bare minimum requirements for RadCom to support V2V communications are the specifications for the ETSI ITS-G5 medium [5]. These are:

- 1) **Data rate:** support 3 Mbit/s, 6 Mbit/s and 12 Mbit/s. The default rate in ETSI ITS-G5 is 6 Mbit/s.
- 2) **Message rate:** maximum 40 Hz and minimum 1 Hz.

The body of work on mmWave systems supporting vehicular applications shows that these requirements can be met by generic mmWave deployments. The work in [19] tests their proposed multi-hop system at Gbit/s rates when exchanging sensor information. The work in [21] assesses the capacity of generic mmWave when coding errors are present. OFDM

waveforms has been proposed for automotive radar enabling wide bandwidth communication [22]. Communication networks may also be instrumental in avoiding interference between wide band radar sensors [23]–[25]. Their results show that, starting with bandwidths of a fraction of a GHz, rates in tens of Mbit/s are possible in line-of-sight scenarios. Thus, we can expect RadCom to be able to accommodate the requirements that are set for ETSI ITS-G5 and beyond.

#### IV. EVALUATION OF CHANNEL OCCUPANCY

We use Artery [26] as our simulation toolkit. It combines OMNET++ and Vanetza — a C++ implementation of the ETSI ITS protocol stack. Our setup uses Artery’s integration with Veins [27] for the physical layer. Finally, SUMO [28] provides the mobility model for the road topology. Simulation parameters are specified in Table I.

TABLE I. SIMULATION PARAMETERS

Parameter	Values
Access Layer protocol	ITS-G5 (IEEE 802.11p)
Channel bandwidth	10 MHz at 5.9 GHz
Data rate	6 Mbit/s
Transmit power	20 mW
Path loss model	Simple Path-loss Model
Maximum transmission range	1500 m
CAM packet size	285 bytes
CAM Traffic Class	TC2
CAM generation frequency	Kinematic-based [3]
PCM packet size	301 bytes
PCM Traffic Class	TC1
PCM generation frequency	Periodic at 2 Hz
RadCom penetration rate	0, 50, 100%

#### A. Simulation Scenario

For our scenario, we simulate a 5 km long road with four lanes in each direction. Vehicles occupy the road with a density of 30 veh/km per lane and are running in a steady state, where we can consider them to have organized platoons of different lengths, and have different roles (platoon leader and platoon member). We take measurements for 30 s after a warm-up period of 120 s. Vehicles send CAMs (generated dynamically following ETSI rules [3]), and PCMs that work for controlling and maintaining the platoon (generated periodically every 500 ms). We send both messages on the same ETSI ITS-G5 channel, with PCMs having higher priority than CAM since we consider them to be more critical, although there is not a standardized priority for PCMs as of now [7].

A subset of platoons offload PCMs to bumper-to-bumper RadCom. This means that these vehicles stop sending PCMs on the ETSI ITS-G5 spectrum and perform platoon control and maintenance “bumper-to-bumper”. We increase the number of RadCom platoons (i.e., penetration rate) until only the platoon leaders send messages on the ETSI ITS-G5 channel (i.e., 100% penetration rate).

We measure conditions in the ETSI ITS-G5 channel. The performance metrics we evaluate from the simulation are:

- **Packet-delivery Ratio (PDR):** the number of successful message receptions divided by the total expected receptions.

- **Smoothed Channel Busy Ratio (S-CBR):** the smoothed average of CBR measurements which is used in the Decentralized Congestion Control (DCC) mechanism [29].

The results above allow the calculation of safety and efficiency metrics presented in Section V. We use the work in [15] to relate network performance to inter-vehicle distances, and then extrapolate them to fuel efficiency.

### B. Simulation results

TABLE II. RESULTS FOR MESSAGES IN THE C-ITS SPECTRUM AT  $d \leq 200\text{M}$  WITH DIFFERENT PENETRATION RATES OF RADCOM

RadCom Penetration Rate	PDR	S-CBR	Latency
0%	0.6985	0.6176	136.80 ms
50%	0.7859	0.6119	109.57 ms
100%	0.9015	0.2217	1.45 ms

Table II shows the results of our experiment. The table shows the average PDR and latency for PCMs. For the 100% rate, only the leaders send messages on the C-ITS spectrum and the rest of the platoon communicates using RadCom. Thus, the PDR for PCMs is mostly affected by propagation phenomena and the interference from CAMs. Therefore, even sending command-and-control messages at a high rate, offloading to RadCom allows platoon members to listen to leaders with significantly increased reliability.

It is worth noting that, even with half of the fleet not sending PCMs, channel occupancy stays at similar levels as when all vehicles send PCMs. This number, slightly above 0.61 is close to the theoretical CBR limit for ETSI ITS-G5 (0.68) and to the point where medium occupancy converges ( $CBR = 0.65$ ) [10]. While occupancy stays similar, the effect of offloading to RadCom is noticeable in PDR and in latency: more packets arrive, and they do so faster. Nevertheless, even at this vehicle density (30 veh/km per lane), the stress on the medium is noticeable. However, when only platoon leaders send PCMs (100% penetration rate), besides the increased PDR, the value for latency significantly better. Delays are minimal, and thus, more messages arrive, and they do so in a timely fashion.

### V. OPTIMAL DISTANCES AND FUEL CONSUMPTION

Increased offloading of V2X channel results in increased PDR (Table II). Consequently, Inter-Vehicle Distances (IVDs) within the platoon can be decreased without compromising safety. Figure 3 shows how distances between vehicles of one platoon can be shortened with the increased RadCom penetration rate. The minimum safe IVDs were obtained as a Pareto optimal solution that minimizes IVDs' weighted sum under safety constraints (see (2), (4) in [15]) for a simulated scenario involving a four-vehicle platoon on a flat and straight road section. Reduced distances between vehicles contribute to a decrease in air drag force, subsequently resulting in reduced fuel consumption. In our simulation, the platoon of four heavy-duty trucks can save 2% of fuel with 50% RadCom penetration rate compared to the scenario when radar communications are

not utilized. Furthermore, a 100% offload of the V2X channel leads to even greater fuel efficiency, with a substantial 5.6% reduction in fuel used. Lower fuel consumption leads to cost savings for individuals and businesses, as well as diminishes environmental impact.

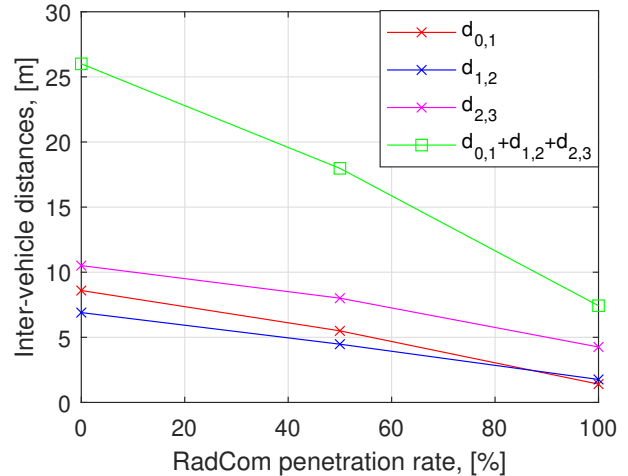


Fig. 3. Safe inter-vehicle distances in a platoon of four vehicles versus RadCom penetration rate. Here,  $d_{i-1,i}$  denotes an inter-vehicle distance between vehicles  $i - 1$  and  $i$  where vehicle 0 is the leader.

### VI. DISCUSSION

Below we discuss various issues related to using RadCom for intra-platooning communications. All of them represent possible directions for further research.

The energy savings in Section V are presented for one particular scenario only. The full mechanical model (see Equations (1,2) in [30]) takes into account road and vehicles' geometry (possible bumps, inclinations, curvatures) as well as their dynamical properties (variable friction and resistance coefficients). One might also consider possible thermal effects. Thus, for Internal Combustion Engine (ICE) vehicles, too small distances imply additional heating that, in turn, increases fuel consumption [31]. However, this is not the case for electrical vehicles.

Another factor that ambiguously affects energy costs is PCM rate. Low PCM rates lead to decreasing service costs (e.g., resource usage, and data transmission costs), whereas the high ones allow for shorter inter-vehicle distances. Thus, energy consumption is determined by the balance between low/high maintenance costs and savings related to shorter/longer distances.

One of the points to evaluate is the pertinence of having PCMs sent at a fixed interval, as considered in [7]. While these *heartbeat* messages keep platoon members informed about the status of the cluster, there are situations where PCM frequencies can be lowered (e.g., in flat, straight stretches of a highway). Further work is required in order to determine if variable PCM rates are energy beneficial and whether RadCom can support such scenarios.

The weather causes interference for radar in general and RadCom specifically. The detection capabilities of radars are affected by adverse weather conditions [32], [33] which are likely to affect RadCom links as they do with certain cases of V2X communications [34]. Further exploration is needed to understand the impact of weather-related failures, assess potential mitigation strategies (e.g., adding re-transmission protocols with or without forward error correction), and evaluate their effects on throughput.

Another issue that can affect performance in general for RadCom-enabled platooning is security. The ETSI ITS framework specifies a security architecture [35] with different requirements for each ITS service. For example, confidentiality and privacy requirements are different for CAMs and for DENMs, given their different nature. In DENM cases, such as road hazard warnings, the trade-off between confidentiality and road safety is leveraged differently. Work has to be performed to assess the need to encrypt RadCom-exchanged PCMs since they have a different dissemination scheme than those exchanged using the C-ITS spectrum.

Finally, one of the contributions of this paper was the evaluation of the effect of RadCom penetration rates. The nature of the vehicular industry creates a phenomenon where the average age of a vehicle is 12 years for passenger vehicles and 14.2 years for trucks [36]. This means that, even if 100% of vehicles produced starting today include RadCom nodes, it is unlikely that the penetration rate will reach 100% before several decades pass. However, one solution could be to retrofit radar-equipped vehicles (especially heavy-duty vehicles) with nodes adapted to their currently existing radars. Further work on the effect of a mixed-capability fleet shall be performed.

## VII. CONCLUSION AND FUTURE WORK

We presented a proposal to offload intra-platoon communications, which are expected to use PCMs sent in the 5.9 GHz V2X spectrum, to RadCom. We measured the potential benefit of the use of this additional access technology in a less congested V2X spectrum when adoption rates are high. Thus, lower congestion is reflected in increased network reliability and reduced end-to-end delays for safety-critical messages.

This increased reliability allows reducing the minimum inter-vehicle distance required for safe platooning. Therefore, other efficiency metrics are also boosted as a consequence of offloading communications to RadCom. We showed that fuel efficiency is increased with reduced distances, and with this efficiency, it can be argued that other beneficial societal and economical impacts occur.

Finally, we elaborated on other issues affecting platooning in general and RadCom-enabled platooning specifically:

- lowered distances effects on platoons of ICE and electric vehicles,
- fixed and dynamic PCMs rates,
- effects of adverse conditions on RadCom, and
- security requirements.

Future work includes the thorough evaluation of RadCom to comply with the requirements set for existing services and

*Future Mobility* services based on V2V communications, such as intention sharing and maneuver coordination.

## ACKNOWLEDGMENT

This work was partially supported by SAFER in the project “Human Factors, Risks and Optimal Performance in Cooperative, Connected and Automated Mobility”, the Knowledge Foundation in the project “SafeSmart – Safety of Connected Intelligent Vehicles in Smart Cities” (2019-2024), and the EL-LIIT Strategic Research Network in the project “6G wireless” – sub-project “vehicular communications”, and Vinnova grant 2021-02568.

## REFERENCES

- [1] United Nations, Department of Economic and Social Affairs - Sustainable Development, “Transforming our world: the 2030 agenda for sustainable development,” p. 16301, 2015, accessed 02-02-2024. [Online]. Available: <https://sdgs.un.org/2030agenda>
- [2] European Commission (EC), “Towards a European road safety area: policy orientations on road safety 2011-2020,” July 2010.
- [3] European Telecommunications Standards Institute (ETSI), “Intelligent Transport Systems (ITS); Vehicular communications; Basic set of applications; Part 2: Specification of Cooperative Awareness basic service,” ETSI, Standard EN 302 637-2 - V1.4.1, April 2019.
- [4] —, “Intelligent Transport Systems (ITS); Vehicular communications; Basic set of applications; Part 3: Specification of Decentralized Environmental Notification Basic Service,” Standard EN 302 637-3 - V1.3.1, April 2019.
- [5] —, “Intelligent Transport Systems (ITS); ITS-G5 Access layer specification for Intelligent Transport Systems operating in the 5 GHz frequency band,” ETSI EN 302 663 V1.3.1, January 2020.
- [6] Q. Delooz, R. Riebl, A. Festag, and A. Vinel, “Design and performance of congestion-aware collective perception,” in *2020 IEEE Vehicular Networking Conference (VNC)*, 2020, pp. 1–8.
- [7] European Telecommunications Standards Institute (ETSI), “Intelligent Transport Systems (ITS); Multi-Channel Operation study; Release 2,” ETSI TR 103 439 - V2.1.1, October 2021.
- [8] O. Amador, I. Soto, M. Urueña, and M. Calderon, “GoT: Decreasing DCC Queuing for CAM Messages,” *IEEE Communications Letters*, vol. 24, no. 12, pp. 2974–2978, 2020.
- [9] A. Baiocchi, I. Turcanu, N. Lyamin, K. Sjöberg, and A. Vinel, “Age of Information in IEEE 802.11p,” in *2021 IFIP/IEEE International Symposium on Integrated Network Management (IM)*, 2021, pp. 1024–1031.
- [10] O. Amador, I. Soto, M. Calderón, and M. Urueña, “Experimental Evaluation of the ETSI DCC Adaptive Approach and Related Algorithms,” *IEEE Access*, vol. 8, pp. 49 798–49 811, 2020.
- [11] C. Bonnet and H. Fritz, “Fuel consumption reduction in a platoon: Experimental results with two electronically coupled trucks at close spacing,” SAE technical paper, Tech. Rep., 2000.
- [12] T. Robinson, E. Chan, and E. Coelingh, “Operating platoons on public motorways: An introduction to the sartre platooning programme,” in *17th world congress on intelligent transport systems*, vol. 1, 2010, p. 12.
- [13] M. Adolfson, “Cooperative dynamic formation of platoons for safe and energy-optimized goods transportation,” in *93rd annual meeting of the transportation research board, Washington, DC, USA (Oral presentation)*, p. 42.
- [14] A. Pezzano and P. D. Idiada, “Enabling safe multi-brand platooning for europe,” 2020.
- [15] G. Sidorenko, J. Thunberg, K. Sjöberg, and A. Vinel, “Vehicle-to-vehicle communication for safe and fuel-efficient platooning,” in *2020 IEEE Intelligent Vehicles Symposium (IV)*, 2020, pp. 795–802.
- [16] European Telecommunications Standards Institute (ETSI), “Intelligent Transport Systems (ITS); Pre-standardization study on co-channel co-existence between IEEE- and 3GPP- based ITS technologies in the 5 855 MHz - 5 925 MHz frequency band,” ETSI TR 103 766, September 2021.
- [17] N. Lyamin, A. Vinel, M. Jonsson, and B. Bellalta, “Cooperative awareness in vanets: On etsi en 302 637-2 performance,” *IEEE Transactions on Vehicular Technology*, vol. 67, no. 1, pp. 17–28, 2018.

- [18] D. H. Nguyen, "Adaptation of etsi dcc for multi-lane platoon scenario," Delft, NL, August 2023, available at <http://resolver.tudelft.nl/uuid:9fac47f4-c240-44a1-89c9-f783b331a29a>.
- [19] F. Zhang, M. M. Wang, R. Deng, and X. Zhao, "High-reliability and low-energy sensor sharing in vehicle platoon based on multihop millimeter-wave communication," *IEEE Internet of Things Journal*, vol. 9, no. 19, pp. 18 514–18 526, 2022.
- [20] T. Paulin and S. Ruehrup, "On the Impact of Fading and Interference on Contention-Based Geographic Routing in VANETs," in *2015 IEEE 82nd Vehicular Technology Conference (VTC Fall)*, 2015, pp. 1–5.
- [21] S. Huang, M. Xiao, and H. V. Poor, "Achievable rate analysis of millimeter wave channels using random coding error exponents," *IEEE Transactions on Wireless Communications*, vol. 21, no. 1, pp. 250–263, 2022.
- [22] G. K. Carvajal *et al.*, "Comparison of automotive fmcw and ofdm radar under interference," in *2020 IEEE Radar Conference (RadarConf20)*, 2020, pp. 1–6.
- [23] H. Hellsten and E. Nilsson, "Multiple access radar using slow chirp modulation," in *2020 IEEE Radar Conference (RadarConf20)*, 2020, pp. 1–6.
- [24] C. Aydogdu *et al.*, "Radar interference mitigation through active coordination," in *2021 IEEE Radar Conference (RadarConf21)*, 2021, pp. 1–6.
- [25] —, "Radar interference mitigation for automated driving: Exploring proactive strategies," *IEEE Signal Processing Magazine*, vol. 37, no. 4, pp. 72–84, 2020.
- [26] R. Riebl, H. Günther, C. Facchi, and L. Wolf, "Artery: Extending Veins for VANET applications," in *2015 International Conference on Models and Technologies for Intelligent Transportation Systems (MT-ITS)*, 2015, pp. 450–456.
- [27] C. Sommer, R. German, and F. Dressler, "Bidirectionally Coupled Network and Road Traffic Simulation for Improved IVC Analysis," *IEEE Transactions on Mobile Computing*, vol. 10, no. 1, pp. 3–15, 2011.
- [28] D. Krajzewicz, J. Erdmann, M. Behrisch, and L. Bieker, "Recent Development and Applications of SUMO - Simulation of Urban MObility," *International Journal On Advances in Systems and Measurements*, vol. 5, no. 3&4, pp. 128–138, December 2012.
- [29] European Telecommunications Standards Institute (ETSI), "Intelligent Transport Systems (ITS); Decentralized congestion control mechanisms for Intelligent Transport Systems operating in the 5 GHz range; Access layer part," ETSI EN 102 687 - V1.2.1, April 2018.
- [30] K.-Y. Liang, J. Mårtensson, and K. H. Johansson, "Heavy-duty vehicle platoon formation for fuel efficiency," *IEEE Transactions on Intelligent Transportation Systems*, vol. 17, no. 4, pp. 1051–1061, 2016.
- [31] C. Zhang and M. P. Lammert, "Impact to cooling airflow from truck platooning," National Renewable Energy Lab.(NREL), Golden, CO (United States), Tech. Rep., 2020.
- [32] V. Sharma and S. Sergeyev, "Range detection assessment of photonic radar under adverse weather perceptions," *Optics Communications*, vol. 472, p. 125891, 2020. [Online]. Available: <https://www.sciencedirect.com/science/article/pii/S0030401820303631>
- [33] S. Walz, M. Bijelic, F. Kraus, W. Ritter, M. Simon, and I. Doric, "A benchmark for spray from nearby cutting vehicles," in *2021 IEEE International Intelligent Transportation Systems Conference (ITSC)*, 2021, pp. 188–195.
- [34] S. Dimce, M. S. Amjad, and F. Dressler, "mmwave on the road: Investigating the weather impact on 60 ghz v2x communication channels," in *2021 16th Annual Conference on Wireless On-demand Network Systems and Services Conference (WONS)*, 2021, pp. 1–8.
- [35] European Telecommunications Standards Institute (ETSI), "Intelligent Transport Systems (ITS); Security; ITS communications security architecture and security management," ETSI TS 102 940 V1.2.1, November 2016.
- [36] European Automobile Manufacturers' Association, "Average age of the EU vehicle fleet, by country," accessed 02-02-2024. [Online]. Available: <https://www.acea.auto/figure/average-age-of-eu-vehicle-fleet-by-country/>

# A Numerical Investigation of Deformable Soil-Tire Interaction

Dhruvin Jasoliya

Department of Mechanical  
Engineering

Virginia Tech, Blacksburg, VA, USA  
email: dhruvinj@vt.edu

Alexandrina Untaroioi

Department of Mechanical  
Engineering

Virginia Tech, Blacksburg, VA, USA  
email: alexu@vt.edu

Costin Untaroioi

Department of Biomedical  
Engineering and Mechanics

Virginia Tech, Blacksburg, VA, USA  
email: costin@vt.edu

**Abstract**— An accurate modeling of soil-tire interaction is necessary to determine and optimize key tire and vehicle performance parameters. In this study, soil is modeled using the Coupled Eulerian-Lagrangian (CEL) method, which is quite stable numerically for large deformation problems such as soil-tire interaction studies. The methodology for material model parameterization and setting up of numerical simulation is developed and validated against experimental data. The realistic stress data and good prediction of tire traction relative to experimental data suggest using the proposed methodology in future studies.

**Keywords:** Soil constitutive material model; Soil-tire interaction; Coupled Eulerian-Lagrangian (CEL).

## I. INTRODUCTION

The study of a deformable soil-tire interaction is important due to its wide applications in mining, agricultural, forestry, and military industries. Several researchers have used analytical and semi-empirical approaches to understand the complex phenomenon of traction mechanics on deformable terrain and optimize tire/vehicle performance [1]. The limitations of these studies include the oversimplification of the soil model by neglecting some of its complex factors (e.g., strain rate, moisture content, confining pressure, and/or drainage conditions) [2]. To overcome these limitations, in the past few decades, numerical methods have been used to study soil-tire interaction problems.

Various formulations of the Finite Element Method (FEM), such as Lagrangian, Arbitrary Lagrangian-Eulerian (ALE), and Coupled Eulerian-Lagrangian (CEL) have been used to model the soil-tire interaction [3-6]. These methods were able to provide a suitable alternative to analytical models because of their ability to capture the soil deformations and stresses in a more detailed manner. Additionally, meshless methods, such as Smooth Particle Hydrodynamics (SPH) and Discrete Element Method (DEM) were also employed [7][8]. Although meshless methods were able to predict the soil separation process occurring during the soil-tire interaction accurately, they have inherent stability issues. Furthermore, there is a lack of

validation of these meshless methods for cohesive soil-tire interaction [9].

The main goal of this work is to investigate the numerical accuracy of tire-deformable soil interaction simulations performed based on literature data. Numerical simulations of a plain rigid tire on deformable soil (Norfolk Sandy Loam) were performed for the traction prediction. The CEL approach is used due to its numerical stability in modeling large deformation problems. The soil is modeled using an elastic-plastic constitutive material model which is parameterized using literature data. The variation of net traction with different normal loads is studied and compared with the experimental data.

The methodology of performing the soil-rigid tire interaction numerical simulation is proposed in Section 2. In Sections 3 and 4 of the paper, numerical simulation results and discussion are provided. In the last section, a summary of the study is provided with the scope of future work.

## II. METHODOLOGY

The methodology of modeling rigid tire interaction with soil is based on the four steps (Figure 1). The first step is to analyze the experimental study of the rigid tire and soil [10] for the collection of traction data at different compaction, moisture content, normal load, and slip ratios.

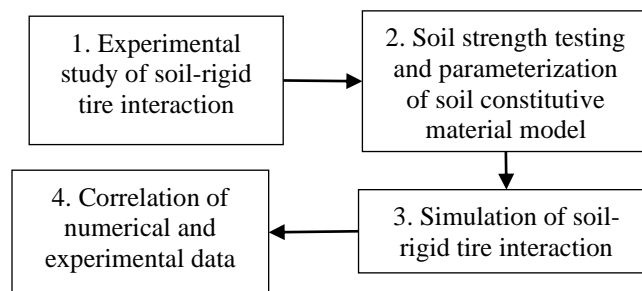


Figure 1: Soil-rigid tire interaction modeling methodology.

Based on the soil type and conditions, an appropriate soil strength test must be conducted for the parameterization of the soil constitutive material model. In the last two steps, the numerical simulation models of soil-rigid tire interaction are

used to predict net traction, and the results are compared with experimental data.

#### A. Experimental study of soil-rigid tire interaction

The experimental data from a rigid tire traction test conducted on Norfolk Sandy Loam (NSL) soil is carefully analyzed [10]. In testing, a rigid tire with dimensions of 1372 mm in diameter and 305 mm in width was used. Before the test, the soil was first rotary-tilled and then leveled with the roller until the required level of compaction was achieved, which was verified with a cone penetrometer. The experiment was designed to study the effect of variation of normal load and slip ratio on the traction of rigid tire (TABLE I). After soil conditioning, the normal load was applied to the rigid tire with a longitudinal velocity of 0.15 m/s. Based on the slip ratio, angular velocity was estimated and applied to the rigid tire. The wheel force transducers were used to record the net traction value for the corresponding normal load and slip ratio.

TABLE I: SOIL-RIGID TIRE INTERACTION TEST DESIGN OF EXPERIMENTS (DOE) [10].

Factor	Levels		
	1	2	3
Normal Load	2.9 kN	5.8 kN	8.7 kN
Slip Ratio	18.5 %	-	-

#### B. Soil testing and constitutive material model parameters

The shear strength of the soil is dependent on moisture content, strain rate, confining pressure, and drainage conditions. The triaxial test is extensively used for determining the shear strength and failure envelope of soil [2]. In triaxial testing, the cylindrical soil specimen is first subjected to predetermined confining pressure and then it is sheared at a constant strain rate until failure. The triaxial testing of the NSL soil used in the soil-rigid tire interaction was done at the three confining pressures (300 kPa, 400 kPa, and 500 kPa), and the failure envelope of the soil was calculated [11]. Based on the failure envelope of the soil, parameterization of the relevant soil constitutive material model is done.

The soil constitutive material models based on the theory of plasticity are frequently used in the modeling of granular materials such as soils and rocks. The elastic-plastic material models such as Mohr-Coulomb (MC), Drucker-Prager (DP), Cap-plasticity, and Cam-Clay are used in commercial FE software such as ABAQUS and LS-Dyna. An appropriate material model must be selected based on the available testing data and the expected output of the numerical simulation. For modeling of soil-rigid tire interaction, the DP material model is used because of its ability to capture the plastic deformations occurring in soil under the tire and its easy parameterization. The yield surface of the DP material model is defined in  $p$ - $q$  space using two plastic parameters, i.e., compressive yield stress ( $\sigma_c$ ) and material friction angle ( $\beta$ ) given by (1) (Figure 2). The DP material model

parameters for NSL soil based on triaxial test results are provided in TABLE II.

$$F(\sigma) = q - 3\sqrt{3}\alpha p - \sqrt{3}k \quad (1)$$

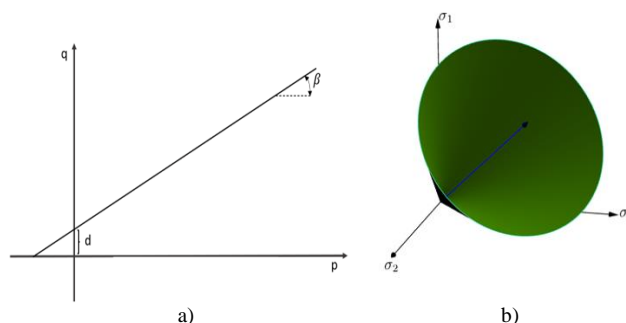


Figure 2: a) 2D DP Yield Surface b) 3D DP Yield Surface.

TABLE II: DP MATERIAL MODEL PARAMETERS FOR NSL SOIL [4].

Parameter	Value
Material friction angle ( $\beta$ ) [deg]	59.41
compressive yield stress ( $\sigma_c$ ) [MPa]	0.001
Mass density [ $\text{kg}/\text{m}^3$ ]	1255
Young's Modulus [MPa]	5
Poisson's ratio	0.3

#### C. Soil-rigid tire interaction numerical simulation

For the soil-rigid tire interaction model, the soil is modeled using Eulerian elements (EC3D8R) and the rigid tire with rigid elements (S4R) in ABAQUS/Explicit (Figure 4) [12]. A void region of a height of 150 mm is also added to capture the soil. Fixed boundary conditions are applied to the sides and bottom face of the soil domain, while the top surface interacting with the rigid tire is kept free. The DP material model is assigned to the soil domain. The soil domain, rigid tire dimensions, and coefficient of friction between rigid tire and soil are defined based on literature (TABLE III) [4].

TABLE III: SOIL-RIGID TIRE INTERACTION NUMERICAL SIMULATION PARAMETERS

Parameter	Value
Rigid tire thickness	304.8 mm
Rigid tire radius	686 mm
Soil domain cross-section	4000x1500 mm
Soil domain height	500 mm
Soil mesh size	20 mm
Friction coefficient between soil and rigid tire	0.4
Applied Longitudinal velocity	150 mm/s
Applied rotational velocity (18.5 % slip rate)	0.26 rad/s

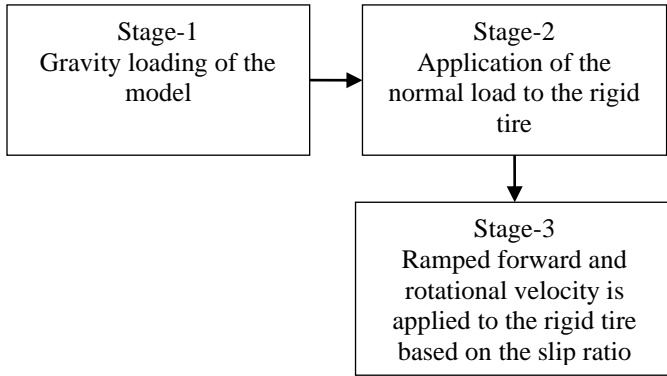


Figure 3: Soil-rigid tire interaction numerical simulation setup.

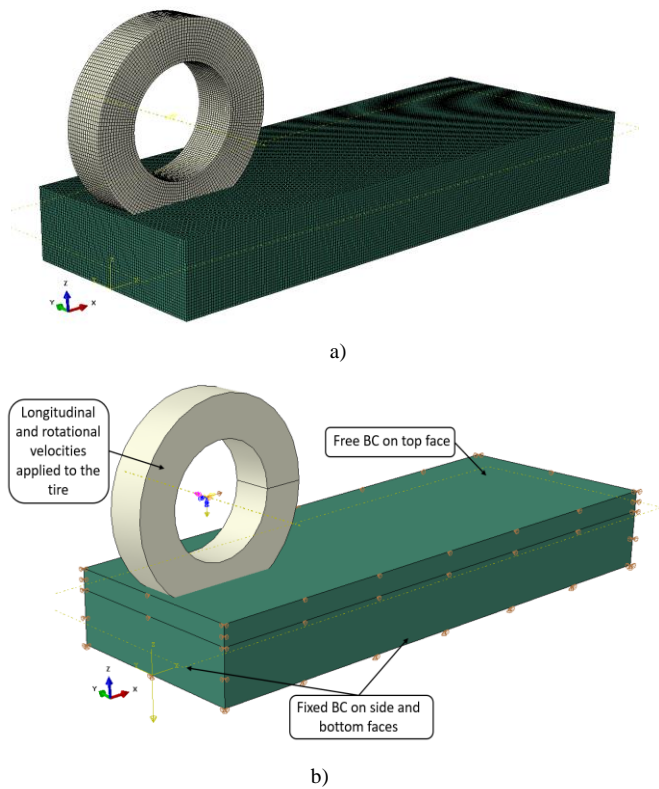


Figure 4: a) CEL model discretization b) CEL model BC.

The numerical simulations are set up in three stages (Figure 3). The net traction force which is the summation of normal and shear contact force is estimated from the total contact forces on the rigid tire.

### III. RESULTS

The normal stress (S33) and in-plane shear stress (S13) components of the soil domain are plotted once the steady state is reached during the traction performance simulation. A formation of the normal stress bulb due to applied normal load and a soil slip plane caused by applied longitudinal and rotational velocities are observed (Figure 5).

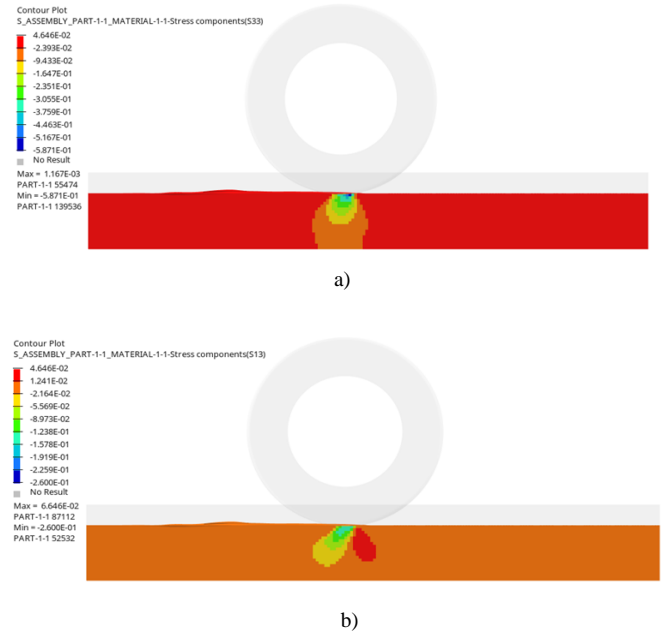


Figure 5: a) Normal stress (S33) b) in-plane shear stress (S13) (Normal load of 8.7 kN and slip rate of 18.5%).

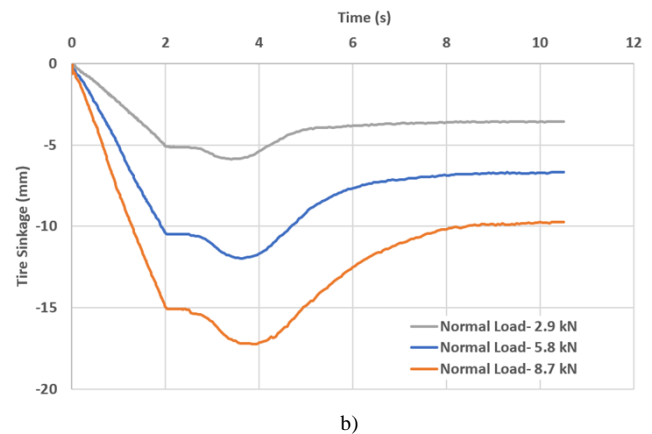
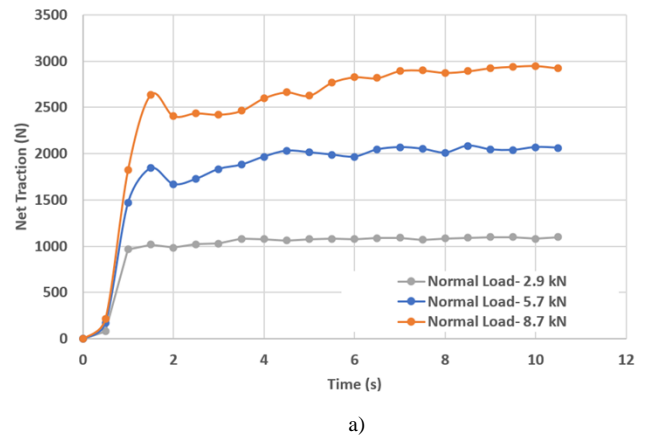


Figure 6: a) Net Traction performance b) Tire Sinkage (Slip ratio- 18.5%).

The unfiltered time history data of net traction and sinkage of rigid tire on soil at three different DOE normal loads is estimated from the numerical simulation runs. Based on the applied normal load, the settling time of the net traction and sinkage varies with time. Further, the net traction and sinkage increased with the increase in normal load (Figure 6).

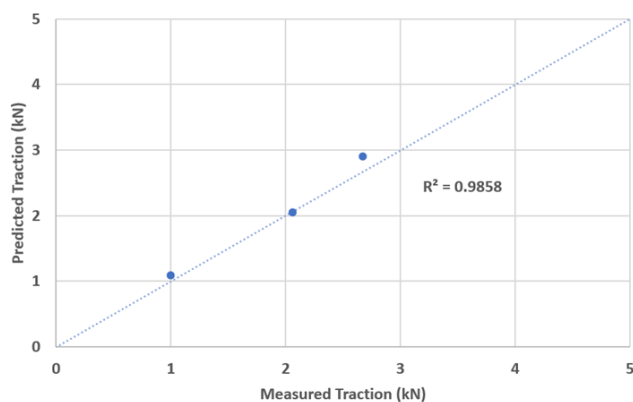


Figure 7: Traction for NSL soil: measured data vs. numerical predictions [10].

The net traction predicted by the numerical simulations is compared with the experimental results provided in the literature [10]. The predicted vs measured values for three normal loads applied at an 18.5% slip rate along with the  $R^2$  for the rigid tire on NSL soil are presented (Figure 7).

#### IV. DISCUSSION

The numerical simulations are performed based on the parameterization of the soil constitutive material model using soil strength testing results and rigid tire soil interaction experimental study DOE [10]. The soil undergoes volumetric and shear deformation when the tire passes over it during the soil-tire interaction process [13]. The stress plots indicate plastic deformation and volumetric changes occurring in the soil. The volumetric deformation in the soil provides information about the compaction state of the soil and soil-tire interface contact area, which directly affect the shear strength of the soil. The stress bulb formation and stress distribution are directly dependent on the soil-tire contact area (Figure 5-a). The shear stress plot indicates the formation of the slip planes under the tire, where the soil in front of the tire provides a negative contribution to the net traction as it is resisting the movement of the tire. The soil under and at the back of the tire provides a positive contribution to the net traction as it assists in the driving process (Figure 5-b). The location of the slip plane is dependent on the applied normal load and slip ratio, shear strength of soil, and tire sinkage [8].

The variation of net traction of the rigid tire is investigated for different applied normal loads. The soil strength is pressure dependent, the increase in applied normal load increases the shear strength of the soil.

Therefore, both net traction and tire sinkage increase with soil shear strength (Figure 6). In numerical simulation, the ramped longitudinal and rotational velocity is applied, therefore there is variation in the initial time duration of the simulation is observed before the net traction and tire sinkage settle down to the steady state values. The measured vs fitted curve of net traction at three different normal loads provided a good correlation with an  $R^2$  value of 0.98.

Overall, a plain rigid tire is used at a low slip rate in this study. Therefore, additional studies are required with a more complex problem definition and extensive validation plan in terms of net traction, tire sinkage, and soil stresses to determine the accuracy of the developed methodology presented in this study for large-scale application.

#### V. CONCLUSIONS AND FUTURE WORK

The modeling of the soil-tire interaction process with traditional numerical methods is infeasible due to stability issues. Further, soil undergoes high plastic deformation, and the use of non-linear elastic-plastic material models is required for accurate results. The CEL approach has been successfully implemented in the simulation of non-linear dynamic problems such as soil-structure interaction. Therefore, in this study, a methodology of numerical simulation of soil-rigid tire interaction is developed using the CEL approach in Abaqus/Explicit. The numerically predicted net traction for three normal loads at a given slip rate of 18.5 % provided a good correlation with the experimental data.

The developed methodology with the CEL approach is suitable for predicting the net traction, tire sinkage, tire-soil contact area, and stress distribution in soil. These performance attributes are important for the design optimization of off-road tires based on the application and properties of terrain. However, the comparison of the relative accuracy of the CEL approach with other meshed and meshless numerical methods is still not undertaken for soil-tire interaction modeling.

The next steps are to model the soil-tire interaction with other numerical formulations used in modeling large deformation problems, such as SPH and ALE. Also, the sensitivity of the net traction to different slip rates and tire parameters will be studied.

#### REFERENCES

- [1] R. He, C. Sandu, A. K. Khan, A. G. Guthrie, P. S. Els, and H. A. Hamersma, "Review of terramechanics models and their applicability to real-time applications," *Journal of Terramechanics*, vol. 81, pp. 3-22, 2019.
- [2] D. Jasoliya, A. Untaroiu, and C. Untaroiu, "A review of soil modeling for numerical simulations of soil-tire/agricultural tools interaction," *Journal of Terramechanics*, vol. 111, pp. 41-64, 2024.
- [3] C. Fervers, "Improved FEM simulation model for tire-soil interaction," *Journal of Terramechanics*, vol. 41, no. 2-3, pp. 87-100, 2004.
- [4] A. G. Varghese, J. L. Turner, T. R. Way, C. E. Johnson, and H. R. Dorfi, "Traction prediction of a smooth rigid wheel in soil

- using coupled Eulerian-Lagrangian analysis," in *Proceedings of 2012 SIMULIA Community Conference*, 2012, pp. 1-15.
- [5] K. Xia, "Finite element modeling of tire/terrain interaction: Application to predicting soil compaction and tire mobility," *Journal of Terramechanics*, vol. 48, no. 2, pp. 113-123, 2011.
- [6] H. Yamashita, P. Jayakumar, M. Alsaleh, and H. Sugiyama, "Physics-based deformable tire-soil interaction model for off-road mobility simulation and experimental validation," *Journal of computational and nonlinear dynamics*, vol. 13, no. 2, p. 021002, 2018.
- [7] Z. El-Sayegh, M. El-Gindy, I. Johansson, and F. Öjjer, "Improved tire-soil interaction model using FEA-SPH simulation," *Journal of Terramechanics*, vol. 78, pp. 53-62, 2018.
- [8] C.-L. Zhao and M.-Y. Zang, "Application of the FEM/DEM and alternately moving road method to the simulation of tire-sand interactions," *Journal of Terramechanics*, vol. 72, pp. 27-38, 2017.
- [9] V. S. Swamy *et al.*, "Review of modeling and validation techniques for tire-deformable soil interactions," *Journal of Terramechanics*, vol. 109, pp. 73-92, 2023.
- [10] W. A. Block, *Analysis of soil stress under rigid wheel loading*. Auburn University, 1991.
- [11] A. C. Bailey and C. E. Johnson, "A soil compaction model for cylindrical stress states," *Transactions of the ASAE*, vol. 32, no. 3, pp. 822-825, 1989.
- [12] D. Systèmes, "Abaqus 6.9 User's guide and theoretical manual, Hibbitt, Karlsson & Sorensen," *Inc.: Providence, RI, USA*, 2009.
- [13] J. Y. Wong, *Theory of ground vehicles*. John Wiley & Sons, 2022.